NORTHWESTERN UNIVERSITY

Mechanistic Studies of the Autoxidative Curing of an Oil-Based Paint Model System

A DISSERTATION

SUBMITTED TO THE GRADUATE SCHOOL

IN PARTIAL FULFILLMENT OF THE REQUIREMENTS

for the degree

DOCTOR OF PHILOSOPHY

Field of Materials Science and Engineering

By

Lindsay H. Oakley

EVANSTON, ILLINOIS

December 2017

Mechanistic Studies of the Autoxidative Curing of an Oil-Based Paint Model System

Lindsay H. Oakley

Microkinetic modeling is a powerful tool for creating dynamic and quantitative descriptions of complex systems. These detailed mechanistic models compliment experimental techniques and provide an ability to achieve deeper insights into chemical processes where numerous intermediates are highly reactive and difficult to quantify in the laboratory. This thesis discusses the development of a microkinetic model for the autoxidative curing of an oil-based paint model system relevant to the cultural heritage science community. Grasping the mechanisms of the formation and resulting composition of crosslinked and non-crosslinked species from autoxidative processes is critical to understanding and predicting the long-term chemical and physical stability of painted objects.

The fatty acid ester studied in this work, ethyl linoleate (EL), is frequently used as a model system for oil paint binders. Consequently, quantitative experimental data was available for model validation and comparison to theoretical predictions for a few key metrics such as the peroxide content and oxygen absorption of the system, as well as the evolution of small volatile molecules such as hexanal and pentanal. The mechanism and parameters for autoxidation were assembled from a variety of literature sources. This preliminary microkinetic model of EL curing catalyzed by cobalt-2-ethyl hexanoate (Co-EH) up to the formation of single crosslinked species revealed that the mechanisms governing the formation of the volatile species hexanal were still not well understood and that a much larger reaction network would be required to thoroughly describe the cured system.

An in depth study of mechanistic postulates for the formation of hexanal was conducted and β-scission of higher rank oligomeric products was demonstrated to be an effective route to form these volatile products at the mild reaction conditions of interest. Gas Chromatography/Mass Spectrometry (GC/MS) headspace analysis was also conducted to provide quantitative targets for hexanal and pentanal production in the early cure regime (< 24 hours) which were previously unavailable.

Quantum chemical calculations were performed to derive a structure-reactivity relationship for the formation of experimentally observed epoxide species. A wide range of chemical space was explored for the first time, including observations for allylic and benzylic radical reactants. This work revealed that the reactant radical type can have a strong effect on the calculated rate parameters and that separate kinetic correlations are required to treat saturated and unsaturated species accurately.

A second generation model for EL autoxidation was constructed incorporating these new mechanistic insights and used computational automation to generate the reaction network. This larger microkinetic model represented a significant improvement in capturing experimentally observed products at longer curing times (up to 100 hours). The larger model was also able to capture accelerated rates of curing in response to increased temperature and Co-EH concentration. Building a detailed microkinetic model for an oil-based model system expanded understanding of the underlying chemical mechanisms involved in the formation of stable paint films.

Acknowledgements

To my excellent advisors, Professors Linda Broadbelt and Ken Shull: I am so grateful for both of your guidance throughout the process of grad school and for your encouragement to take advantage of opportunities outside of the box for typical PhDs. You have modeled both academic excellence and a generosity with your time and knowledge that I have greatly benefited from and hope to emulate.

To my committee members, Dr. Katherine Faber, Dr. Wesley Burghardt and Dr. Francesca Casadio: Thank you so much for your thoughtful questions and constructive feedback. In particular I would like to thank Dr. Casadio for the mentorship and advice you have provided towards preparing for a career in the conservation science field.

To Dr. Kristin Wustholz and Shelley Svoboda: One of the main reasons I decided to pursue a PhD is because of you two and the invaluable research experience you provided me as a William & Mary undergraduate. Thank you for teaching me, challenging me and believing in me.

To Broadbelt and Shull Research Group members past and present: This work would not have been possible without your valuable questions and contributions at group meetings and conversations around the office(s). Your work ethic, moral support, creativity and participation in scientific outreach events were continually inspiring to me and I am so grateful to have been a part of two such encouraging and collaborative groups.

To treasured friends: I would not have survived all the ups and downs of grad school without an amazingly supportive network of colleagues in my department that shared in the struggles and thrills of coursework and academic milestones, in particular Stephanie, Madeleine, Josh & Ashwin. Thank you to many friends from GCF who challenged me to think deeply about life's

big questions and who once showed up to help me move on the hottest day of the year. Thank you to the most wonderful string of roommates a person could ask for, Sarah, Christina, Lois, Heather, Anne, Danielle & Nathalia, living with each of you was a joy and kept me sane. Thanks to my gym buddy and fellow Shull group member Lauren who got me up early each day with the promise of exercise and excellent companionship. A special thanks to Nayo for your words of wisdom always exactly when I needed them, as well as to Anne and Josh for keeping me fed, happy and healthy as the process of thesis writing became consuming.

To my family: Mom, Dad, Cate, Miles, grandparents and more, I have felt your love and support my entire life in tangible and intangible ways that are too numerous to count. Thank you for constantly encouraging me to pursue hard and challenging things and for always being there when I needed you. This work is dedicated to you.

Financial support for this work from the National Science Foundation Division of Materials Research (DMR-1241667) and the Northwestern University/Art Institute of Chicago Center for Scientific Studies in the Arts (NU-ACCESS) is gratefully acknowledged. This work used the Extreme Science and Engineering Discovery Environment (XSEDE), which is supported by National Science Foundation grant number ACI-1053575. GC/MS Headspace analysis experiments were performed at the Northwestern Integrated Molecular Structure and Education Research Center (IMSERC) which has received support from the Soft and Hybrid Nanotechnology Experimental (SHyNE) Resource (NSF NNCI-1542205); the State of Illinois and International Institute for Nanotechnology (IIN). Helpful conversations with Dr. Ken Sutherland (AIC) and Director of IMSERC Mass Spectrometry, Dr. S. Habibi Goudarzi are also gratefully acknowledged.

Table of Contents

Table of Contents 7
List of Figures 9
List of Tables 13
Chapter 1 14
Introduction 14
Chapter 2 21
Microkinetic modeling of the autoxidative curing of an alkyd and oil-based paint model system 21
2.1 Introduction 21
2.2 Mechanism Development 24
2.3 Computational Methods 31
2.4 Results and Discussion 33
2.5 Conclusions 41
Chapter 3 43
An examination of the mechanisms for the formation of volatile aldehydes from the autoxidation of oil-based systems 43
3.1 Introduction 43
3.2 Computational Techniques 46
3.2.1 Quantum Chemical Calculations 46
3.2.2 Microkinetic Modeling 47
3.3 Experimental Details 48
3.3.1 Materials 48
3.3.2 GC/MS Headspace Instrumentation and Procedures 48
3.4 Reactions Studied 49
3.4.1 Korcek and Korcek-like Reactions 49
3.4.2 Intramolecular Hydrogen Shifts 51
3.4.3 Reactions Involving Allyl Peroxy Species 53

3.4.4. Formation of Volatile Products from Dimers and Other Higher Order Species 54
3.5 Results and Discussion 55
3.5.1 Experimental Results 55
3.5.2 Computational Results and Implications 56
3.6 Conclusions 67
Chapter 4 69
Theoretical study of epoxidation reactions relevant to hydrocarbon oxidation 69
4.1 Introduction 69
4.2 Computational Methods 72
2.3 Results and Discussion 73
4.4 Conclusions 84
Chapter 5 86
An expanded microkinetic model for the condensed phase, cobalt catalyzed autoxidative curing of ethyl linoleate 86
5.1 Introduction 86
5.2 The EL model system and autoxidation mechanism 88
5.2.1 Ethyl linoleate as a model system 88
5.2.2. Mechanism and kinetic parameters 89
5.3 Computational Methods 90
5.3.1 Automated Mechanism Generation 90
5.3.2 Microkinetic Modeling 93
5.4 Results 94
5.5 Conclusions 107
Chapter 6 109
Summary and Future Perspectives 109
References 113

List of Figures

Figure 1.1. Flow chart for the development of a microkinetic model. 18

Figure 2.1. A schematic of the chemistry incorporated into the microkinetic model. 26

Figure 2.2. Ethyl linoleate molecule. The most reactive hydrogens located at position 11 are *shaded darkly*, with positions of decreasing reactivity corresponding to progressively *lighter shading.* 30

Figure 2.3. Comparison of total peroxide content of the system output by the KMC dimer model (line) to experiment (points)[30] 35

Figure 2.4. Oxygen uptake, or mass gain, of the system from the KMC dimer model (line) compared to experiment (points)[30] 36

Figure 2.5. Hexanal (*solid line*) and pentanal (*dashed line*) yields predicted by the KMC dimer model. At 10 h of curing time, expected values from experiment are approximately 1.0 mmol/mol EL and 0.05 mmol/mol EL, respectively[30] 38

Figure 2.6. Schematic of the β-scission mechanism for the formation of pentanal and hexanal. Qualitative experimental trends for the production of pentane and pentanal are matched by the model using scission reaction 1 and subsequent pathways, but scission reaction 2 yields extremely low levels of hexanal. 39

Figure 3.1. Proposed mechanism for a Korcek-like reaction in ethyl linoleate containing residual unsaturation in the carbon chain. The first step (1) is the formation of a cyclic peroxide from a keto-hydroperoxide which can be acid catalyzed followed by the (2) fragmentation of the keto peroxide into hexanal and a carboxylic acid. 51

Figure 3.2. Proposed mechanism for the formation of hexanal and an allylic radical from a series of elementary steps involving (1) hydrogen abstraction from a conjugated alcohol, (2) fast isomerization, (3) an internal hydrogen shift and (4) the subsequent β-scission of the resulting alkoxy radical. 52

Figure 3.3. Proposed mechanism forming hexanal through the (1) cyclization of an allylic peroxy radical and (2) subsequent concerted decomposition into two carbonyl-containing species. 53

Figure 3.4. Proposed mechanism for the formation of the small volatile molecules hexanal and pentanal (through the further oxidation of pentyl radicals) from a dimer or higher oligomeric species. Alkoxy radicals are produced by the catalytic activity of cobalt decomposing hydroperoxides, and β-scission can subsequently proceed via pathway 1 or 2. 55

Figure 3.5. Amount of volatile species hexanal (open squares □) and pentanal (open triangles Δ) detected by GC/MS headspace analysis during the oxidation of EL with a cobalt catalyst. Results are compared to those of Oyman et al.[30] which are designated using closed symbols. ... 56

Figure 3.6. Free energy surfaces for the formation of a six-membered cyclic (a) saturated and (b) unsaturated peroxide species. The unsaturated keto-hydroperoxide must undergo *trans* to *cis* isomerization to obtain the necessary geometry for cyclization to occur. 58

Figure 3.7. A free energy surface for 1,3-intramolecular hydrogen shift involving a hydroxyl group. Geometries are also shown for the reactant (a), transition state (b) and product (c). 60

Figure 3.8. Free energy surface for the formation of two terminal carbonyl species from the decomposition of a peroxy radical. Results are in good agreement with those that Juita et al.[79] were able to report, with the addition of a definitive transition state for the decomposition of the dioxetane intermediate. 63

Figure 3.9. Structure of the transition state for the concerted decomposition of a conjugated hydroperoxide into an aldehyde and an alcohol. Relevant interatomic distances are included in Angstroms (Å). 63

Figure 3.10. Scheme for the formation of a dimeric species through 1) peroxy radical addition across conjugated double bonds followed by 2) the potential isomerization of the allylic radical and 3) oxygen addition and hydrogen abstraction to form the second hydroperoxide group..... 65

Figure 3.11. Concentration profiles for the volatile aldehydes, hexanal and pentanal, generated by the microkinetic model (lines). Agreement with measured experimental values (hexanal ■, pentanal ▲) is vastly improved from previous versions of the model that did not allow for volatiles to be formed from higher rank products. 67

Figure 4.1. Reactant radicals undergoing direct epoxidation through homolytic O−O bond cleavage that were examined using quantum chemical calculations. 72

Figure 4.2. Representative free energy profile for reactant 6 in Figure 4.1 from G4 calculations. Values are referenced to reactant structure A. Also shown are the (B) transition state geometry, as well as the structures of the (C) epoxide product and (D) alkoxy leaving group. Key bond lengths and angles are also indicated in Angstroms and degrees, respectively. 74

Figure 4.3. Evans-Polanyi plot of the forward exothermic epoxidation reactions (filled) and the reverse endothermic radical addition reactions (open). Reactant characteristics assigned in Table 4.1 are represented by the following symbol shapes: alkylperoxy (□), alkylhydroperoxy (◊), allylic alkylperoxy (×), allylic alkylhydroperoxy (Δ), benzylic hydroperoxy(○) and benzylic alkylperoxy(*). Species numbers from Table 4.1 are also listed with their associated data point for ease of reference. 80

Figure 4.4. A closer examination of the Evans-Polanyi plot in the region of -15 to -20 kcal/mol. A new regression for only these points is provided. An example of the basic alkylhydroperoxy radical structure exhibited by the species in this region is shown and species numbers from Table 4.1 are also listed with their associated data point for ease of reference. 81

Figure 4.5. Representative enthalpy landscape constructed from G4 enthalpies at 298 K for reactant 10. This diagram reveals the formation of a low-energy complex. When the heat of reaction is referenced to this complex, an Evans−Polanyi relationship with a slope less than 1 is recovered. 82

Figure 5.1. An example β-scission reaction matrix transformation where a C-O bond is broken by a carbon radical creating a C=C double bond and an oxygen radical. 91

Figure 5.2. The evolution of the total peroxide content of the system (blue line) compared to results from Oyman et al.[30] The total peroxide content of the system predicted by the microkinetic model is broken down in the contributions from hydroperoxide functional groups (red line) and peroxide functional groups (yellow line). 95

Figure 5.3. Comparison of the model prediction of the total oxygen uptake of the system (line) to experimental data from Oyman et al.[30] (points). 96

Figure 5.4. A comparison of the production of volatile species to experimental data for the small molecules pentanal (blue lines and points) and hexanal (red lines and points). 97

Figure 5.5 Model predictions for the peroxide content of the system generated with 67 model parameters. The two additional parameters suppressed the addition of oxygen to larger radicals and therefore reduced the amount of peroxides in the system to better agree with experiment[30] 101

Figure 5.6. Schematic of representative mechanistic steps that lead to hexanal from over-oxidized reactant C). Ideally if mechanistic step 3 could be avoided by increasing the competition to form reactants D) & E) and ensuring routes exist in the model to form hexanal from these species, model agreement could be improved. 102

Figure 5.7. The evolution of the concentration of oligomeric species. Species were classified as dimers, trimers, etc. based on the number of carbons in the molecule. 103

Figure 5.8. The microkinetic model predictions for key functional groups containing oxygen during the first 100 hrs of cure time. These species were observed experimentally but not necessarily well quantified for model comparison. 104

Figure 5.9. Microkinetic model predictions for the consumption of double bonds over 100 hours of curing time. The inset tracks the percentage of double bonds that exist in conjugated form. 105

Figure 5.10. Microkinetic model predictions of the concentration profiles for lumped hydroperoxide species at catalyst concentrations ranging from 0.07 to 1.4 wt%. Increasing the amount of cobalt in the system dramatically increased the rate of consumption of these functional groups to form radicals. 106

Figure 5.11. Microkinetic model predictions for the consumption of double bonds at increasing temperatures from 25 to 60°C for 25 hours. 107

List of Tables

Table 1.1. The fatty acid composition of some common drying oils (wt%)[6,9] 16

Table 2.1. Kinetic parameters for the microkinetic model with units for k and A in L/mol•s (bimolecular) or s^{-1} (unimolecular) and E_0 in kcal/mol. 29

Table 3.1. A summary of reaction mechanisms for the production of small volatile aldehydes. Reaction barriers (E_A) in kcal/mol and pre-exponential factors (A) in L/mol s (bi-molecular) or s^{-1} (unimolecular) for rate-determining steps are provided, the types of calculations performed to determine these values are indicated and relevant literature describing the mechanism in detail is cited. 57

Table 3.2. Arrhenius parameters calculated for the forward cyclization and corresponding reverse reactions of the minimum free energy pathways shown in Figure 3.6. 59

Table 4.1. Kinetic and Thermodynamic Properties Calculated for the Reactants Shown in Figure 4.1 Based on G4 Energies and Corrected for Internal Rotations, Including Key Aspects of the Reactant Radical Structure (Alkyl, Allylic, Cyclic, or Benzylic) and the Alkoxy Leaving Group (Hydroperoxy or Alkylperoxy). 75

Table 4.2. Comparison of calculated kinetic parameters with those presented in previous theoretical studies. 78

Table 5.1. Input variables *s* and ε for the automatically generated mechanism meeting the key criteria. The resulting size descriptors are presented in terms of the number of species, reactions and size of the largest oligomeric species generated. 93

Table 5.2. Kinetic parameters for the microkinetic model with units for k and A in L/mol•s (bimolecular) or s^{-1} (unimolecular) and E_0 in kcal/mol. 98

Chapter 1

Introduction

The field of cultural heritage science evolved into the robust discipline it is today in response to the many challenges that arise in caring for and preserving objects of historic, aesthetic and cultural significance for future generations. A major objective of science in this interdisciplinary space is to develop an understanding of how materials age and degrade over time.[1] This is important information for conservators to have as they make decisions about how to care for and display objects, ensuring their survival for future generations.

Paintings in particular present unique challenges to conservation scientists. Due to their multi-layered structure comprised of non-homogenous mixtures of pigment, binder and other additives included to adjust the working qualities of the paint either by manufacturers or the artist themselves, determining the chemical and physical properties of an object that has aged for many years is non-trivial. The complexity makes it difficult to anticipate how a particular object may respond to environmental conditions, cleanings or other treatments. Currently, strategies for the prediction of long-term chemical aging and stability primarily consist of artificial aging. Samples of material are painted onto suitable substrates such as canvas, glass slides or Mylar® and are typically then subjected to either UV light exposure or increased temperature in ovens in an attempt to produce a paint film with physical and chemical properties that mimic those of naturally aged paints in a substantially shorter period of time.[2] These artificially aged samples can be used to test mechanical strength before treatments and stresses are applied to valuable

cultural heritage objects. However, studies have shown that artificial aging protocols, particularly those using elevated temperature, may not as accurately capture the behavior of actual historic objects as previously thought.[3,4]

This research aims to introduce kinetic modeling to the field of cultural heritage science as a tool for developing a detailed mechanistic understanding of how materials age and degrade as well as having predictive capabilities for a variety of scenarios including variances in the composition of an object and its environmental conditions. More specifically, this work focuses on the development of a microkinetic model of the autoxidative curing of model systems for oil-based binding media.

Natural oils, such as linseed oil, have been used for centuries as paint binders. Some modern binders, such as alkyds, are also oil-rich as they have a polyester polymer backbone modified by fatty acid residues.[5] Oil-based paint binders are characterized by their ability to autoxidatively cure and dry to form a crosslinked network that provides for the structural stability of a paint coating. The fatty acid residues in these drying oils contain varying degrees of unsaturation which play an important role in the curing chemistry. The fatty acid composition of some common drying oils is reproduced from Lazzari et al.[6] in Table 1.1. Palmitic and stearic acids are completely saturated while oleic, linoleic and linolenic acid contain one, two and three double bonds respectively. The mixing ratios of these fatty acids can be unique even between sources of the same oil type which leads to complexity of the crosslinked network that is formed during the curing process and presents an obstacle to the development of models for these types of systems. However, insights into the overall key mechanisms of polymerization and drying can still be discerned from the examination of single component analogs. The fatty acid ester ethyl

linoleate (EL) was utilized in this work as a model system to approximate an oil binder with an average degree of unsaturation of ~2. Knowledge of the mechanisms that lead to the formation of crosslinked material is a critical foundation to understanding the long term stability of oil paintings, as are the mechanisms that lead to non-crosslinked components. These non-crosslinked small molecules can have a high mobility within the paint layer and may be particularly susceptible to volatilization or solvent extraction during cleaning which could have an impact on the appearance and physical stability of the object (e.g. embrittlement).[7,8]

Table 1.1. The fatty acid composition of some common drying oils (wt%)[6,9]

Oil	Palmitic	Stearic	Oleic	Linoleic	Linolenic
Linseed	6-7	3-6	14-24	14-19	48-60
Walnut	3-7	0.5-3	9-30	57-76	2-16
Poppyseed	10	2	11	72	5
Tung[a]	3	2	11	15	3

[a] The main component is elaecostearic acid (59%)

Microkinetic modeling is a powerful tool for investigating curing phenomena because all mechanistic elementary steps are considered explicitly. Since no rate-limiting steps are assumed, the model is easily extensible to a variety of conditions and can be rapidly expanded to account for new mechanistic postulates. Key factors that influence the kinetics of reactions on the molecular level can be explored and can provide insight into competing mechanisms and potential inform strategies to optimize processes. This theoretical method can contribute significant value in cases of long time scales that are difficult to capture in the laboratory, or when multiple intermediates are highly reactive and difficult to quantify experimentally.

Developing a microkinetic model is an iterative process as shown in the flow chart in Figure 1.1. First a mechanism must be proposed and kinetic parameters (usually Arrhenius A and

E_A) describing each elementary reaction step obtained. Ideally, values are available from experiment, but given the nature of the autoxidative process with reactive radical intermediates, this is not possible for all of the elementary steps involved. Often correlations that relate kinetic parameters to thermodynamic quantities for a specific type of reaction chemistry are used to achieve rigorous estimates for these values that can have a strong fundamental basis in quantum chemical calculations and statistical mechanics using transition state theory.[10–12]

The mechanism can be solved by either stochastic or deterministic methods, each with their own strengths and limitations. This work presents models based on both a kinetic Monte Carlo (KMC) framework and a system of ordinary differential equations (ODEs) and the benefits and limitations of each are discussed. For either mathematical method, the output is the concentration profiles of all the species which can be compared to expected experimental yields. By optimizing the set of kinetic parameters within a reasonable range of expected error, a descriptive mechanistic model is created which can be used to make predictions for other experimental conditions.

In Chapter 2, the development a of microkinetic model for an EL model system containing a cobalt catalyst to accelerate the decomposition of key hydroperoxide intermediates into oxygen-centered radicals is presented using a kinetic Monte Carlo framework. The process of assembling key mechanistic steps and parameters from the literature is discussed in detail and the model performance compared to three quantitative experimental metrics is evaluated in the early cure regime (<10 hrs, up to the formation of single crosslinks). This preliminary model revealed that the mechanisms governing the formation of small volatile species, particularly hexanal, were still not well understood and merited further scrutiny.

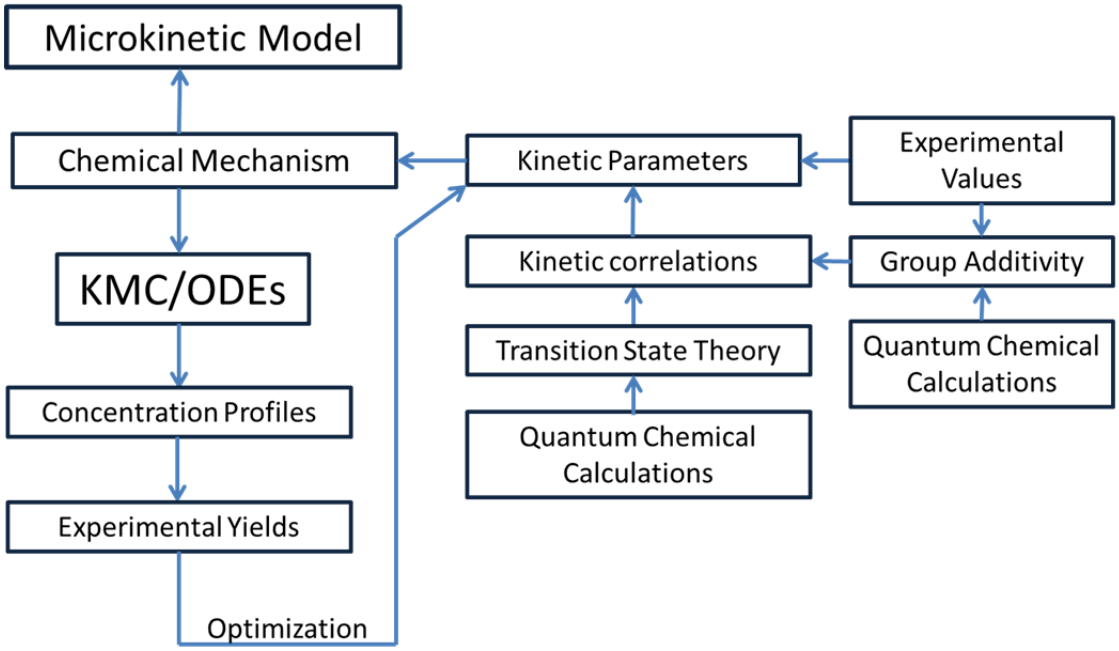

Figure 1.1. Flow chart for the development of a microkinetic model.

Chapter 3 expands on this research by performing an in depth analysis of mechanistic postulates for the formation of hexanal. When kinetic parameters were not available for these reactions, quantum chemical calculations were utilized to fill in missing information necessary to test these routes within the context of the microkinetic model developed in Chapter 2. Using the kinetic rates of these reactions to assess the contributions of these pathways to the formation of hexanal was critical to improving model performance as many of the tested pathways were not kinetically significant at the room temperature, condensed-phase conditions of interest but could play a role at other reaction conditions. Also, since experimental data in the early curing regime which the model was designed to predict was unavailable, GC/MS headspace analysis was performed to provide quantitative targets for comparison.

In some instances where kinetic rate parameters or kinetic correlations for necessary reaction channels leading to the formation of observed product moieties were not available, a structure-reactivity relationship had to be calculated. Chapter 4 discusses a particular instance where a kinetic correlation, in Evans-Polanyi form,[13] for the production of epoxide species was determined from a series of quantum chemical calculations for 25 different molecules. This set of reactant molecules was specifically selected to explore a diverse chemical space, in particular including allylic and benzylic radical species for the first time. Exploring a wide range of values for the heat of reaction, ΔH_R, revealed that the radical type has a major influence on the calculated kinetic parameters and that in order to accurately treat both saturated and unsaturated species in the mechanism at least one subdivision of the kinetic correlation is recommended. This has important implications for a variety of contexts where models of hydrocarbon oxidation have been applied.

Finally, Chapter 5 represents the culmination of the work in the previous chapters into an expanded model for cobalt-catalyzed EL autoxidation. This model included the new mechanistic postulates for the formation of volatile hexanal as well as routes and parameters for the formation of epoxide species. Since previous versions of the model struggled to capture behavior at longer curing time scales (up to 100 hours) due to a lack of routes to form higher rank oligomeric species, the automated mechanism generator NetGen[14] was used to generate a much larger reaction network which was solved deterministically and optimized using gradient-based search methods. Model predictions were again compared to quantitative metrics and other qualitative experimental observations and represented a significant improvement over previous

generations of the microkinetic model. The model was also used to make predictions about autoxidative behavior at increased concentrations of cobalt catalyst and at elevated temperatures.

Chapter 6 discusses the major conclusions of this work and the future possibilities for expanding the contributions of microkinetic modeling in the field of cultural heritage science to increasingly complex oil paint mimics as well as other material systems.

Chapter 2

Microkinetic modeling of the autoxidative curing of an alkyd and oil-based paint model system

Material in this chapter is reproduced from the article "Microkinetic modeling of the autoxidative curing of an alkyd and oil-based paint model system" by Lindsay Oakley, Francesca Casadio, Kenneth Shull and Linda Broadbelt; *Applied Physics A*, **121**, 869-878.[15]

2.1 Introduction

Oil and oil-based paints have been ubiquitous in Western artwork for centuries.[16] Cleaning, displaying and preserving important objects of cultural heritage significance containing these materials can present numerous scientific challenges. Consequently, a fundamental grasp of the interactions of the different paint components is critical to maintaining chemical stability and structural integrity. Dynamic and quantitative models of chemical phenomena in these paints would be useful to conservators and scientists interested in understanding and predicting how environmental conditions and treatment interventions will impact works of art on timescales difficult to replicate in the laboratory.

To this end, a kinetic model can be constructed to describe the chemical and structural changes occurring in a curing and aging oil-based paint. Similar to other hydrocarbons, curing proceeds via an autoxidative mechanism where chemically cross-linked oligomers form the basis of a matrix holding the paint together and providing mechanical strength.[17,18] A kinetic model facilitates the investigation of the mechanisms and driving factors that govern network formation and degradation within the medium. More

specifically, a microkinetic, or mechanistic, model constructed from elementary steps can connect key insights at the molecular level to macroscale properties of interest.[19] Assembling a complete reaction mechanism at this level of detail from experiments alone would be difficult since many reactive intermediates are not easily isolated and quantified. A microkinetic model is also inherently flexible enough to be continuously improved and expanded as new information becomes available.

This chapter describes the construction of such a detailed microkinetic model within a kinetic Monte Carlo (KMC) framework and its validation against experiment.[20] Kinetic Monte Carlo simulations allow an even more precise statistical description of an aging paint to be developed because species are tracked explicitly, including sequence data for the larger cross-linked oligomers.[21–23] This stochastic formulation for dynamic systems is attractive since it naturally handles the large numbers of species that are required to model hydrocarbon autoxidation and track sequence data for this system. Additionally, KMC uses simple algebraic expressions for each reaction event to adjust the system composition, mitigating potential issues of system stiffness.[24]

Since paints are complex mixtures, previous experimental work has employed single-component analogs such as linseed oil for oil paint and ethyl linoleate for more modern alkyds. On the timescales associated with curing, numerous analytical tools including FTIR spectroscopy,[6,25–29] Raman spectroscopy,[29–31] NMR,[29,32–34] mass spectrometry[32,35] and size exclusion chromatography (SEC)[6,30,36] were applied to determine the progression of network formation. Other data such as peroxide content[27,29,30,36,37] and oxygen uptake[29,30] have also been reported for these model systems. This work focuses on an ethyl linoleate (EL) model

system in order to leverage this information to validate the kinetic model. Utilizing this model system presumes that all of the critical curing chemistry is taking place in the unsaturated fatty acid tail and that hydrolysis mechanisms that are known to degrade oil paint networks by breaking ester bonds and releasing free acid groups over much longer timescales[38] can be neglected in the early stages of matrix formation.

Recent work by Iedema and coworkers employed a similar strategy to develop a mathematical description of a maturing oil paint.[39] They modeled triacylglycerides (TAGs) by assuming an average concentration of bi-allylic hydrogens in the fatty acid tails comparable to that of linseed oil. They obtained the evolution of lumped functional group concentrations using 70 equations and also determined a set of kinetic parameters characterizing the mechanism by optimization against experiment. Lumping kinetic model outputs by functional groups for hydrocarbon-based systems is often done to match available experimental data or to speed simulations depending on the desired application.[40] However, resolving species explicitly allows for rigorous interrogation of the proposed reaction network. Obtaining kinetic parameters strictly from optimization procedures may also obscure errors in the mechanism and makes the model less extensible to a variety of conditions, a major value proposition for the conservation community where each artwork encountered is unique. Building a model that contains the necessary detail requires employing methods developed to facilitate the modeling of large-scale and complex reaction networks for processes, such as catalytic cracking, pyrolysis and oxidation, and applying them for the first time to problems in conservation science. For instance, the model exploits advances in computational chemistry allowing kinetic parameters not easily resolved by

experiment to be calculated from first principles, providing an increased fundamental underpinning to mechanistic investigations.[41] Developing a reliable model of a well-cured oil-based paint network is a vital first step toward investigating the chemistry of long-term aging as well as to assess the impact of a variety of environmental factors. This knowledge will ultimately be translated into important decisions about treatment and control of the museum environment to optimize display and storage conditions for these works of art.

2.2 Mechanism Development

Construction of a microkinetic model requires detailed knowledge of the chemistry involved since the method requires elementary steps to be enumerated. Numerous reviews of condensed-phase, low-temperature hydrocarbon oxidation mechanisms have been produced,[42–44] and the mechanisms proposed by the conservation science community for oil-based paint curing overlap significantly.[45,46] Based on this literature, a mechanistic model for autoxidation must at a minimum include pathways for the initiation, propagation and termination of free radicals.

In this model, the included transition metal catalyst, cobalt ethyl-hexanoate, played an active role in initiating alkyl radical species.[36] These free radicals rapidly reacted with dissolved molecular oxygen to form peroxy radicals, which were subsequently converted into critical hydroperoxide intermediates. These intermediates can be detected and quantified, and their decomposition rates into peroxy and alkoxy radicals are accelerated by the transition metal catalyst. The work of Spier et al.[47,48] investigated the effects of different cobalt ligands on the decomposition of hydroperoxides both experimentally and computationally. Their data indicated the existence of parallel catalysis cycles which are

populated according to the ligand type. Both cycles are explicitly included in the microkinetic model. Termination reactions are radical recombinations to form peroxy, ether and alkyl cross-links as well as disproportionation reactions to form alcohols and ketones. Reactions competing with network formation such as alkoxy β-scission events were also included. The literature also suggests that these pathways lead to the evolution of small volatile molecules such as hexanal and pentanal.[30,49,50] Finally, reaction channels from the hydrocarbon oxidation literature leading to other secondary products, such as carboxylic acids, were incorporated.[51] If multiple mechanistic pathways were found in the literature for the formation of a certain species, they were included and their kinetic relevance assessed. A schematic representation of these chemical pathways is laid out in Figure 2.1. More specific information about each reaction type incorporated is presented below when the kinetic parameters are discussed.

Although the number of different types of reaction channels included in the schematic is relatively low, the number of possible elementary steps and chemically unique species is quite large, typically on the order of 10^4 for hydrocarbon oxidation systems because of the wide range of possible "R" groups. Consequently, a major challenge associated with microkinetic modeling is not only assembling the mechanism to be solved, but also obtaining kinetic parameters for each step. If available, rate constants or Arrhenius factors derived from experiment were used. If experimental data were not available for elementary steps, parameters were estimated using kinetic correlations.

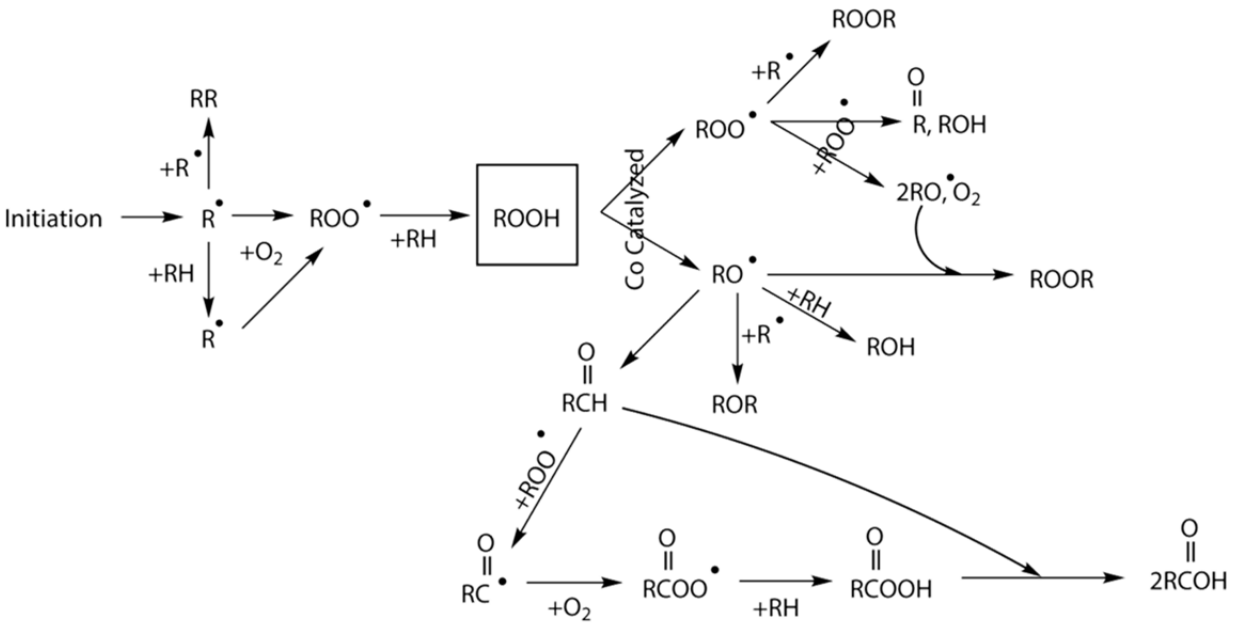

Figure 2.1. A schematic of the chemistry incorporated into the microkinetic model.

Kinetic correlations are useful for kinetic modeling because they relate the rate constant to a value that is more straightforward to determine, such as a thermodynamic quantity. A widely used kinetic correlation based on thermodynamic quantities is the Evans–Polanyi relationship, $E_A = E_0 + \alpha \Delta H_R$, where E_A is the activation energy, E_0 is the intrinsic reaction barrier, α is the transfer coefficient, and ΔH_R is the heat of reaction.[13] An Evans–Polanyi relationship can be constructed for reactions of similar chemistry possessing similar reaction coordinates grouped into reaction "families." Related forward and reverse reaction families have the same E_0 value, and the sum of their transfer coefficients is equal to one. The difference in the entropy of activation between reactions in a given family is assumed to be negligible so all reactions within a family have the same pre-exponential factor, and forward and reverse reaction family pairs will have pre-exponential factors that are thermodynamically consistent. This dramatically reduces the number of parameters

required to construct a kinetic model because rate constants for all elementary steps grouped in a family can be calculated based on only having to specify the heat of reaction for each specific step. Heats of reaction can be obtained from experiment, but another strategy used in the absence of experimental data is the group additivity method developed by Benson.[52] For this work, a library of kinetic correlation parameters[53] in conjunction with the *NIST Structure and Properties Database* was used to determine rate coefficients.[54] This information is summarized in Table 2.1.

The Evans–Polanyi parameters for each reaction family are specified based on regression against known experimental values or from quantum chemical calculations and transition state theory.[55] For the reaction families applied here, many of the Evans–Polanyi parameters were available from the previous literature. It should be noted that studies utilizing composite model chemistries such as Gx or CBS-x to derive these relationships can predict thermochemical data very accurately[56–59] and have also demonstrated some success calculating kinetic parameters for radical chemistry.[60,61] The uncertainty in these calculated parameters provides bounds for executing parameter optimization routines. The range utilized in this work to achieve the agreement shown in Section 2.4 was narrow and conservative (1–2 kcal/mol in barrier height which translates to a factor of approximately 5–10 in the rate constant at room temperature) when compared to the broader bounds of accuracy typical of quantum chemical calculations or kinetic correlations derived from them. Applying representative values for the frequency factors can also be interrogated as an assumption, as the frequency factors for members of a given reaction family are not precisely equal.

Although the techniques described above greatly reduce the number of parameters required to construct the model and provide an approach to automate their determination, it is still beneficial in the case of large oxidation mechanisms to limit the number of reaction channels and species based on eliminating pathways that are kinetically insignificant at all conditions of interest. For the KMC model created here, some chemically reasonable simplifications were made. First, the reactivity of different positions along the hydrocarbon chain were assessed using a group additivity scheme and the NIST *Structures and Properties Database*.[54] As anticipated, the most reactive hydrogens were the bi-allylic hydrogens located on carbon number 11 as shown in Figure 2.2. Hydrogen abstraction at positions 8 and 14 as well as from positions adjacent to conjugated double bonds (introduced after initiation) were also determined to have potential kinetic relevance. Alkyl hydrogens are on the order of 10^5 times less reactive than their bi-allylic counterparts and can be reasonably excluded from abstraction reactions on the timescales and temperatures associated with paint curing. Peroxide bond fission reactions were also excluded from the current model since the unimolecular decomposition barriers ranged from 40 to 45 kcal/mol,[53] making them kinetically irrelevant compared to the catalytic decomposition of those species under the mild reaction conditions.

Table 2.1. Kinetic parameters for the microkinetic model with units for k and A in L/mol•s (bimolecular) or s^{-1} (unimolecular) and E_0 in kcal/mol.

Reaction Family	Representative Reactions	Reported *k*	Parameters A	E_0	α_{fwd}[a]	References
Initiation	$Co^{II} + O_2 \leftrightarrow Co^{III}OO\bullet + RH \rightarrow Co^{III}OOH + R\bullet$	0.666, 5×10^{-5}				36
	$Co^{III}OOH \rightarrow Co^{II} + HO_2\bullet$	0.5				
O_2 Addition	$R\bullet + O_2 \rightarrow ROO\bullet$		10^8	0	0	53
Hydroperoxide formation	$ROO\bullet + RH \rightarrow ROOH + R\bullet$	6.6 (for bi-allylic)				62,63
Hydroperoxide decomposition	$ROOH + Co^{II} \rightarrow RO\bullet + [Co^{III}OH^-]$	0.5				47,64,65
	$ROOH + [Co^{III}OH^-] \rightarrow [Co^{III}OOR] + H_2O$	2				
	$[Co^{III}OOR] \rightarrow Co^{II} + ROO\bullet$	.0095				
	$[Co^{III}OOR] + R'OOH \rightarrow [Co^{III}OOR,HOOR']$	900(×2)				
	$[Co^{III}OOR,HOOR'] \rightarrow R'O\bullet + [Co^{III}OOR,OH]$	.0095				
	$[Co^{III}OOR,OH] \rightarrow ROO\bullet + [Co^{III}OH^-]$					
β-Scission	$RO\bullet \rightarrow R'C(O)H + R''\bullet$		10^{14}	9.5	0.85	53
Hydrogen Transfer	$R\bullet + R'H \rightarrow RH + R'\bullet$		10^7	9.1	0.7	53
	$RO\bullet + R'H \rightarrow ROH + R'\bullet$			11.9	0.91	
	$ROO\bullet + R'C(O)H \rightarrow ROOH + R'C(O)\bullet$			6.2	1	
	$RC(O)OO\bullet + R'H \rightarrow RC(O)OOH + R'\bullet$			3.05	1.1	
Disporportionation	$2ROO\bullet \rightarrow R(O) + ROH + O_2$		10^6	0	0	53,66
	$2ROO\bullet \rightarrow 2RO\bullet + O_2$					
Recombination	$2R\bullet \rightarrow RR$		10^8	RT	0	53
	$ROO\bullet + R\bullet \rightarrow ROOR$	5×10^7				62,63
	$RO\bullet + R\bullet \rightarrow ROR$	1×10^8				
	$RO\bullet + RO\bullet \rightarrow ROOR$	2×10^7				
Baeyer-Villiger	$RCOOOH + RC(O)H \rightarrow 2RCOOH$		1.2×10^4	8.5	0	53

[a]See Pfaendenter and Broadbelt [53] for definitions of $\alpha_{fwd.}$

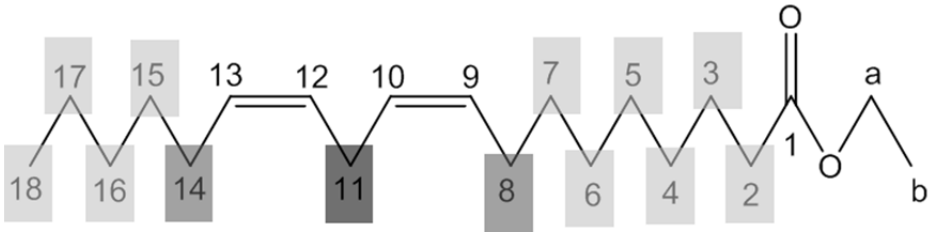

Figure 2.2. Ethyl linoleate molecule. The most reactive hydrogens located at position 11 are *shaded darkly*, with positions of decreasing reactivity corresponding to progressively *lighter shading.*

Research has also investigated the importance of singlet oxygen in hydrocarbon oxidation. Singlet oxygen can add directly to the unsaturated carbons in the alkyl chain via an "ene" reaction.[67] Reactions with singlet oxygen are usually detected by examining the isomeric forms of the hydroperoxide intermediates. Non-conjugated hydroperoxides with functional groups located on carbons 10 or 12 in the alkyl chain are an indicator of singlet oxygen "ene" reactions.[68] Frankel examined the hydroperoxides formed from the oxidation of methyl linoleate, and non-conjugated hydroperoxides were not detected until a photosensitizer was added to the reaction mixture.[69] This suggests that with sufficient photosensitizers, such as pigments or dyes, these reactions may become important but can be excluded for the reaction conditions examined here. In the first-generation model presented in this chapter, reactions were coded up to the formation of dimers, or single cross-links. Emphasis was also placed on including pathways responsible for secondary products that could be compared to experimental data such as the volatile aldehydes hexanal and pentanal. The final model included 160 species and approximately 400 reaction channels.

2.3 Computational Methods

Using the classic stochastic simulation algorithm (SSA) developed by Gillespie, a kinetic Monte Carlo (KMC) framework was constructed to evaluate the mechanism outlined in Section 2.2.[20,70,71] This algorithm calculates the probability that a given reaction, R_μ, will occur inside a well-stirred, scaled reaction volume during the time interval, δt, for given sets of species, $\{S_1, S_2,\ldots,S_N\}$, and available reaction channels, $\{R_1, R_2,\ldots,R_M\}$. This calculation requires the reaction parameter, c_μ, which can be mathematically related to the more familiar deterministic reaction rate constant, k, through the following equations, where k_i is the rate constant for a unimolecular reaction, k_{ii} is the rate constant for a bimolecular reaction between two molecules of the same species, and k_{ij} is the rate constant for a reaction between two different species. The factors of volume and Avogadro's number appear because rate constants in the stochastic formulation are based on the explicit number of species in the reaction volume as opposed to concentrations.

$$c_i = k_i \tag{2.1}$$

$$c_{ii} = \frac{2k_{ii}}{VN_A} \tag{2.2}$$

$$c_{ij} = \frac{k_{ij}}{VN_A} \tag{2.3}$$

Using these inputs, the probability, p_r, for each reaction, r, is determined based on its current reaction rate, R_r, and the sum of all possible reaction rates as shown in Equation 2.4. The quantity R_r is calculated as the product of c_r and the current number of available species that are defined as the reactants for case r.

$$p_r = \frac{R_r}{\sum_{i=1}^{N} R_i} \tag{2.4}$$

After calculating the probabilities, the reaction to be executed is selected based on Equation 2.5, where x_1 is a random number from a uniform distribution between zero and one.

$$\sum_{i=1}^{\mu-1} p_i < x_1 < \sum_{i=1}^{\mu} p_i \tag{2.5}$$

The time step to advance is also determined based on a uniformly distributed random number, x_2, as demonstrated in Equation 2.6.

$$\tau = \frac{1}{\sum_{i=1}^{N} R_i} \ln\left(\frac{1}{x_2}\right) \tag{2.6}$$

The system is then updated to reflect the reaction and time step selected. Time is set to $t = t + \tau$, and the species' populations are adjusted to reflect the occurrence of reaction i. If the total desired reaction time has not been reached, then the algorithm recalculates the reaction probabilities to reflect the changes that occurred before a new reaction and time step are selected. This cycle continues until the desired reaction time has been reached.

This model was initialized with system conditions matching those described in Oyman et al.[30] (e.g., 40 g of technical grade EL, 0.07 wt% Co-EH catalyst). Impurities in the ethyl linoleate, mostly ethyl oleate and other saturated esters, were treated as inactive solvent due to their low reactivity in comparison with the bi-allylic hydrogens of ethyl linoleate. The dissolved oxygen content of the system was held constant at the saturation limit at 25 °C, 0.00218 mol/L, approximated from dissolved oxygen concentration values

for soybean oil which has a high linoleic acid content[72,73] and the system was treated as a well-stirred, homogenous batch reaction.

The KMC framework was constructed in *C*++, and simulations of up to 100 h were performed. Data were captured at 100-s intervals. The number of initial molecules in the system, which is a required input parameter for a KMC model, was set at 10^8, and the system was determined to be fully converged.[74]

2.4 Results and Discussion

The model output provides the temporal evolution of all radical and molecular species. From the generated concentration profiles, key quantities were selected for comparison with experimental data. The evolution of peroxides, a primary product of autoxidation, and the absorption of oxygen by the system are measurable quantities often used to gauge the progression of curing. Although the model allows the resolution of the precise values of structural isomers, the peroxide content of the system is presented as a lumped quantity of all peroxide-containing species. Oxygen absorption by the model paint was determined by tallying the number of times a reaction channel was selected that required O_2 as a reactant.

Examination of these values as a function of time revealed that the simulations qualitatively matched experimental trends over 100 h of curing time, but were not in good agreement with quantitative benchmarks at longer timescales. Scrutiny of experimental SEC data offers some insight into this observation.[30] At the time of reaction initiation, a single peak is resolved for ethyl linoleate and its other fatty acid ester impurities. After 8 h of reaction time, the chromatogram is still dominated by the ethyl linoleate peak, but has also

developed a significant adjacent shoulder for EL hydroperoxides as well as a distinct peak for cross-linked dimers and what is best described as an elevated baseline indicating the presence of higher oligomers, representing less than 10 % of the system content. At times beyond 24 h, peaks associated with higher oligomers increase as the other peaks decline. Since the model focuses on chemistry leading to the formation of hydroperoxides and single cross-links, the model should achieve good qualitative and quantitative agreement with experiment for the first 8–10 h of curing time and will be evaluated within this time window.

The peroxide content of the system during the curing stage is shown in Figure 2.3. This result is sensitive to two major kinetic parameters, the rate of hydroperoxide formation where a peroxy radical abstracts a bi-allylic hydrogen and the rate-limiting step of the cobalt-catalyzed decomposition cycle which releases a peroxy radical. An experimental value was available for the first parameter which was not adjusted. The Arrhenius equation parameters for the dissociation of an ROO• species from the cobalt complex was assumed to be representative for the hydroperoxide isomers tracked uniquely in the system. This rate constant was adjusted within the previously mentioned range for values obtained from quantum chemical calculations, and the good agreement shown in Figure 2.3 was obtained. At longer timescales, the predicted hydroperoxide content does indeed peak and decline to a baseline value as demonstrated experimentally, but the model under represents this value due to the lack of higher oligomers in the system which could contain peroxy functional groups.

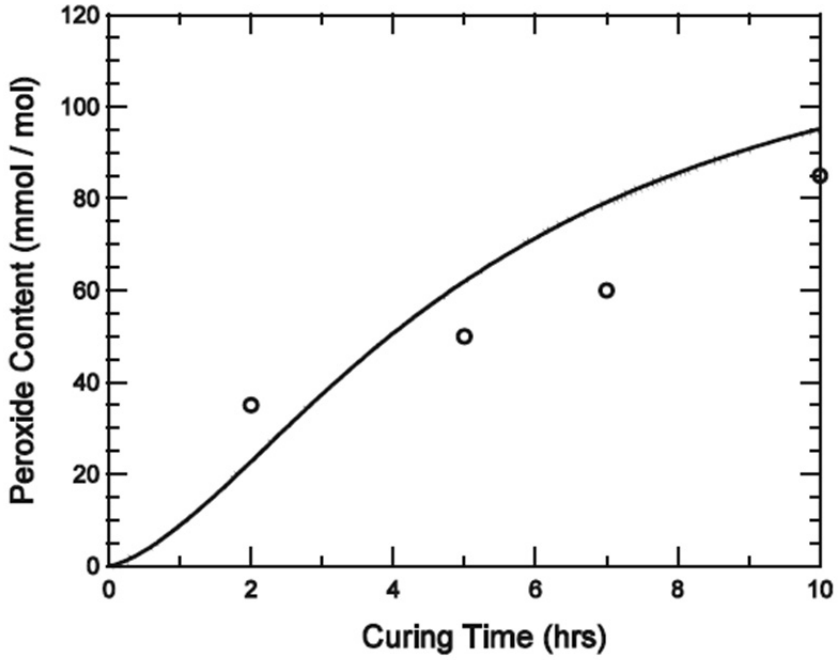

Figure 2.3. Comparison of total peroxide content of the system output by the KMC dimer model (line) to experiment (points)[30]

The results for the oxygen uptake of the system are presented in Figure 2.4 which indicates that the model is again under-predicting the amount of mass that the model paint absorbs by a factor of three. It is proposed that this disagreement stems from the fact that not all major reaction channels involving the absorption of oxygen have been accounted for in this model. In particular, dimers are treated as dead chains in the system despite the fact that they have remaining functionalities that could continue to react with oxygen and other radical species, placing a stoichiometric limit on the amount of O_2 the system can absorb. It is anticipated that oxygen incorporation would increase with a higher-order model. However, including these pathways would dramatically increase the size of the reaction network and would become an impractical undertaking without the assistance of computational automation to ensure the model is as comprehensive as possible.

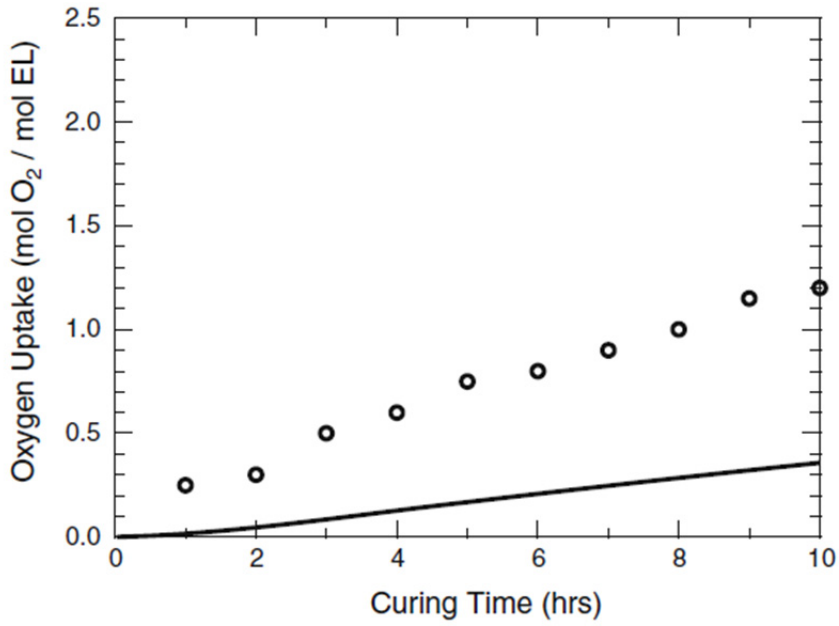

Figure 2.4. Oxygen uptake, or mass gain, of the system from the KMC dimer model (line) compared to experiment (points)[30]

The production of small volatile aldehydes by the model was also quantified and compared to experimental results from the analysis of the headspace of a third experimental setup with GC/MS.[30] Although few experimental data points are available for this range, extrapolation between data collected at 2 and 24 h of curing time can allow some conclusions to be drawn about the model performance, which is shown in Figure 2.5. At 10 h of curing time, expected values from experiment are approximately 1.0 mmol hexanal per mol EL and 0.05 mmol pentanal per mol EL. The first important point of note is that the model appears to over-predict the production of pentanal in comparison with experiment. This may be due to thermodynamic effects; the model currently assumes that all small aldehyde molecules that have not been further oxidized to carboxylic acids, a small effect at these timescales, have effectively volatilized from liquid phase. The second important point,

however, is that the model does not predict the appropriate levels of hexanal, which is predicted to be present in trace quantities. The ratio of pentanal to hexanal observed experimentally is clearly not recapitulated by the model.

The model assumes that the production of these two key volatile aldehydes is closely associated with β-scission reactions in direct competition with network formation. The conjugated alkoxy radical shown in Figure 2.6 can undergo two different scission reactions leading to an aldehyde and a carbon-centered radical. From scission reaction one, a pentyl radical and a dienal are produced. Pentanal can be formed from the further oxidation of the radical species. Additional confirmation for the veracity of this mechanism can be obtained by certifying that the model successfully accounts for and reasonably quantifies other downstream products such as the saturated hydrocarbon pentane. Pentane has been detected by other research groups in substantial quantities.[49,75,76] The mechanistic model similarly produces this product in substantive amounts from the facile abstraction of a hydrogen atom by the alkyl radical.

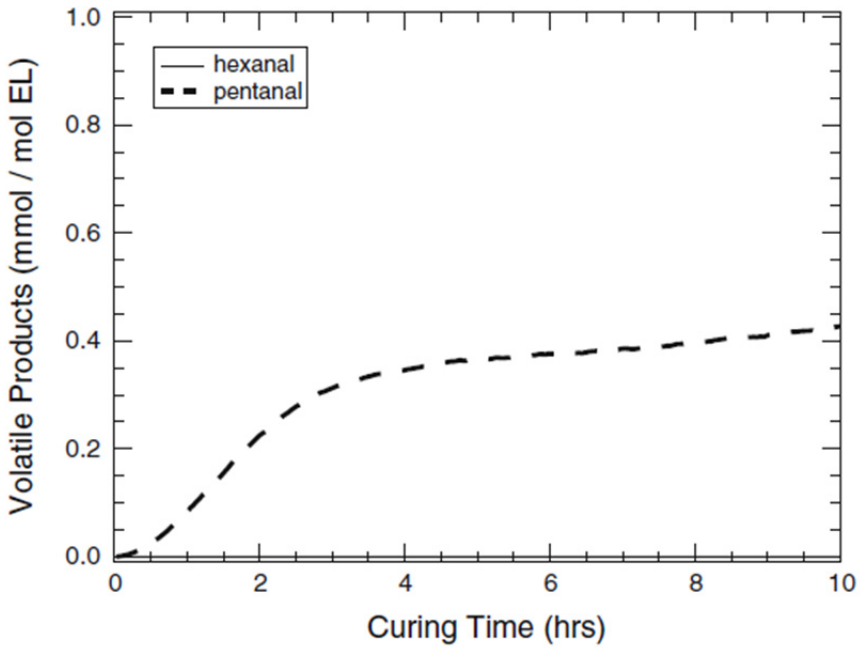

Figure 2.5. Hexanal (*solid line*) and pentanal (*dashed line*) yields predicted by the KMC dimer model. At 10 h of curing time, expected values from experiment are approximately 1.0 mmol/mol EL and 0.05 mmol/mol EL, respectively[30]

Scission reaction two is a plausible mechanism for hexanal production since it is formed directly. However, the simultaneous production of an unstable vinyl radical makes this reaction very endothermic, and consequently, it has a high activation energy barrier based on the Evans–Polanyi kinetic correlation. The difference in calculated barrier height between the two scission reactions is ~13 kcal/mol, making the formation of pentane and pentanal highly favored at these low temperatures. Frankel acknowledged this phenomenon in his work on the production of volatiles from food oils, suggesting that the relative stability of the resulting aldehydes might balance the effect of the instability of the vinyl radical, but that the question remained open.[49] These factors suggest that alternative mechanisms for the production of hexanal should also be investigated.

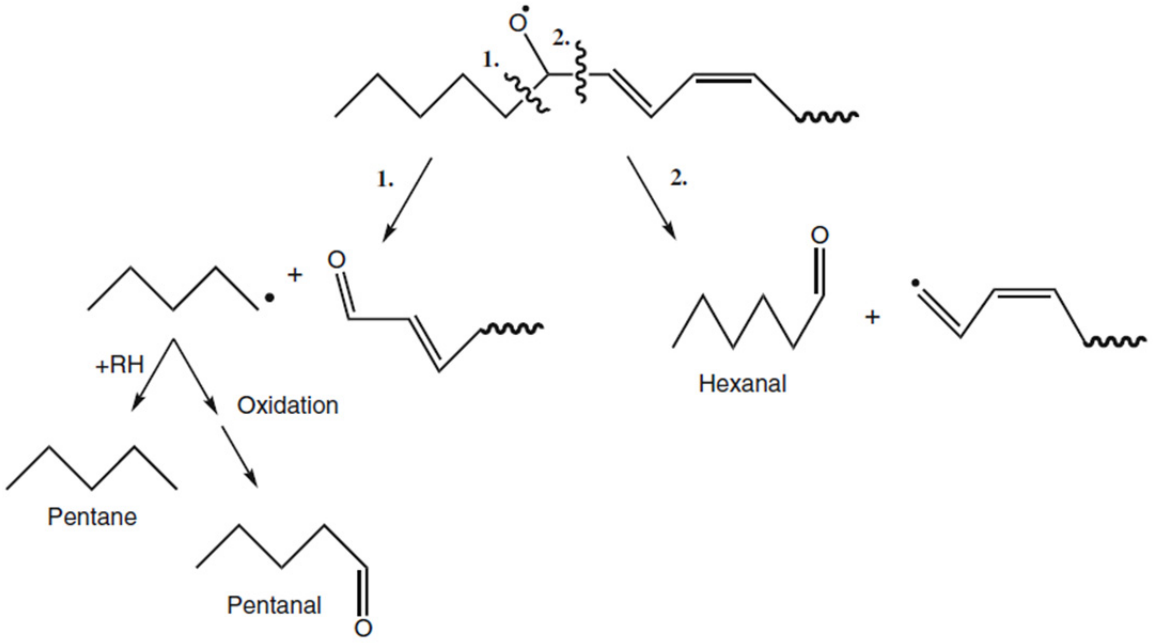

Figure 2.6. Schematic of the β-scission mechanism for the formation of pentanal and hexanal. Qualitative experimental trends for the production of pentane and pentanal are matched by the model using scission reaction 1 and subsequent pathways, but scission reaction 2 yields extremely low levels of hexanal.

Candidate mechanisms should have target energies of activation in the range of approximately ~11–17 kcal/mol. Korcek-like reactions examined by Jalan et al.[77] in a recent publication show promise for producing volatiles of interest at higher temperatures, but activation barriers of about 30 kcal/mol and low levels of the necessary keto-peroxide reactant made these reactions insufficient to produce the expected level of hexanal at room temperature. Preliminary candidates that will be evaluated further in Chapter 3 include Hock cleavage of an allylic hydroperoxide,[78] endoperoxide cleavage into two carbonyl species[79] and decomposition of a peroxide linked oligomer containing additional hydroperoxide moieties.[80] Although Hock cleavage is usually described as an acid-catalyzed mechanism,[81] it can occur without any added acid.[82,83] Evaluating this pathway in the context of a

microkinetic model would allow for the assessment of its contributions to the production of volatile molecules which has yet to be determined quantitatively in the literature. Often it is considered as one of many possible pathways that cannot be excluded from consideration due to difficulties isolating critical intermediates.[83,84]

Additional pathways to hexanal are suggested by Juita et al.[79] They propose a mechanism derived from quantum chemical calculations where allylic peroxy radicals cyclize into four- or five-membered ring endoperoxide species that can decompose into aldehyde species. They describe a possible concerted splitting of the C–C and O–O bonds in the case of the four-membered ring and the production of a biradical intermediate in the case of the five-membered ring. It is possible that after the same initial cyclization steps, stepwise scission reactions of the C–C and O–O bonds would lead to the facile creation of these products of interest with a reasonable overall barrier to the reaction.

The final option is a mechanism suggested by Morita and Tokita[80,85] involving the homolytic decomposition of peroxide linked polymers with hydroperoxide functionalization into hydroxy radicals and aldehydes. They confirmed the formation of hydroxy radicals by adding methyl benzoate which reacts with the radicals to form methyl salicylate which was tracked over time. Testing this mechanism in future iterations of the model similarly requires determining kinetic parameters from quantum chemistry. With parameters for these potential pathways, microkinetic modeling can aid in resolving the mechanisms that contribute to the formation of undesirable volatile products and determine the extent to which they compete with network formation.

2.5 Conclusions

In summary, a microkinetic model has been constructed for the autoxidative curing of an oil-based paint model system. The model can be expanded, currently using ethyl linoleate and single cross-links to remain manageable without the assistance of computational automation. Nevertheless, the model shows promise, with good agreement on short timescales for common curing metrics such as peroxide content and oxygen uptake. Significant disagreement was discovered when evaluating the formation of secondary products, specifically the volatile species hexanal. A reasonable range for activation energies was established to screen candidate alternative mechanisms, and several have been selected for further evaluation within future iterations of the model which will be discussed in detail in the following chapter. It should be noted that this work has highlighted the benefits of resolving individual species within the microkinetic model. If the model were not fully specified, lumped data for the concentration of aldehydes in the system might have led to erroneous conclusions about the accuracy of the mechanism. It is suggested that efforts to understand the chemical changes in curing and aging oil-based paints should be tested at this level of specific detail before they can be generalized and applied broadly for use in the conservation science field.

Additional opportunities to improve model agreement and extend to longer timescales of interest to the conservation science community include increasing mechanism coverage by automating the generation of a reaction network and the necessary kinetic parameters. Subsequent chapters will discuss the adaptation existing automation tools such as NetGen[14,86] to handle the critical chemistry of oil paint maturing and aging.

Once these approaches are optimized, microkinetic modeling offers the promise of an accurate and flexible tool to develop a realistic and dynamic description of the composition of oil-based paint coatings. This in turn can facilitate the exploration of the effects of various environmental conditions on these paints' long-term chemical stability, effectively complementing and enhancing experimental testing on artificially aged mock-ups.

Chapter 3

An examination of the mechanisms for the formation of volatile aldehydes from the autoxidation of oil-based systems

The mechanisms responsible for the production of small volatile aldehydes during low temperature condensed phase oxidation have been the subject of extensive research, and many pathways have been proposed in the literature. However, many of these mechanisms have yet to be explored quantitatively in the context of a kinetic model. In this chapter, a variety of mechanistic postulates for the formation of the volatile species hexanal, were assembled, and quantum chemical calculations were performed where necessary to obtain estimates of kinetic parameters in order to test each reaction's kinetic relevance in the microkinetic model described in Chapter 2. A more detailed experimental data set than previously available in the literature with information in the early (< 24 hr) time window was obtained by GC/MS headspace analysis in order to more effectively asses the model efficacy and performance with new mechanistic postulates.

3.1 Introduction

The molecules responsible for the characteristic odor of drying oil-based paints or other bio-based coatings and products have been captured and identified in several studies, particularly pinpointing the role of small volatile aldehydes.[87–89] While the composition of these volatiles has been established, the mechanisms by which they are produced remain obscured. Understanding these mechanisms is important in multiple contexts. In modern industrial settings, minimizing the production of these volatiles from coated surfaces is desirable to reduce their environmental impact and improve safety.[89–91] In foods containing natural oils, volatile aldehydes sour the taste,

and packaging and cooking conditions may need to be optimized to prevent waste.[92–95] Finally, in the context of cultural heritage science for oil paintings and other cultural heritage objects containing oil-based polymers, understanding these mechanisms may lead to crucial insights for preserving and maintaining priceless artworks.[96,97]

Often, volatile aldehydes are used as a metric to monitor surfaces for aging, and an increase in the concentration of these molecules is associated with increased degradation.[98] However, this information is chiefly obtained from artificially aged samples where elevated temperatures or UV radiation is used to affect observable changes in reasonable time periods in the laboratory. Experimental work has indicated that artificial aging may create samples similar to naturally aged samples in terms of physical properties like brittleness, but may lack the chemical similarity desired for testing cleaning techniques or idealizing environmental conditions using mock-ups.[3,4]

Microkinetic modeling is a powerful tool that can facilitate the exploration of the mechanisms governing the production of these molecules and lead to new mechanistic understanding.[24] This technique is based on elementary steps providing the level of detail required to resolve the mechanistic questions of interest on the molecular level.[99] In the previous chapter, a microkinetic model was utilized to explore the autoxidation of an oil paint model system comprised of ethyl linoleate and a cobalt catalyst.[15] Available experimental data on the production of volatile molecules from the system included headspace analysis for the period of 100 hours, specifically tracking the evolution of hexanal and pentanal with data taken approximately every 24 hours.[30] Most of the literature sources explored suggested that the β-scission of a single conjugated alkoxy radical was responsible for the formation of both products, and these routes were included into the microkinetic model for testing. [6,33,44,46,49,100] However,

quantitative comparison of the model results with experimental data confirmed that these routes were kinetically insignificant. The model predicted that almost no hexanal was formed despite the fact that it is considered a major volatile product, produced in much higher concentrations than pentanal. This is largely due to the fact that a highly unstable vinyl radical is simultaneously created when forming hexanal via β-scission, making the reaction barrier for this elementary step too high to be kinetically relevant at room temperature. This discovery motivated an in depth exploration of alternative mechanisms for the production of hexanal. It should be noted that while this β-scission mechanism may not be the primary pathway for hexanal production at room temperature, it may become important at elevated temperatures used to simulate conditions for artificial aging or other condensed phase, low temperature oxidation scenarios of interest. Thus, additional reaction mechanisms for hexanal formation were sought to add to the model to account for the formation of hexanal at low temperature as well as preserve its ability to account for alternative routes at higher temperatures.

This work examined in detail and tested a number of alternative mechanistic postulates in the context of the previously constructed microkinetic model. Specifically, Korcek and Korcek-like reactions, intramolecular hydrogen shifts followed by subsequent β-scission events, and the cyclization and decomposition of allylic peroxy radicals through a dioxetane intermediate were probed. While these mechanisms have been gleaned from or inspired by chemical mechanisms in the literature, supporting kinetic information was provided in only a few instances. Consequently, missing kinetic information was filled in using quantum chemical calculations. Since many of the intermediate species proposed in these pathways would be extremely difficult to isolate and track with analytical techniques due to their short-lived nature or low

concentrations, quantum chemical calculations provide quantitative information about free energy barriers that can be used to compare and assess the kinetic relevance of these alternative mechanisms. Finally, an alternative mechanism not previously proposed in the literature was examined, namely the concerted decomposition of a hydroperoxide and the cobalt-catalyzed decomposition of a dimer formed from the primary products of a conjugated hydroperoxide and a peroxy radical into an alkoxy radical that undergoes a facile β-scission reaction. Each of these mechanisms, their kinetic parameters, and their ability to capture the experimental data are presented below.

The experimental data used to evaluate the model results was derived from two main sources. As previously mentioned, literature data for the reaction conditions of interest exists, but the lack of data in the early curing regime (< 24 hr) which the model was designed to capture was problematic. Rather than interpolating the data between 0 and 24 hours, it was decided to replicate the experiment, with a focus on obtaining data points previously unavailable for these conditions in the early cure regime.

3.2 Computational Techniques

3.2.1 Quantum Chemical Calculations

To effectively reduce the time and computational resources required for the calculations, a simplified molecule was utilized for computational study. It was ensured that the reacting atoms and any surrounding moieties that could influence the chemical reaction were captured. Quantum chemical calculations were performed in Gaussian09[101] using the composite method G4.[102] Transition states were identified as first order saddle points with a single imaginary, high amplitude mode. Intrinsic reaction coordinate (IRC) scans were used to confirm that the

transition state was connected to the reactants and products of interest. To extract the kinetic quantities of interest, the frequencies for each stationary point were used to determine the temperature-dependent total partition function in the program Calctherm[103] which could in turn be used to determine the rate constant as a function of temperature via transition state theory.[104] A Wigner tunneling correction was also applied.[105] This allowed the familiar frequency factor, A, and activation energy, E_A, to be extracted from a linear fit of an Arrhenius plot of ln(k) versus 1/T. Temperatures ranged from 300-1500 K in 100 K increments.

3.2.2 Microkinetic Modeling

Microkinetic modeling is a powerful method of exploring key factors that influence the kinetics of reactions on the molecular level, and can provide insight into competing mechanisms and potential ways to optimize desired processes. The model was built from elementary reaction steps and requires a detailed knowledge of the chemistry. A list of reaction steps for autoxidation including reactions for initiating, propagating and terminating radicals, and associated kinetic parameters and reaction conditions are listed in the previous chapter.[15] Because a microkinetic model from elementary steps feasible for hydrocarbon autoxidation can have on the order of 10^4 unique species, kinetic correlations quantifying the kinetic parameters of reactions of similar chemistry were employed to reduce the number of parameters. In instances where experimental values could not be determined, an Evans-Polanyi correlation was used which linearly correlates the heat of reaction with the energy of activation: $E_a = E_0 + \alpha\Delta H_R$, where E_0 is the intrinsic activation barrier and α is the transfer coefficient.[13] Values for ΔH_R for a specific reaction can be extracted from experimental literature or calculated using a Benson group additivity method and software available from the *NIST Chemistry WebBook*.[54] Concentration profiles for each species were generated using a kinetic Monte Carlo (KMC) framework based on the classic stochastic

simulation algorithm developed by Gillespie.[70,71,106] Additional mechanistic steps and parameters enumerated in the following sections were added to this foundational KMC model to test for their kinetic relevance for the production of volatile species at room temperature.

3.3 Experimental Details

3.3.1 Materials

The reactants, technical grade ethyl linoleate (EL) and Co(II) 2-ethylhexanoate (Co-EH, 65% w/w in mineral spirits), and analytical standards (cyclohexane, hexanal and pentanal) were purchased from Sigma Aldrich and used as received.

3.3.2 GC/MS Headspace Instrumentation and Procedures

The reaction mixture was created by combining 1.014 mL EL with 0.7 μL Co-EH catalyst. The time was noted immediately as the initiation of the autoxidation reaction. The reaction mixture was then spiked with 92 μL of 0.342 M cyclohexane in xylenes solution as an internal standard. A series of vials, one for each desired time point, was created by placing a 12 μL aliquot of the spiked reaction mixture into each 20 mL vial which was subsequently closed with an aluminum and Teflon® cap and sealed with a crimper. The time between the initiation of the reaction and the analysis of the first time point was approximately 30 minutes.

Experiments were conducted using an Agilent 7697A Headspace Sampler connected to a 6890 GC system. Vials were allowed to cure in lab atmospheric conditions in a sample tray and at 1 hr intervals for the first 20 hrs; samples were automatically agitated and loaded into a temperature controlled oven at 70°C. Additional time points were taken at approximately 30, 50, 70 and 95 hr. In the oven, a 100 μL headspace sample was immediately removed by syringe to prevent further sample oxidation and transferred to the GC via a fused silica transfer line held at

115 °C. The syringe was automatically purged for 1 min with helium after the injection was made. Helium was also used as a carrier gas.

The GC system was equipped with a FFAP capillary column (30.0 m long × 250 μm diameter × 0.25 μm film thickness). The GC oven was held initially at 50 °C for 2 min and then ramped up to a maximum temperature of 245 °C at a rate of 20.5 °C/min and held for 8 min. The Quadrapole MS analyzer was operated in electron impact (EI+) ionization mode. Retention times and relative response factors for the compounds of interest were determined from analytical standard references of hexanal, pentanal and cyclohexane. Integrated peaks from the extracted ion chromatograms for characteristic masses for each compound were used to determine the amounts of volatile compounds produced during the course of the reaction.

3.4 Reactions Studied

3.4.1 Korcek and Korcek-like Reactions

Korcek reactions were originally proposed by Korcek and coworkers in the context of the oxidation of lubricant oils.[107–110] A recent computational study performed by Jalan et al. confirmed some of the main ideas behind the mechanistic propositions of Korcek and coworkers, but with some differences.[77] Using high levels of theory, Jalan and coworkers laid out two separate fragmentation pathways for the formation of aldehydes or ketones and carboxylic acids from keto-hydroperoxides via a cyclic peroxide intermediate. The formation of this cyclic peroxide intermediate could also be strongly catalyzed by the presence of organic acids in the system and can shift the rate-limiting step when a critical concentration threshold is exceeded. Their conclusions highlighted the potential applications for these reactions in many low temperature hydrocarbon oxidation scenarios. The microkinetic model contained mechanisms to

produce the desired reactant, the ketohydroperoxide, and thus the Korcek reaction family was a natural extension of the mechanism underlying the microkinetic model.

Specifically, elementary steps analogous to path A described in their work would produce hexanal if one can imagine extending the C3 keto-peroxide system probed by Jalan et al. to the C20 ethyl linoleate model system. The highest barrier reported for this reaction pathway was 34.7 kcal/mol for the formation of the cyclic peroxide intermediate composed of a 5-membered ring. This translates to Arrhenius parameters of $A = 2.1\times10^{8}\ s^{-1}$ and E_A= 28.0 kcal/mol. Since this barrier was too high to be kinetically relevant at the room temperature conditions of interest, either the reaction mixture needed to contain the critical concentration of acid to catalyze the ring formation reaction, or it was hypothesized that a less strained, 6-membered ring as seen in the mechanism shown in Figure 3.1 could lower this barrier. Since peroxide functional groups are likely to form at the carbon γ to the carbonyl moiety, tracing out this pathway is also highly relevant to the system of interest because it contains a high degree of unsaturation. The effect of unsaturation on the cyclization of the keto-hydroperoxide was also explored for new insights into how this chemistry would be applied in the context of lipid peroxidation.

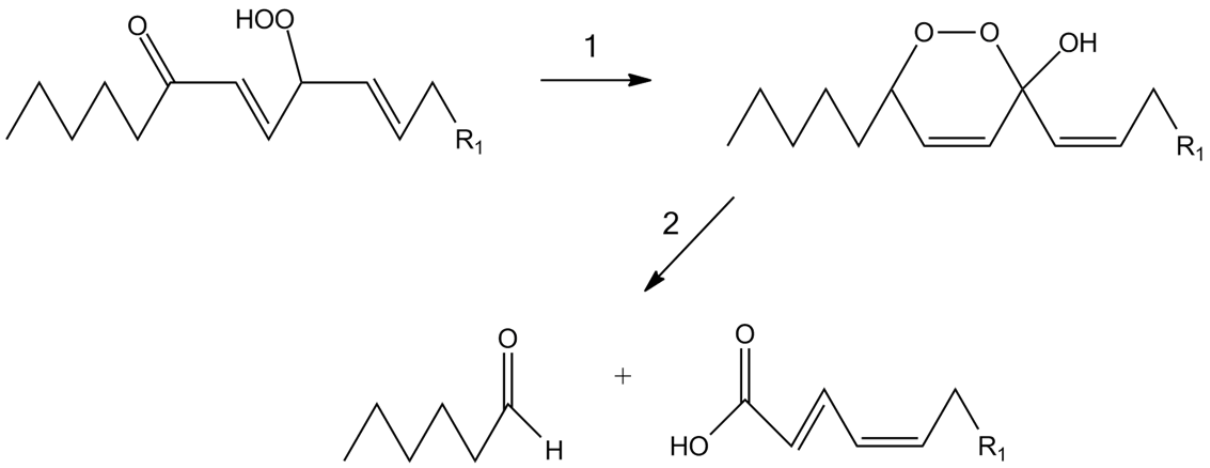

Figure 3.1. Proposed mechanism for a Korcek-like reaction in ethyl linoleate containing residual unsaturation in the carbon chain. The first step (1) is the formation of a cyclic peroxide from a keto-hydroperoxide which can be acid catalyzed followed by the (2) fragmentation of the keto peroxide into hexanal and a carboxylic acid.

3.4.2 Intramolecular Hydrogen Shifts

Intramolecular reactions are another method proposed in the literature related to oxidation of oils and paints for creating hexanal.[111] In the postulated mechanism, a hydrogen is abstracted from an alcohol that is a secondary product. The resulting conjugated radical can then rapidly isomerize to move the double bond in proximity to the alcohol functionality. An intramolecular hydrogen abstraction reaction was then invoked to create an alkoxy radical capable of undergoing β-scission to form hexanal and a terminal allylic radical that is more stable than the vinylic radical produced from the direct β-scission of an alkoxy radical. A schematic of this series of reactions is shown in Figure 3.2.

To determine the kinetic parameters for this reaction, a combination of existing information in the literature and data from new quantum chemical calculations was applied. Calculated parameters for the hydrogen abstraction reaction creating the conjugated radical of interest were compared to those derived from existing data in the literature.[112,113]

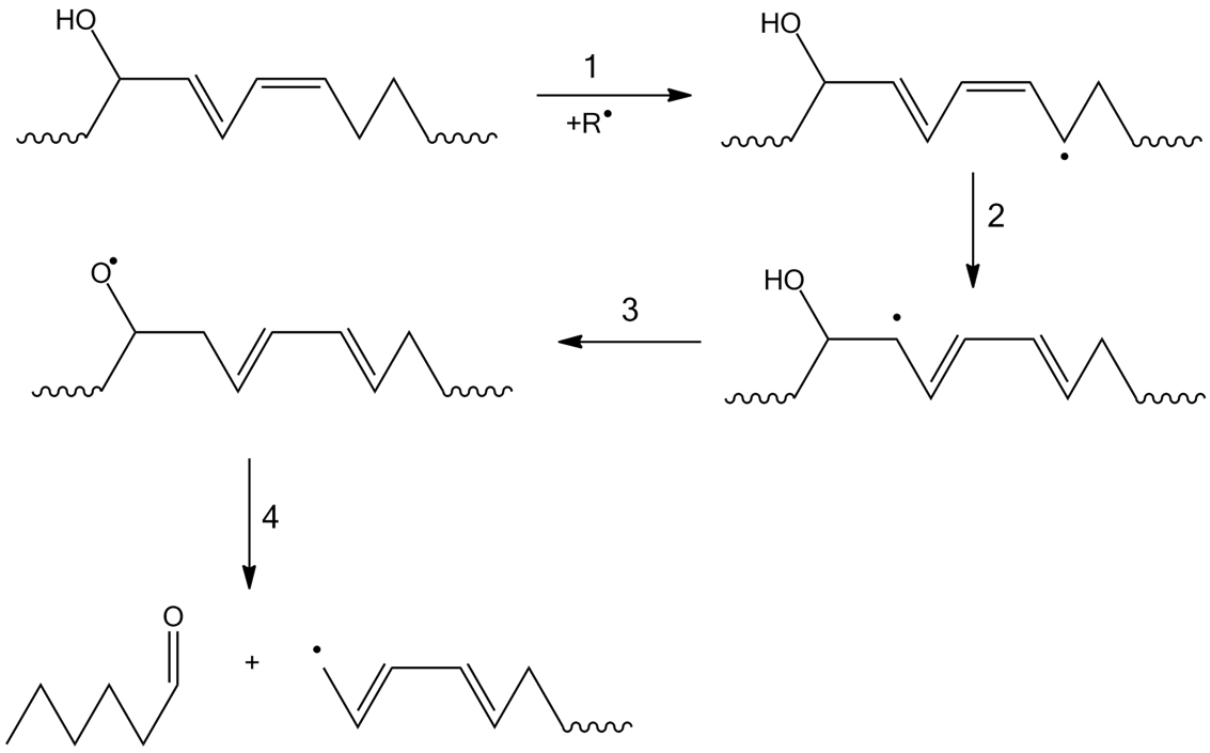

Figure 3.2. Proposed mechanism for the formation of hexanal and an allylic radical from a series of elementary steps involving (1) hydrogen abstraction from a conjugated alcohol, (2) fast isomerization, (3) an internal hydrogen shift and (4) the subsequent β-scission of the resulting alkoxy radical**.**

Since these kinetic correlations from the literature were originally developed for short chain saturated hydrocarbons and other work discussed in Chapter 4 demonstrated the importance of thoroughly exploring a range of chemical space when constructing structure-reactivity relationships,[114] it was sought to confirm their application to systems with increased functionalization and polyunsaturation through a quantum chemical calculation using the hybrid model chemistry G4 described above on a representative allylic alcohol molecule to ensure accuracy.

3.4.3 Reactions Involving Allyl Peroxy Species

Many additional mechanisms for the formation of volatile products lay out pathways starting from an allyl peroxy species. These mechanisms all include cyclization steps before decomposition into small molecules. In work by Juita et al., an allyl peroxy radical species, an early species formed by oxygen addition to a conjugated radical, was examined as a major producer of volatiles.[79] Their computational study followed two pathways for the production of small volatile molecules via either a four-membered dioxetane intermediate or a five-membered ring that could decompose in two elementary steps. These pathways are relevant to systems that contain mixtures of fatty acids with multiple points of unsaturation. The desire to produce hexanal from a linoleic acid derivative guided focus to the formation of volatile products via a four-membered ring. This pathway is reproduced from the work of Juita et al. in Figure 3.3. Researchers were also unable to locate a transition state along the minimum energy path for the formation of these volatile products from the dioxetane intermediate, but estimated the energy barrier to be ~20.1 kcal/mol. This barrier is high to be relevant at room temperature, so additional high level quantum chemical calculations were performed here, using the same G4 method described above, to ensure that no transition states remained unexplored that lead to a lower energy pathway for the production of volatiles at low temperatures.

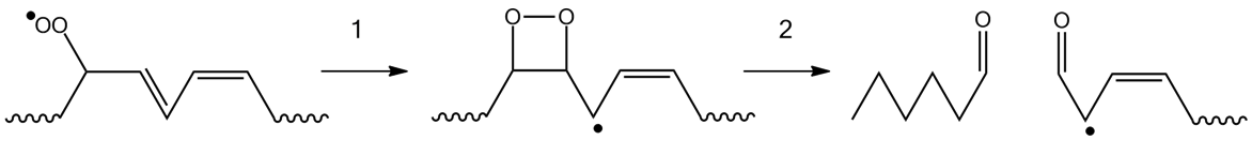

Figure 3.3. Proposed mechanism forming hexanal through the (1) cyclization of an allylic peroxy radical and (2) subsequent concerted decomposition into two carbonyl-containing species**.**

Due to the demonstrated importance of hydroperoxide species in the kinetic model, a mechanistic pathway starting from a critical conjugated hydroperoxide intermediate was also proposed and investigated using G4. The postulated mechanism was inspired by Hock cleavage reactions,[82,84] which are typically acid-catalyzed but can occur without the presence of any added acid though a suggested zwitterion geometry by Farmer and Sundralingham.[83,115]

3.4.4. Formation of Volatile Products from Dimers and Other Higher Order Species

A final mechanism considered for the formation of the volatile product hexanal was inspired by the work of Morita and Tokita.[80,85] Their work proposed and experimentally tested a mechanism for aldehyde formation from the homolytic decomposition of peroxide-linked polymers with hydroperoxide functionalization into hydroxy radicals and aldehydes. This scheme suggested that three bonds would need to be broken, either sequentially or in a concerted fashion, forming four product molecules. This proposed mechanism inspired the proposal of a series of elementary steps involving the decomposition of dimers and other higher order product species to produce volatiles as shown in Figure 3.4, where a dimer species formed through radical addition and containing hydroperoxide functionalization forms a precursor to an alkoxy β-scission reaction that then forms hexanal and an allylic radical. The model system of ethyl-linoleate assumes the presence of cobalt-2-ethyl hexanoate which catalytically decomposes hydroperoxides into oxygen-centered radicals, thereby facilitating the first step in this pathway. Parameters for the competing reaction that forms pentanal (through the further oxidation of the pentyl radical) were also calculated to assess the relative contribution of this pathway to the quantity of small aldehydes experimentally quantified. The attractive features of the proposed mechanism in Figure 3.4 are that it is comprised of classic free-radical reaction types and that parameters are available from experiment or structure-reactivity relationships.

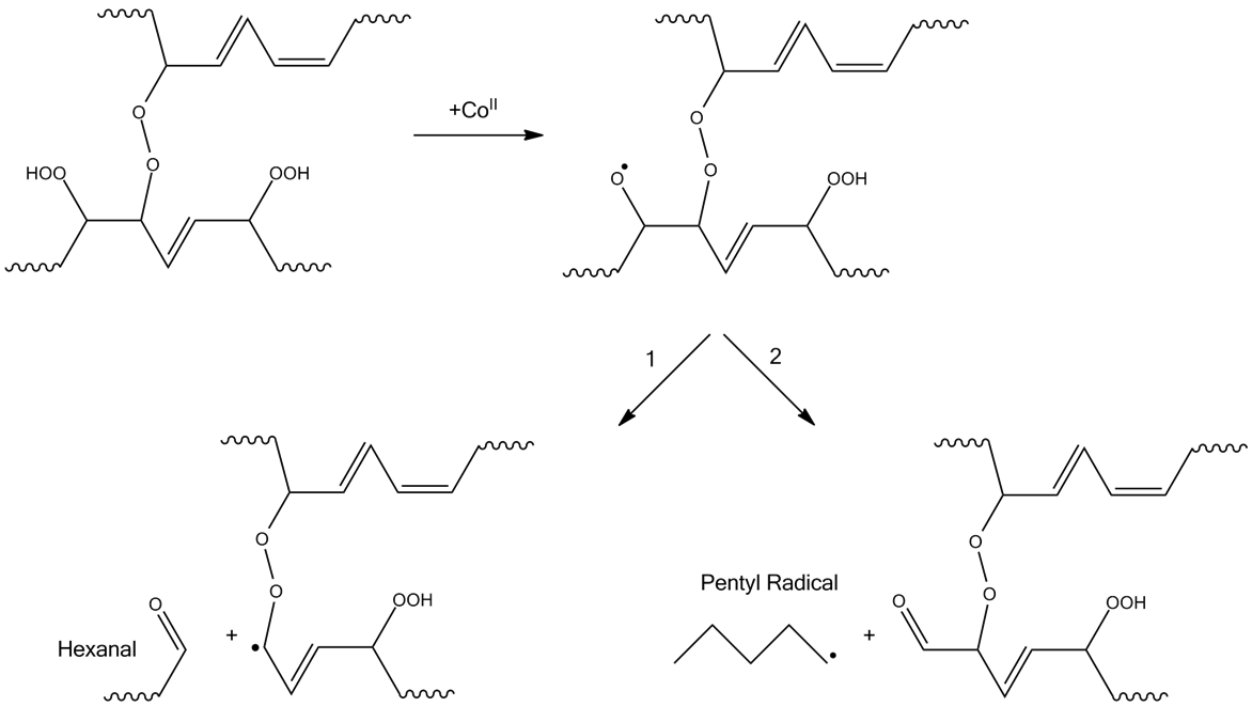

Figure 3.4. Proposed mechanism for the formation of the small volatile molecules hexanal and pentanal (through the further oxidation of pentyl radicals) from a dimer or higher oligomeric species. Alkoxy radicals are produced by the catalytic activity of cobalt decomposing hydroperoxides, and β-scission can subsequently proceed via pathway 1 or 2.

3.5 Results and Discussion

3.5.1 Experimental Results

Results from the headspace analysis are presented in Figure 3.5. The experimental error was determined to be approximately 7.5%. The results were compared to the existing literature data from Oyman et al.[30] in the units of mmol per mol of EL, and agreement is generally good for the available data points. New data in the region of 0-20 hr again highlighted the expected ratio of the production of hexanal to pentanal which the earliest kinetic models struggled to capture. Hexanal was initially generated at a rate of about 9.5:1 compared to pentanal and decreased to a ratio of 6:1 as oxidation proceeded. These early curing time points were then used for comparison to kinetic modeling results.

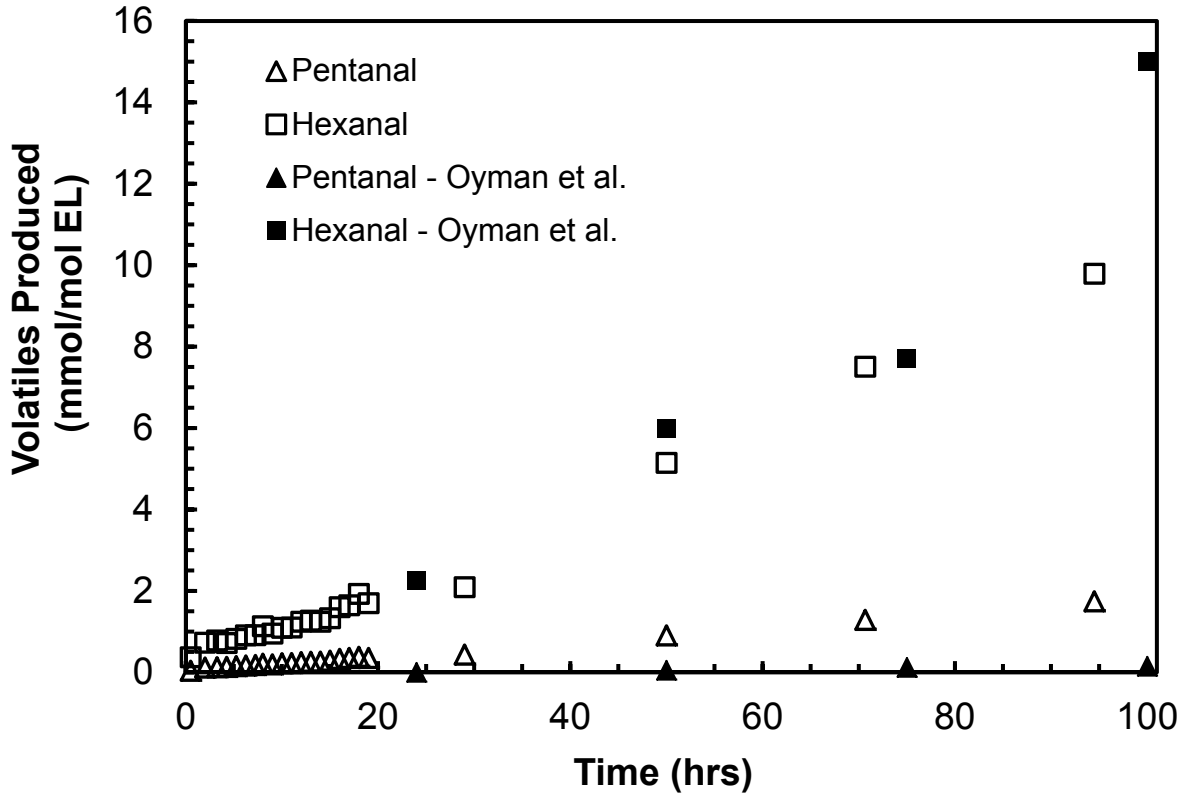

Figure 3.5. Amount of volatile species hexanal (open squares □) and pentanal (open triangles Δ) detected by GC/MS headspace analysis during the oxidation of EL with a cobalt catalyst. Results are compared to those of Oyman et al.[30] which are designated using closed symbols.

3.5.2 Computational Results and Implications

A summary of all the mechanisms studied and the associated kinetic parameters is presented in Table 3.1. The original reactions included in the kinetic model are labeled as β-scission pathways 1 and 2. Pathway 1 corresponds to the breakdown of a conjugated alkoxy radical into a dienal and an alkyl radical, and pathway 2 leads to the formation of hexanal and the vinyl radical. A sensitivity analysis revealed that the reaction energy barrier of pathway 2 would need to be nearly halved in order to obtain yields of hexanal and pentanal that would be in reasonable quantitative agreement with experiment assuming that the pre-exponential factor used for the β-scission family remained consistent.

Table 3.1. A summary of reaction mechanisms for the production of small volatile aldehydes. Reaction barriers (E_A) in kcal/mol and pre-exponential factors (A) in L/mol s (bi-molecular) or s^{-1} (unimolecular) for rate-determining steps are provided, the types of calculations performed to determine these values are indicated and relevant literature describing the mechanism in detail is cited.

Mechanism	E_A (kcal/mol)	A (L/mol s or s^{-1})	Calculation Performed	References
β-Scission, Path 1	11.7	10^{14}	Evans-Polanyi parameters [53] and group additivity [54] to determine ΔH_R	17,36,37
β-Scission, Path 2	24.3	10^{14}	Evans-Polanyi parameters [53] and group additivity [54] to determine ΔH_R	49,75,76
Korcek Decomposition	28.0	2.1×10^{8}	Cyclization to a five-membered ring, M06-2X/MG3S	77
	36.7	1.2×10^{11}	Cyclization to a six-membered ring, G4	
	38.1	2.4×10^{10}	Cyclization to a six-membered ring with unsaturation, G4	
Intramolecular H-shift	41.5	8.73×10^{11}	G4	111
Concerted Reaction	52.0	6.8×10^{11}	G4	49,83
Dioxetane Intermediate	24.6	3.9×10^{11}	G4	83,116
Dimer Decomposition	8.7	10^{14}	Evans-Polanyi parameters [53] and group additivity [54] to determine ΔH_R	80

3.5.2.1. Korcek and Korcek-like Reactions

The results of the quantum chemical calculations are presented in Figure 3.6 as minimum free energy pathways for the cyclization of representative keto-hydroperoxide species to cyclic peroxides both with and without unsaturation in the final ring. The calculation was designed to mimic the reaction coordinate achieved by Jalan et al. for a slightly larger C4 model keto-peroxide and with the introduction of unsaturated chemical functionality that is integral to lipid oxidation. Overall, the effect of unsaturation on the free energy barrier was mild, only increasing the required energy by ~1.5 kcal/mol, but some structural observations can be made based on following the reaction coordinate. The lowest energy reactant configuration containing a carbon-

carbon double bond is *trans*, but in order for cyclization to occur, the *cis* isomer must be adopted, which is about 3 kcal/mol higher in energy.

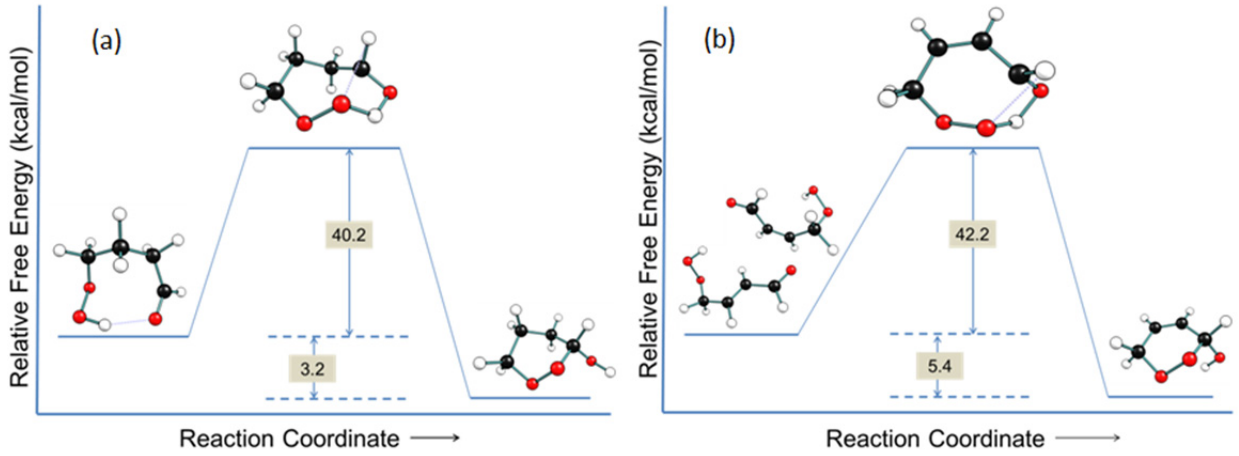

Figure 3.6. Free energy surfaces for the formation of a six-membered cyclic (a) saturated and (b) unsaturated peroxide species. The unsaturated keto-hydroperoxide must undergo *trans* to *cis* isomerization to obtain the necessary geometry for cyclization to occur.

Arrhenius parameters were calculated for both the forward and reverse reactions and are summarized in Table 3.2. According to Jalan et al., this step is rate-limiting, and based on the relatively high activation energy, incorporating these reactions into the kinetic model did not change the concentration profiles of hexanal and pentanal, as expected. However, the availability of an acid-catalyzed bimolecular pathway for the formation of the cyclic peroxide that significantly lowers the activation energy (essentially barrierless) provides another mechanism for the Korcek decomposition chain to proceed. At the temperature of interest, the critical concentration of carboxylic acid functional groups that will shift the rate-determining step from the initial formation of the cyclic peroxide to its subsequent fragmentation was not as low as the literature value (fM quantities) because of the presence of the cobalt catalyst that can compete to

decompose the keto-hydroperoxide, but is still achievable via other oxidation pathways such as Baeyer-Villiger. However, the reaction barriers for fragmentation into the desired aldehyde and acid products were also high (E_A=36.8 kcal/mol), and not much is known about the decomposition of six-membered cyclic peroxide rings. The rate constant for the C3 cyclic peroxide decomposition of a five-membered ring was substituted and used as a lower bound for the rate of the unimolecular decomposition reaction, but for the reaction conditions of interest and the early cure time scale, the experimental targets were still not met.

Table 3.2. Arrhenius parameters calculated for the forward cyclization and corresponding reverse reactions of the minimum free energy pathways shown in Figure 3.6.

Reaction	**A_{fwd} (s^{-1})**	**$E_{a,fwd}$ (kcal/mol)**	**A_{rev} (s^{-1})**	**$E_{a,rev}$ (kcal/mol)**
Saturated	1.2×10^{11}	36.7	4.1×10^{12}	42.3
Unsaturated	2.4×10^{10}	38.1	6.8×10^{12}	46.8

This observation, however, does not rule out the potential importance of this pathway at longer time scales or at higher temperatures, which could be easily tested using the microkinetic model. Additionally, for lipid systems without added transition metal catalysts to decompose hydroperoxide moieties, the contribution of this reaction pathway again increases in significance and may particularly influence the formation of organic acids. Further theoretical study of cyclic peroxide fragmentation reactions of larger molecules more representative of unsaturated lipids would play a critical role in determining the responsibility of Korcek decomposition in these types of reaction systems. Deeper mechanistic insights could also be achieved with more quantitative experimental data such as the organic acid concentration profiles for this model EL system.

3.5.2.2 Intramolecular Hydrogen Shift

The calculated minimum free energy pathway for the 1,3-intramolecular shift of a hydrogen atom of a hydroxyl group is displayed in Figure 3.7. The geometries of the lowest energy reactant, transition state and product alkoxy radical are included, which were determined by interrogating all conformational degrees of freedom based on rotations of all dihedral angles. Arrhenius parameters for the forward reaction were calculated to be $A=8.73\times10^{11}$ s^{-1} and E_a= 41.4 kcal/mol. The structure-reactivity relationship presented in the literature for this type of an intramolecular reaction is actually a regression for the energy of activation as a function of TS ring size,[113] as opposed to ΔH_R typical of an Evans-Polanyi relationship, but the concept is similar. When applied to this mechanism, the relationship yielded estimated values of E_a=41.4 kcal/mol and $A = 3.16\times10^{12}$ s^{-1} which align very closely with the value calculated for this molecule using quantum mechanics.

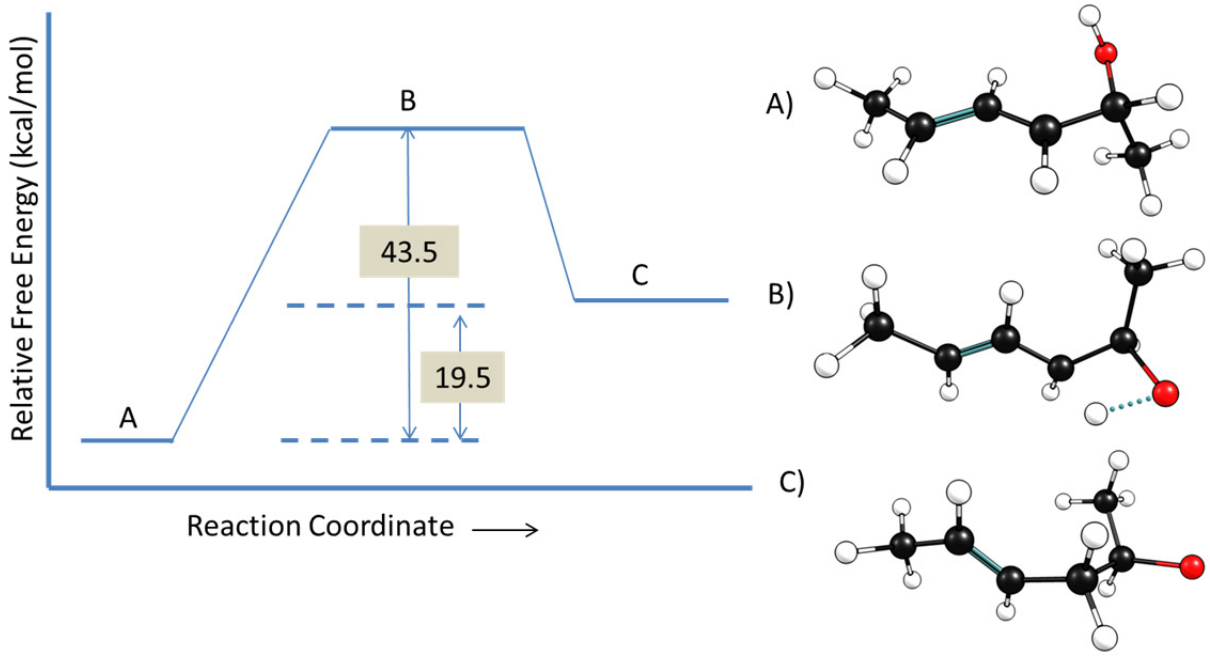

Figure 3.7. A free energy surface for 1,3-intramolecular hydrogen shift involving a hydroxyl group. Geometries are also shown for the reactant (a), transition state (b) and product (c).

While this reaction mechanism does ensure that β-scission of the final alkoxy radical product favors the formation of hexanal and an allylic radical, the high ring strain in the four-membered ring transition state rendered this pathway kinetically inconsequential at room temperature.

3.5.2.3 Reactions with Allylic Peroxy Species

3.5.2.3.1 A Dioxetane Intermediate

The previous alternatives involving β-scission reaction pathways all proceed through high barriers and thus with small rate constants that cause these mechanisms to be kinetically irrelevant at room temperature. However, rates are a function of both the rate constant and the concentration of the reactant(s), and given the facile formation of peroxy radicals, they were attractive candidates to lead to the formation of aldehydes. Formation of many small molecules directly from a peroxy radical was proposed by Juita et al.[79] Although other volatiles may be formed via lower energy pathways through more stable ring structures, the proposed pathway of interest to form hexanal proceeds through a strained four-membered ring. Given that the researchers were unable to isolate a stable transition state for the decomposition of the dioxetane intermediate, it was sought to confirm the lowest energy pathway for this mechanism with G4 since it has recently been demonstrated to have a high level of chemical accuracy for oxygenated and radical species.[117] As seen in Figure 3.7, the calculated value for the energy barrier for the first elementary reaction step, cyclization, using the G4 method faithfully reproduced their result of 24 kcal/mol within the expected error for quantum chemical calculations. The Arrhenius parameters subsequently regressed for the forward and reverse reaction steps were determined to be E_a = 24.6 kcal/mol and 18.8 kcal/mol, respectively, with pre-exponential factors of $A=3.9\times10^{11}$ s^{-1} and 4.02×10^{12} s^{-1}.

For the decomposition of this ring, a transition state was located and is shown on the potential energy surface in Figure 3.8. Key structural parameters were a C-C bond length of 1.64 Å and an O-O bond length of 1.87 Å in the fracturing dioxetane ring. The predicted $\Delta G^{\ddagger}$ was slightly higher than that proposed in the literature. The Arrhenius parameters yielded for this reaction were determined to be E_a = 23.7 kcal/mol and $A=4.45\times10^{12}$ s^{-1}. The associated rate constant was once again too low to be competitive at room temperature for hexanal production as the required peroxy radical reactant readily abstracts abundant bi-allylic hydrogen atoms from the EL substrate in the early curing regime of interest. However, these reactions were incorporated into the kinetic model to enhance the accuracy of experiments run at a variety of temperatures.

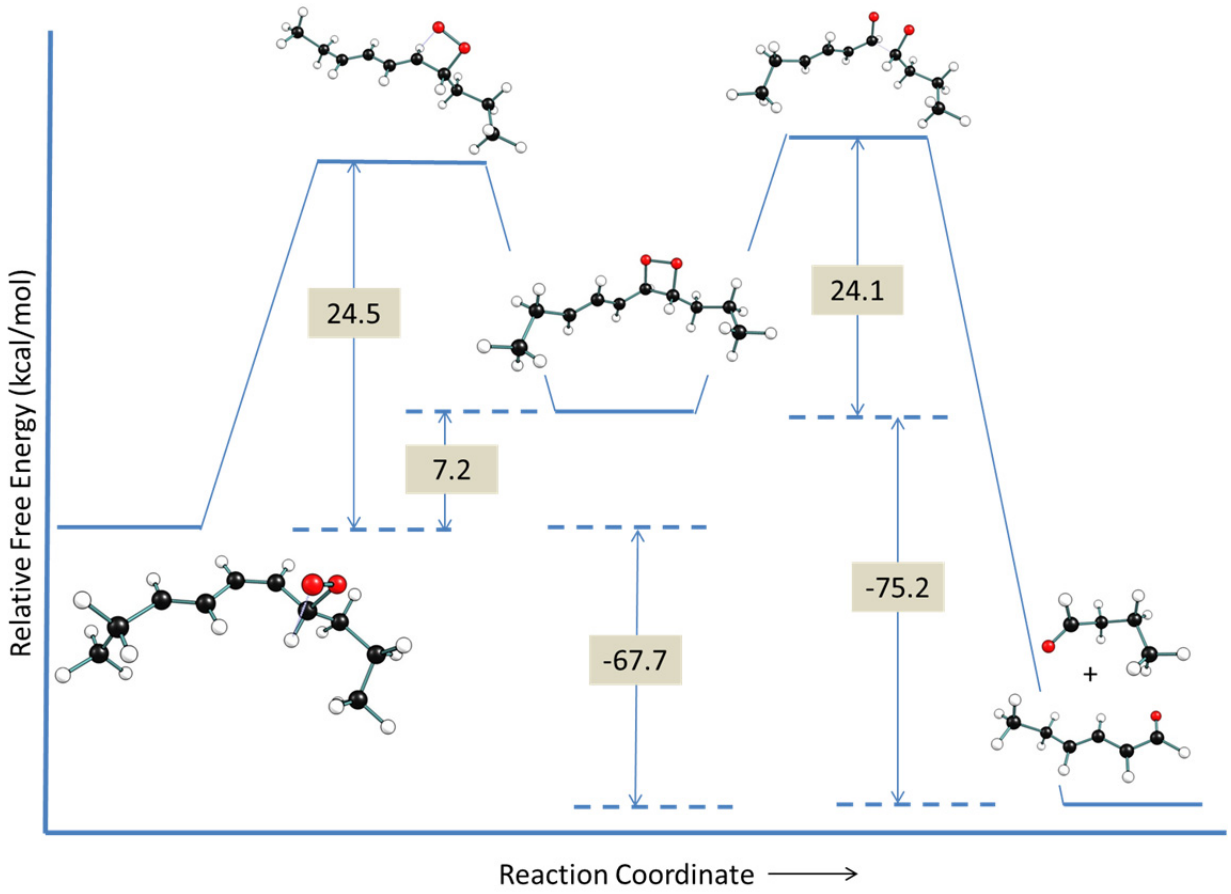

Figure 3.8. Free energy surface for the formation of two terminal carbonyl species from the decomposition of a peroxy radical. Results are in good agreement with those that Juita et al.[79] were able to report, with the addition of a definitive transition state for the decomposition of the dioxetane intermediate**.**

3.5.2.3.2. A Concerted Reaction Pathway

Like the conjugated peroxy radical, an allylic hydroperoxide is a critical reaction intermediate that can build up in the reaction mixture at quite high concentrations until it is catalytically decomposed. Exploring reaction pathways from this species led to an attempt to determine kinetic parameters for a mechanistic postulate proceeding through a zwitterion as originally proposed by Farmer and Sundralingham.[115] While it was not possible to stabilize a zwitterion, the exploration did lead to the discovery of a concerted decomposition reaction. The transition state geometry of this intramolecular reaction is shown in Figure 3.9. Key parameters for the breaking bonds were O-O = 1.80 Å and C-C = 1.57 Å, and the forming bond between the oxygen of the transferring hydroxyl group and the sp^2 carbon was 1.80 Å at the transition state.

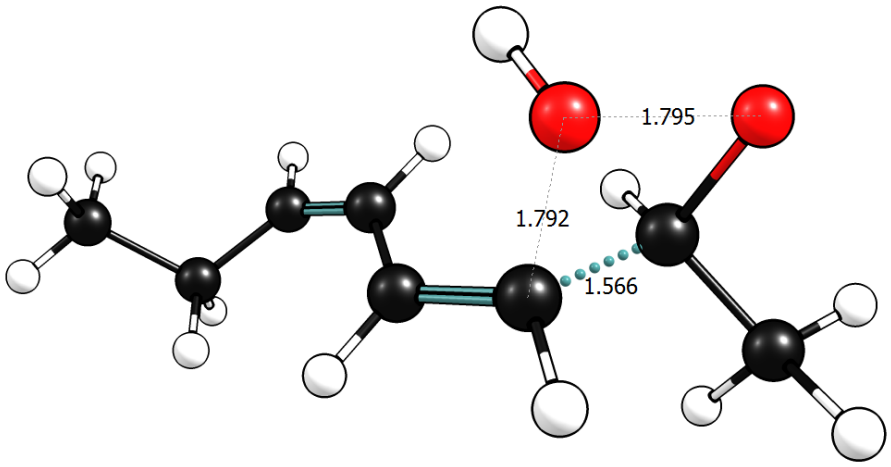

Figure 3.9. Structure of the transition state for the concerted decomposition of a conjugated hydroperoxide into an aldehyde and an alcohol. Relevant interatomic distances are included in Angstroms (Å).

While the activation energy for this reaction, E_a= 52.0 kcal/mol, and the pre-exponential factor, A= 6.8×10^{11} s^{-1}, resulted in a calculated rate constant that excluded this reaction as a possible candidate for hexanal formation, it offers a new pathway for the formation of volatiles during hydrocarbon oxidation at much higher reaction temperatures that could be relevant to, for example, oil oxidation in food applications.[118]

3.5.2.4 Formation of Volatiles from Dimers and Other Higher Order Species

The final mechanistic postulate was inspired by the work of Morita et al.[80] In their work they offered a key insight that small volatiles may actually be primarily produced from larger secondary products rather than from reactants or primary products. Previous mechanistic alternatives to β-scission pathway 2 (Table 3.1) all required routes that involved high energy barriers as conjugated double bonds were re-oriented into a position convenient for hexanal formation. However, in this mechanistic postulate, the presence of the conjugated double bonds was exploited as shown in Figure 3.10 to create a dimeric species with a low energy barrier to forming hexanal through traditional alkoxy β-scission.

Radical addition reactions by peroxy radicals across conjugated double bonds are highly exothermic and facile. Using Evans-Polanyi parameters[19] and heats of reaction calculated using Benson group additivity values,[54] the energy of activation for radical addition to form a dimeric species is 6.7 kcal/mol. In addition, a typical frequency factor for this reaction family is A = 1×10^{8} M^{-1} s^{-1}. Once this radical species is formed, oxygen addition is rapid. Another hydrogen abstraction reaction forms the dihydroperoxide dimeric species depicted in Figure 3.4 and Figure 3.10.

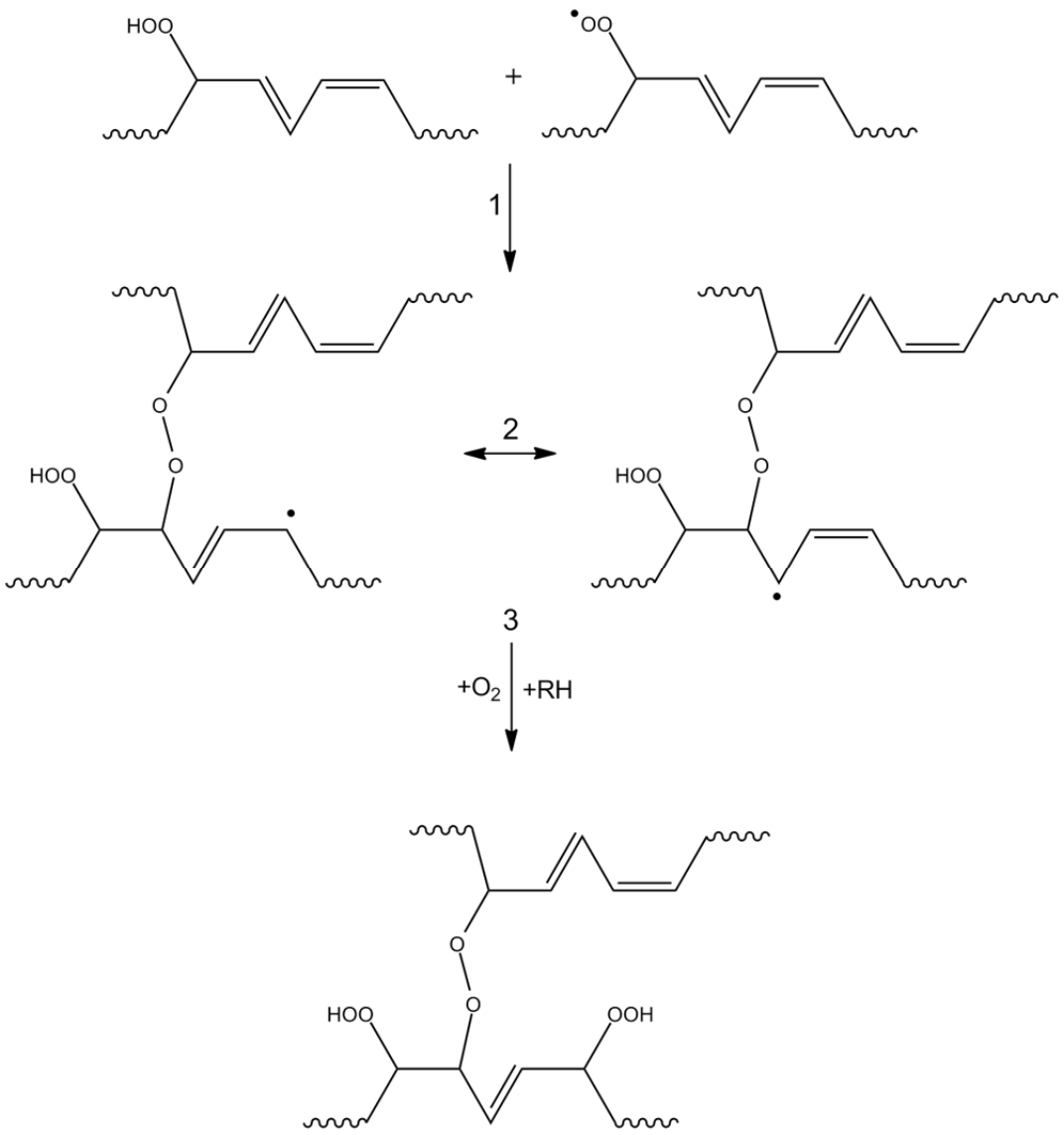

Figure 3.10. Scheme for the formation of a dimeric species through 1) peroxy radical addition across conjugated double bonds followed by 2) the potential isomerization of the allylic radical and 3) oxygen addition and hydrogen abstraction to form the second hydroperoxide group.

Next, the kinetic model included routes for hydroperoxide functionalities to be catalytically decomposed by the presence of cobalt metal ions into peroxy and alkoxy radicals. The alkoxy radical resulting from this catalytic decomposition could then undergo β-scission, leading to hexanal via a much lower barrier of 8.7 kcal/mol compared to pathway 2 (Table 3.1).

When each of these reactions and kinetic parameters were incorporated into the kinetic model, the result was a significant increase in hexanal production and a decrease in overall pentanal production as shown in Figure 3.11 relative to the previous results.[15]

These mechanisms imply an induction time for the formation of hexanal relative to pentanal, although it was ultimately a major product formed in much higher quantities than pentanal at these temperatures. This new mechanism offers promising pathways for the formation of these species at room temperature. Given the fast curing rate of EL, and other metal catalyzed oil-based systems, several data points within the first 24 hours of curing time were needed to develop a thorough mechanistic understanding of the formation of volatile species, a gap that was sought to be filled by the experimental data presented in this work. Data at these lower temperatures offer valuable quantitative targets for comparison during the iterative process of model development and optimization.

A comparison of the theoretical prediction of the model to experiment indicates that the further oxidation of pentyl radicals produced from β-Scission pathway 1 was indeed the main source of volatile pentanal. The model still underestimates the experimental predictions of hexanal relative to experiment, but this could be due to the stoichiometric limits placed on the model by restricting the model size to only include monomeric and dimeric species as well as constraining the peroxy radicals allowed to undergo radical addition to the two major conjugated radical C20 isomers found in the system. Theoretically, the identity of the peroxy radical that adds to the double bond need not be so limited and any higher rank oligomer with the appropriate alkoxy radical β to a peroxy bond should be able to form hexanal from the chain end

scission. One can imagine that with a larger reaction network generated automatically, as well as parameter optimization, the model can be further improved as will be discussed in Chapter 5.

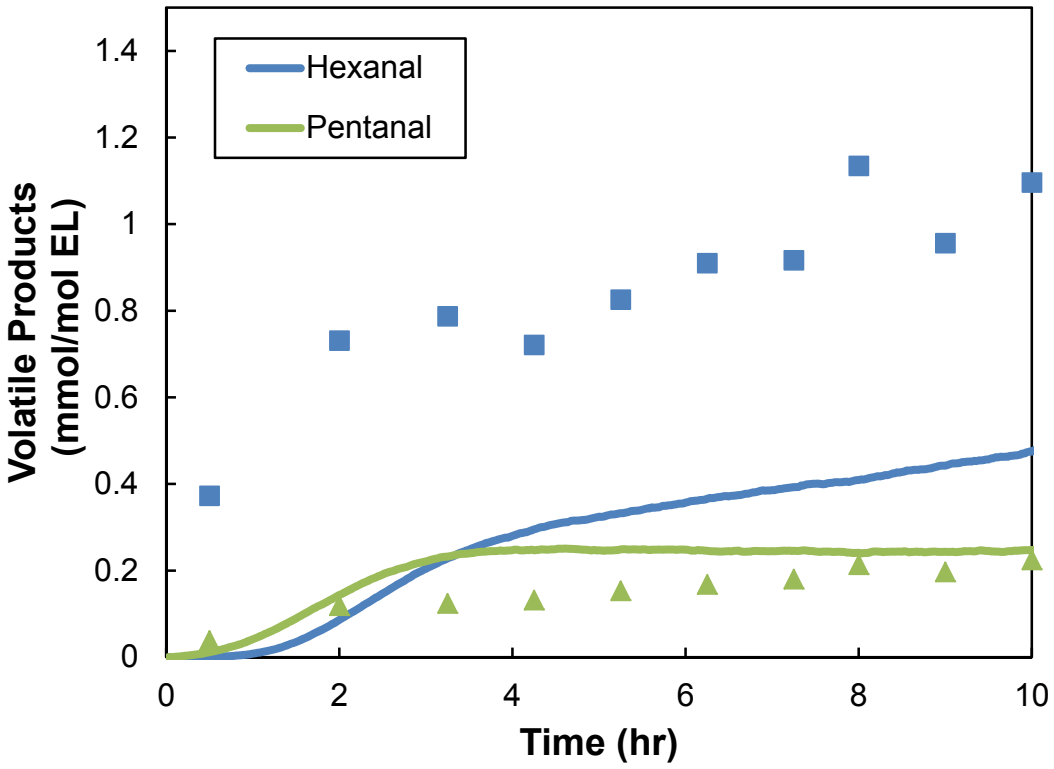

Figure 3.11. Concentration profiles for the volatile aldehydes, hexanal and pentanal, generated by the microkinetic model (lines). Agreement with measured experimental values (hexanal ■, pentanal ▲) is vastly improved from previous versions of the model that did not allow for volatiles to be formed from higher rank products.

3.6 Conclusions

Through the use of computational approaches, this work explored numerous mechanisms for the formation of volatile products, focusing on hexanal in particular. In the context of a microkinetic model, mechanistic postulates parameterized by theory or structure-property relationships such as the Evans-Polanyi relationship were tested for their kinetic relevance within the range of expected computational error. Most of the pathways tested in this work were

appropriate for oxidation chemistry performed at conditions more extreme than room temperature. The results indicated that a reasonable mechanism for the formation of volatile products at room temperature could be accomplished by the scission of chain ends from higher order (dimeric or larger oligomeric) species. This conclusion was tested through the comparison of newly obtained experimental data from GC/MS headspace analysis in the early cure regime.

This mechanism also has important implications for the formation of an overall cured coating. If elevated temperatures shift the competition between intermolecular addition and abstraction reactions that propagate chain growth to favor intramolecular reactions that lead to chain scission, artificially aged mock-ups of paint layers will not demonstrate the same level of stability as their naturally aged counterparts, making treatment decisions for art objects based on the response of samples aged in this way less meaningful. Computational models have the ability to readily explore the effects of a variety of environmental conditions and could be used to quickly optimize artificial aging parameters. With newly acquired headspace data in the early cure regime now available to calibrate model parameters, the benefits of constructing detailed models of chemical pathways to develop a fundamental understanding of oil-based materials' evolution in time as demonstrated here could extend to other systems involving oxidation chemistry.

Chapter 4

Theoretical study of epoxidation reactions relevant to hydrocarbon oxidation

Material in this chapter is reproduced from the article "Theoretical study of epoxidation reactions relevant to hydrocarbon oxidation" by Lindsay Oakley, Francesca Casadio, Kenneth Shull and Linda Broadbelt; *Industrial & Engineering Chemistry Research*, **56**, 7454-7461.[114]

4.1 Introduction

Hydrocarbon oxidative processes play an important role in many industries, ranging from machine manufacturing to food science to coatings. Depending on the application, it is often desirable to mitigate or promote these types of reactions. For instance, in the case of lubricants or edible oils, oxidative reactions shorten product lifetimes[76,119–121] whereas in the case of oil-based paint coatings, autoxidative mechanisms play an essential role in the curing and stability of the paint films.[3,29,122] Microkinetic modeling is one powerful method of exploring key factors that influence the kinetics of these reactions on the molecular level and can provide insight into potential ways to optimize desired processes. These models can also be continuously expanded to accommodate and test new pathways as they are proposed.

However, there are challenges associated with assembling a reaction network at the elementary-step level for condensed- phase oxidation. The construction of a microkinetic model requires detailed knowledge of the kinetic parameters of the relevant chemistry to enumerate all of the elementary steps in the reaction mechanism. For hydrocarbon oxidation, the number of steps can be quite large, making the task of parametrizing each one formidable. Many

researchers in the modeling community have adopted the practice of using structure−reactivity relationships to estimate rate coefficients.[123−125] In early instances, these kinetic correlations were determined empirically, but the advent of computational chemistry has allowed such correlations to be derived using quantum chemical methods in conjunction with transition state theory.

As applied to hydrocarbon oxidation, several relevant Evans−Polanyi[13] or Blowers-Masel[126] type correlations have been investigated and calculated for the fundamental free-radical pathways.[53,113,127] Yet, pathways for more minor products have not been as thoroughly investigated, either because of their lack of kinetic relevance or because they can be fit using empirical methods. However, use of a derived kinetic correlation will offer more flexibility in a kinetic model for exploring a range of environmental conditions without having to repeatedly perform fitting procedures. A seminal work by Muizebelt et al. demonstrated that, during the early stages of oleoresinous paint curing under ambient conditions, a nontrivial concentration of epoxide functional groups is present that slowly disappears as the curing and aging of the coating progress over time.[32] Understanding the mechanisms that lead to the formation and transient nature of these epoxide intermediates is of interest. Budnik and Kochi proposed a mechanism for the epoxidation of hydrocarbons from alkylperoxy radicals and unsaturated species,[128] and Benson also discussed these reactions, remarking on the lack of experimental data for comparison that appears to persist today,[129] with only a handful of studies available in the literature. Baldwin et al. proposed Arrhenius parameters for the formation of oxirane at high temperatures (400−500 °C) but commented on the difficulties of accurately measuring low product levels.[130] Bloodworth and co-workers were able to determine a rate constant for the formation of oxiranes from *tert*-butylperoxyalkyl radicals at 298 K of 4×10^3 s^{-1} using electron

spin resonance (ESR) spectroscopy.[131] Theoretical studies of the formation of oxiranes from alkylhydroperoxy radicals are catalogued in the kinetics database of the National Institute of Standards and Technology (NIST),[112] including the works reported in references [132–134], as well as more recent works,[135–138] yet these calculations have not been extended beyond aliphatic systems to include allylic radicals or to investigate larger species with more highly substituted alkoxy leaving groups. Ascertaining the effects of these types of substituent groups is critical to the calculation of a structure−reactivity relationship for this relationship to be widely generalizable to hydrocarbon systems that include long chains and varying degrees of unsaturation.

The aim of this work was to use quantum chemistry to generate a kinetic correlation for hydrocarbon epoxidation reactions that is suitable for use in microkinetic models of low-temperature oxidation reactions and that has a much broader substrate range and thus applicability. Toward this end, the substrates included in Figure 4.1 were selected to contain a variety of substituent groups to explore broader chemical space and, in turn, a wide range of heats of reaction while still being computationally tractable. Notably, cyclic allylic peroxy and benzylic radical species were also included to thoroughly assess the generalizability of these structure−reactivity relationships to a variety of oxidizing substrates. In particular, this work was motivated by the desire to model the curing of linseed oil, a triacylglycerol with highly unsaturated fatty acid tails that is a widely used binding medium in fine arts paintings and other works of art.

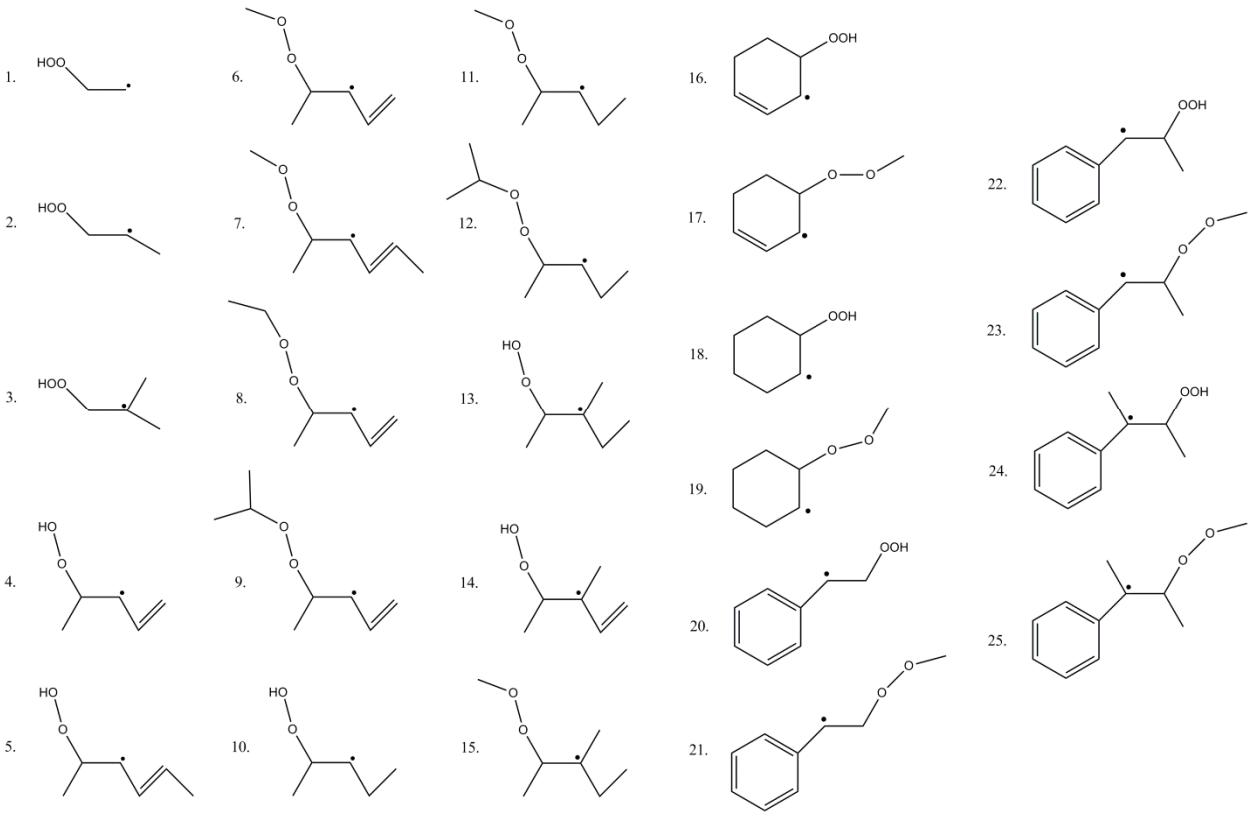

Figure 4.1. Reactant radicals undergoing direct epoxidation through homolytic O−O bond cleavage that were examined using quantum chemical calculations.

4.2 Computational Methods

All quantum chemical calculations were executed using the Gaussian 09[101] software package. For each reaction, conformers of reactants, products, and transition states were explored, and minimum-energy structures were optimized using the Berny algorithm.[139] When the algorithm identified a first-order saddle point on the potential energy surface as a transition state, a frequency calculation was used to confirm the presence of only a single large-amplitude imaginary vibrational mode. A visualization of this mode and additional intrinsic reaction coordinate (IRC) scans confirmed that the proper transition state was connected to the desired reactant and products. The hybrid G4 method[102] was selected to calculate thermochemical

properties because it was demonstrated to provide accurate values of kinetic and thermodynamic parameters involving reactions of radical species in previous studies.[59,140,141] As the first steps in the G4 energy calculation routine, the geometries were optimized and the frequencies were calculated using the B3LYP functional with the 6-31G(2df,p) basis set. Subsequent steps included zero-point energy calculations at the MP-2(full) level of theory. Solvent effects were determined to be negligible by comparing vapor-phase energy barriers for two reactions (those of species 1 and 6) to the same barriers determined using a solvent continuum model with four different solvents described by dielectric constants ranging from 1.9 to 9.8. The dielectric constants of oils at 298 K are between 2 and 4. The resultant frequencies were scaled by a factor of 0.9854 according to the recommendation of Curtiss et al.[142] Ultimately, the frequencies were used to determine the temperature-dependent total partition function with corrections for internal rotation treated as hindered rotors using the program Calctherm,[143] which, in turn, was used to determine the rate constant as a function of temperature using transition state theory.[104] A Wigner tunneling correction was also applied.[105] This allowed the Arrhenius frequency factor, A, and activation energy, E_A, to be extracted from a linear fit of the traditional Arrhenius plot of $\ln(k)$ versus $1/T$. Temperatures ranged from 300 to 1000 K in 100 K increments.

2.3 Results and Discussion

Systematic searches for the lowest-energy transition state revealed the importance of minimizing the effects of hydrogen bonding between the alkoxy leaving group and the newly formed three-membered ring. The presence of hydrogen-bonding interactions resulted in lower-amplitude, highly coupled imaginary vibrational modes in the transition state. An example free

energy profile and the associated geometric characteristics of the reactant, products, and transition state, with key bond lengths and angles included, are shown in Figure 4.2.

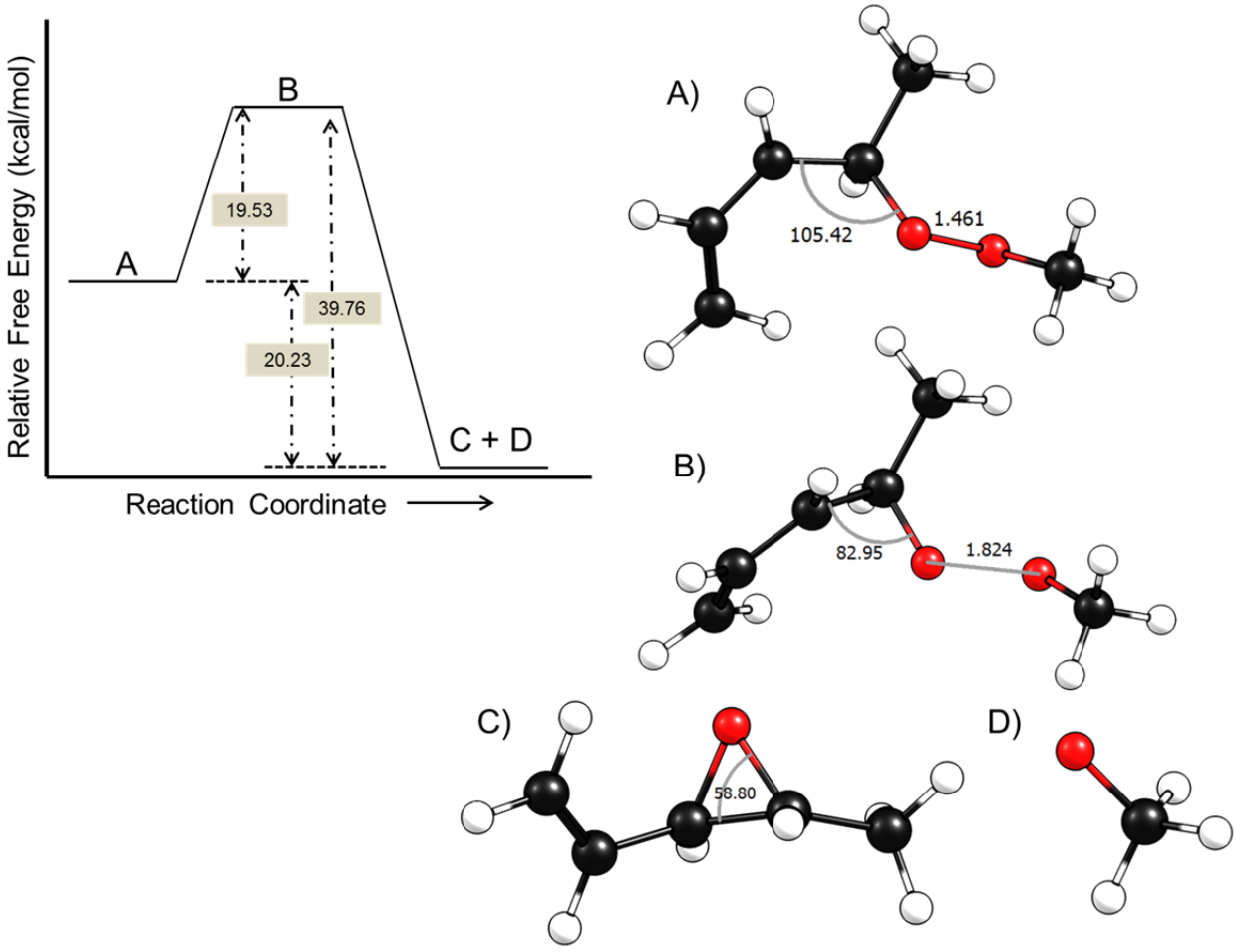

Figure 4.2. Representative free energy profile for reactant 6 in Figure 4.1 from G4 calculations. Values are referenced to reactant structure A. Also shown are the (B) transition state geometry, as well as the structures of the (C) epoxide product and (D) alkoxy leaving group. Key bond lengths and angles are also indicated in Angstroms and degrees, respectively.

This diagram highlights the exergonic nature of the forward reaction. For all species observed, when the C−C−O bond angle moved past 85°, the O−O bond ruptured, and the epoxide group formed. The kinetic and thermodynamic properties derived from the quantum chemical

calculations carried out as described above for the homolytic cleavage of the O−O bond in reactants 1−25 (Figure 4.1) are presented in Table 4.1.

Table 4.1. Kinetic and Thermodynamic Properties Calculated for the Reactants Shown in Figure 4.1 Based on G4 Energies and Corrected for Internal Rotations, Including Key Aspects of the Reactant Radical Structure (Alkyl, Allylic, Cyclic, or Benzylic) and the Alkoxy Leaving Group (Hydroperoxy or Alkylperoxy).

Reactant	Reaction Characteristics	ΔH_R^{fwd} (kcal/mol)	E_A^{fwd} (kcal/mol)	$\log A^{fwd}$ (s^{-1})	E_A^{rev} (kcal/mol)	$\log A^{rev}$ (s^{-1})
1	alkylhydroperoxy	-15.1	15.9	13.0	30.4	4.95
2	alkylhydroperoxy	-16.0	14.0	12.6	29.2	4.06
3	alkylhydroperoxy	-16.5	12.6	12.6	27.4	2.60
4	allylic hydroperoxy	-4.3	20.1	13.6	23.5	4.61
5	allylic hydroperoxy	-3.7	19.3	13.0	22.5	4.75
6	allylic alkylperoxy	-8.9	19.3	13.0	27.6	2.21
7	allylic alkylperoxy	-8.3	17.7	11.1	25.7	1.13
8	allylic alkylperoxy	-8.3	19.0	13.0	26.6	1.29
9	allylic alkylperoxy	-7.8	17.8	11.6	25.6	1.09
10	alkylhydroperoxy	-16.7	11.9	12.7	27.9	3.78
11	alkylperoxy	-21.3	11.6	12.6	32.0	1.23
12	alkylperoxy	-20.6	10.2	11.2	30.7	1.06
13	alkylhydroperoxy	-17.6	10.2	12.5	26.9	3.77
14	allylic hydroperoxy	-4.6	17.8	13.7	21.5	4.58
15	alkylperoxy	-22.4	10.1	12.5	31.9	2.21
16	cyclic allylic hydroperoxy	-1.0	18.9	13.1	20.2	6.75
17	cyclic allylic alkylperoxy	-6.1	18.6	13.2	25.4	5.87
18	cyclic hydroperoxy	-15.5	14.3	13.5	29.4	5.81
19	cyclic alkylperoxy	-20.0	14.6	13.8	34.1	3.43
20	Benzylic hydroperoxy	-6.4	19.5	13.3	25.1	4.28
21	Benzylic alkylperoxy	-11.4	18.3	12.9	29.1	2.34
22	Benzylic hydroperoxy	-7.3	17.9	13.8	24.4	4.75
23	Benzylic alkylperoxy	-11.9	16.7	12.7	28.0	2.04
24	Benzylic hydroperoxy	-7.9	17.2	13.3	24.2	4.46
25	Benzylic alkylperoxy	-12.0	17.2	13.9	28.2	2.02

It should be noted that hybrid chemistry CBS-QB3 calculations were also attempted.[144] As similarly reported in several previous studies, these calculations suffered from high spin contamination in the transition state, which caused the barriers to be consistently underestimated because of the use of an empirical correction term utilizing the result of the spin operator. This problem was first noted by Wijaya et al., and a ~2.5 kcal/mol barrier height correction was added in their work to remove the empirical correction and account for this discrepancy. It was determined that these corrected CBS-QB3 calculations were in good agreement with the G4 results.

Other studies using CBS-QB3 did not clearly apply any correction to the barrier and obtained values that were consistent with each other and with the uncorrected results from the CBS-QB3 results presented here and those of Wijaya et al.,[133] varying only in their selection of conformers and treatment of low-frequency vibrational modes and tunneling, which mostly affected pre-exponential factors.[135–137] Cord et al. compared simulated lumped concentration profiles to experimental data and observed an overestimation of the predicted oxirane products, confirming that the uncorrected barrier was indeed too low. Similarly, Zhang et al.[145] reduced the kinetic parameters taken from the work of Villano et al.[137] to match their experimental results for the formation of cyclic ethers in *n*-hexane oxidation, which indicates that the method might be systematically underestimating barrier heights. Recently, Somers and Simmie[117] performed an important benchmarking study comparing CBS-*x*, G*n*, and W1 methods for determining the thermodynamic properties of small oxygenated radical and closed-shell species. Their results strongly suggested the use of G4 methods for radicals if the highest degree of chemical accuracy

is sought. Consequently, despite its higher computational expense, G4 was selected for the calculations carried out in this work.

The data collected in Table 4.1 capture three important trends. First, the presence of an allylic radical dramatically increases the barrier height for the epoxidation reaction through cyclization by an average of 6.6 kcal/mol compared to the corresponding values for alkyl radicals, which was determined by comparing species 4 to species 10, species 6 to species 11, species 9 to species 12, and species 13 to species 14. This increase equates to a difference in rate coefficient of approximately 5 orders of magnitude at room temperature, a relationship that holds as well for cyclic saturated compounds (species 18 and 19) and their unsaturated counterparts (species 16 and 17, respectively). The benzylic radical species examined were not found to exhibit any clear trend in activation energies, especially relative to their allylic radical counterparts, but they did play a crucial role in extending the range of reaction enthalpies explored. Second, the trend that activation energy decreases as the radical becomes more highly substituted (i.e., 1° > 2° > 3°) first described by Wijaya et al[133] was reproduced. This is most easily observed in the series of reactants 1, 2, and 3. Finally, the results suggest that increasing the size of the alkoxy leaving group has only a minor effect on activation energy. It is known that the O−O bond dissociation energy of a hydroperoxide (ROOH) is larger than that of its ROOR counterpart,[146] so it was anticipated that this effect would influence the overall relative enthalpy of reaction, and indeed, this effect was observed, for example, in the difference in ΔH_R values between reactants 4 and 6. However, extending the carbon chain length on the radical leaving group did not appear to contribute significantly to further reductions in the activation energy unless the additional atoms increased the degree of substitution near the oxygen radical as seen

in the comparison among species 6, 8, and 9, where the barrier decreased by about 1 kcal/mol as the leaving radical changed from methoxy to ethoxy to 2-propoxy. These emerging patterns and their interactions emphasize the importance of investigating a diversity of substituent groups to establish a kinetic correlation for modeling complex mixtures, such as drying oils, that have varying degrees of unsaturation, usually ranging from zero to three double bonds, in each fatty acid constituent.

It is also possible to compare some of the results with the limited values presented in the literature. Kinetic parameters for the formation of oxirane are highlighted in Table 4.2 and compared with values from previous theoretical studies. It should be noted that the calculated rate constant, $k_{fwd} = 1.57 \times 10^4$ s^{-1}, for species 11 at 298 K matches well with the solution-phase experimental rate constant, $k = 4 \times 10^4$ s^{-1}, derived by Bloodworth et al.[131] for a reactant with a comparable radical structure.

Table 4.2. Comparison of calculated kinetic parameters with those presented in previous theoretical studies.

	Method	E_A (kcal/mol)	Log(A/s^{-1})
•CH_2CH_2OOH→•OH + oxirane			
Present Work	G4	15.9	13.0
Present Work	CBS-QB3+2.5 kcal barrier adjustment	16.8	13.1
Wijaya et al. *	CBS-QB3	17.0	12.6
	BH&HLYP /6-311G**	16.7	12.7
Villano et al.	CBS-QB3	13.3	9.2
Cord et al.	CBS-QB3	14.2	11.0
Miyoshi	CBS-QB3	14.9	13.0
Bugler et al.	M06-2X/6-311++G(d,p)	11.7	7.2
Sheng et al.	CBS-Q//B3LYP/6-31G(d,p)	15.4	10.1
Chan et al.	BH&HLYP	16.5	14.0
* also corrects barrier heights for spin contamination			

Using the results presented in Table 4.1, activation energies for both forward and reverse reactions were plotted as a function of reaction enthalpy to establish a kinetic correlation. As shown in Figure 4.3 the data could be fit well by a linear regression to produce an Evans−Polanyi relation of the form the form of Equation 4.1, where E_A is the activation energy, ΔH_R is the heat of reaction, E_0 is the intrinsic barrier and α is the transfer coefficient.

$$E_A = \alpha \Delta H_R + E_0 \tag{4.1}$$

The parameters of the fit were constrained such that $\alpha_{fwd} + \alpha_{rev} = 1$, and the intrinsic reaction barrier, $E_{0,}$ was made equivalent for the exothermic and endothermic regimes to satisfy thermodynamic consistency. The overall relationship is summarized in Equation 4.2.

$$E_A = \begin{cases} 0.51(\Delta H_R) + 21.4 & for\ \Delta H_R \leq 0 \\ 0.49(\Delta H_R) + 21.4 & for\ \Delta H_R > 0 \end{cases} \tag{4.2}$$

The line of best fit reveals a relationship with an α value very close to 0.5. Such a value provides insight into the transition state geometry. An α value less than 0.5 indicates a transition state geometry that is very "reactant-like", whereas a value approaching 1 indicates a very "product-like" geometry. The geometry implied by a value of ~0.5 is approximately symmetric and is common for transfer reactions. The regression is reasonable over the entirety of the chemical space explored, with an R^2 value of 0.82 in the endothermic regime and an R^2 value of 0.80 in the exothermic regime and largest residuals of 3.3 kcal/mol for species 19 and 2.7 kcal/mol for species 21. This would introduce a maximum possible error of approximately 1−2 orders of magnitude into the calculation of rate constants, assuming oxidation at 25°C. However, the remaining residuals were within the expected computational error of 1−2 kcal/mol for barriers calculated by G4.

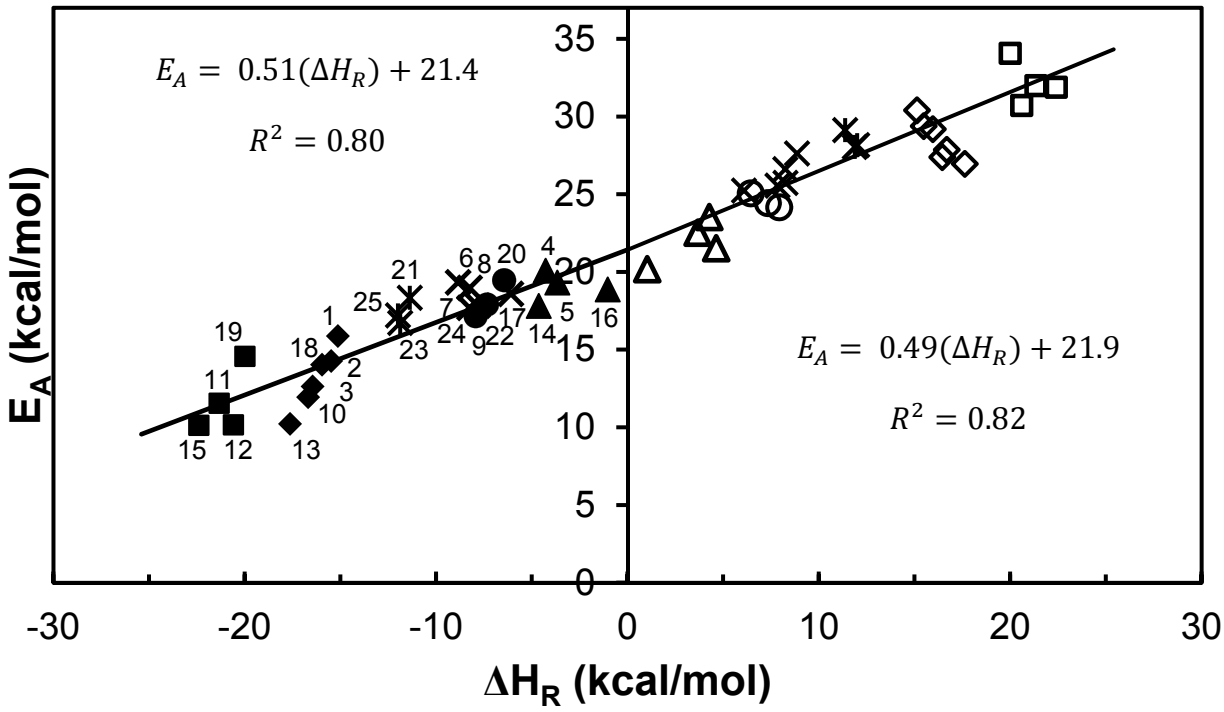

Figure 4.3. Evans-Polanyi plot of the forward exothermic epoxidation reactions (filled) and the reverse endothermic radical addition reactions (open). Reactant characteristics assigned in Table 4.1 are represented by the following symbol shapes: alkylperoxy (□), alkylhydroperoxy (◊), allylic alkylperoxy (×), allylic alkylhydroperoxy (Δ), benzylic hydroperoxy(○) and benzylic alkylperoxy(*). Species numbers from Table 4.1 are also listed with their associated data point for ease of reference.

A closer examination of Figure 4.3 highlights the necessity of exploring a diversity of chemical space to derive widely applicable kinetic correlations. A visual inspection of the Evans−Polanyi relationship reveals several groupings based on similar chemical features that can be explored in further detail. For example, the points in the cluster between $\Delta H_R = -15$ and $\Delta H_R = -20$ kcal/mol shown in the close up in are all associated with alkylhydroperoxy species.

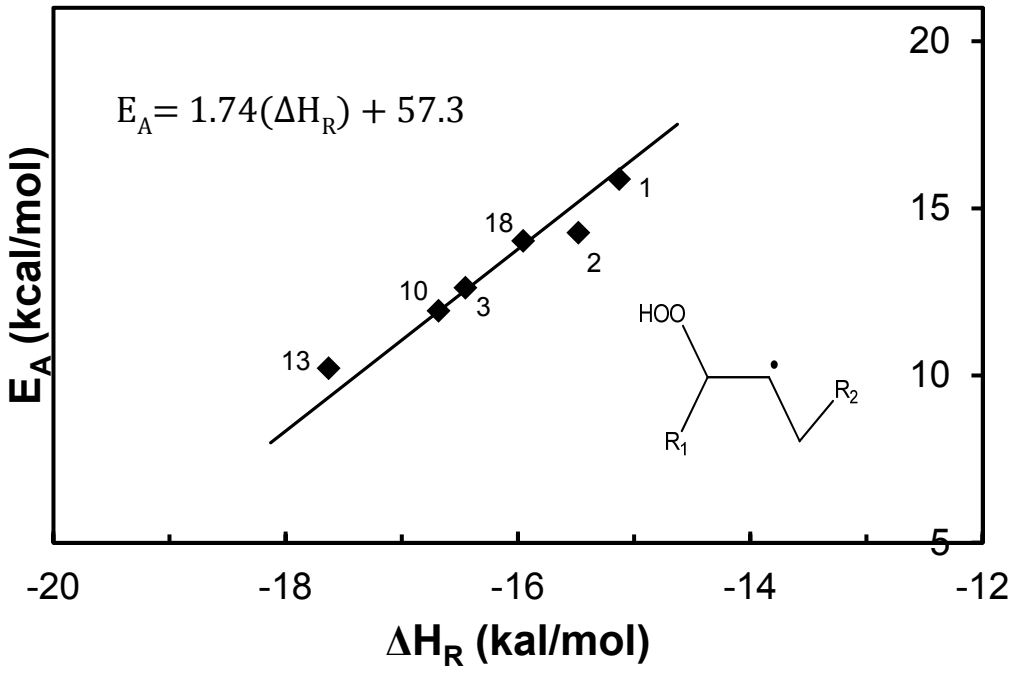

Figure 4.4. A closer examination of the Evans-Polanyi plot in the region of -15 to -20 kcal/mol. A new regression for only these points is provided. An example of the basic alkylhydroperoxy radical structure exhibited by the species in this region is shown and species numbers from Table 4.1 are also listed with their associated data point for ease of reference.

If these species are examined in isolation, a dramatically different structure−property relationship emerges. Linear regression in this region yields a relationship much more in line with previous structure−property relationships presented for this family by Wijaya et al.[133] and Villano et al.[137] as evidenced by the fact that the slope of the line is greater than 1. This effect arises because of the formation of a lower-energy product complex, as shown in Figure 4.5. As the O−O hydroperoxy bond lengthens, the small •OH leaving group is able to reorient and form a strong hydrogen bond with the oxygen atom of the epoxide group. Such lower-energy product complexes tend not to form for larger alkyl radical leaving groups because it is more difficult for the larger leaving groups to move into favorable conformations. Allylic hydroperoxy species such as 4, 5, and 14 also exhibit this complexation behavior and could ultimately form a separate

correlation with a steep slope greater than 1 as well, but the points were clustered over too small of a range of heats of reaction to draw such a conclusion. It is interesting to note that referencing the product complex when calculating the heat of reaction instead of the infinitely separated products shifts and collapses the points collected in Figure 4.4 into a more conventional Evans-Polanyi relationship with a slope less than one.

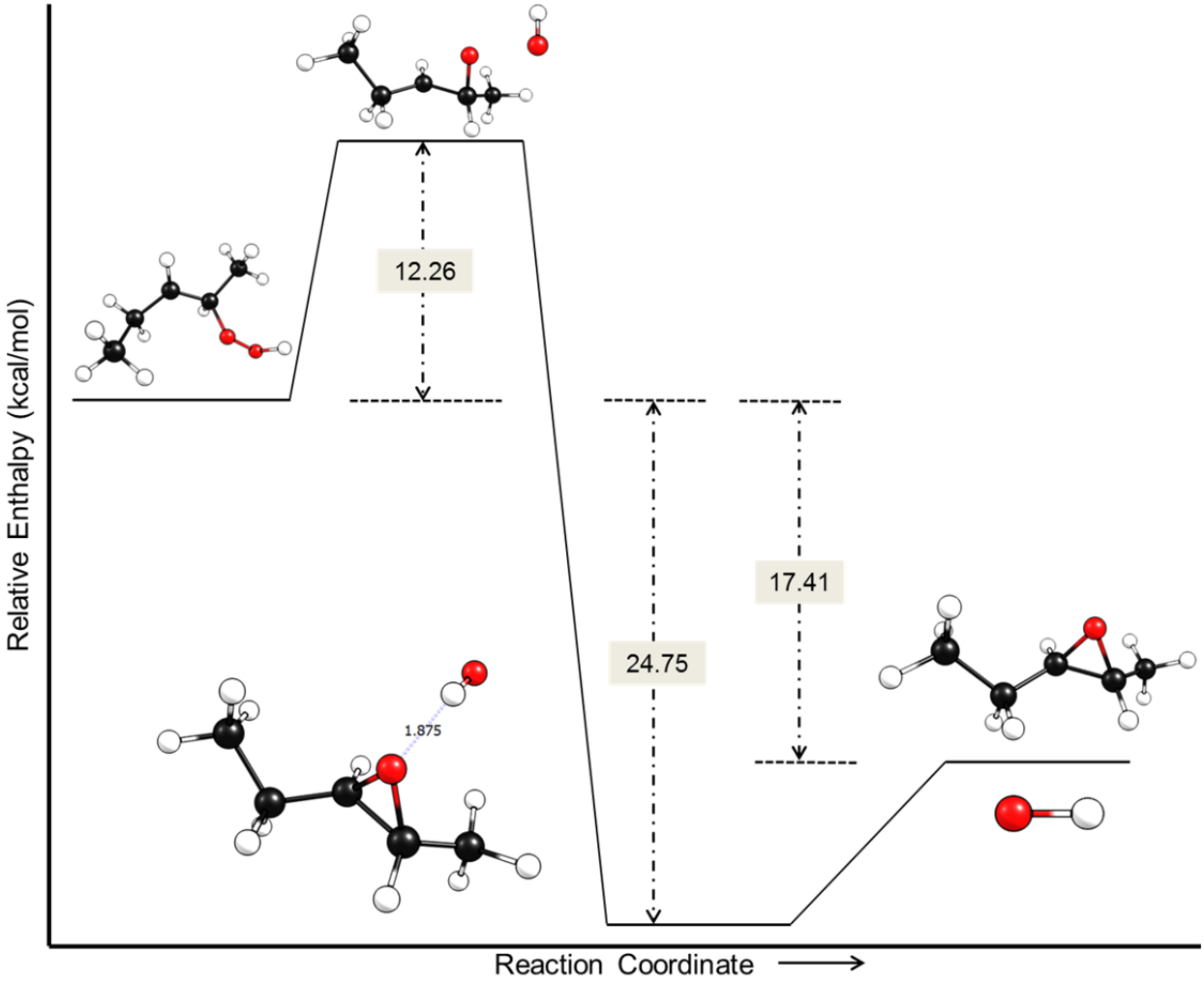

Figure 4.5. Representative enthalpy landscape constructed from G4 enthalpies at 298 K for reactant 10. This diagram reveals the formation of a low-energy complex. When the heat of reaction is referenced to this complex, an Evans−Polanyi relationship with a slope less than 1 is recovered.

However, as noted in a previous work,[147] it is more valuable to maintain an Evans−Polanyi relationship that is based on heats of reaction of the true reactants and products as these are the species for which heats of formation are available experimentally, from group additivity, or from straightforward quantum chemical calculations. Therefore, the relationship shown in Figure 4.4 would be the one used in the context of kinetic modeling.

This then raises the question of how finely chemical space should be divided such that a reaction family is broken into subfamilies. For example, if the points in Figure 4.4 were removed from the larger data set and a new overall correlation were regressed, the relations E_{fwd} = 0.44(ΔH_R) + 21.4 would emerge with improved R^2 values of 0.83 and a maximum residual of 2.5 kcal/mol. For kinetic models of the combustion of small alkanes for which only alkylhydroperoxy (QOOH) species are relevant, the more specific correlation derived in Figure 4.4 is more appropriate for use, especially because the largest deviations from the general correlation in Figure 4.2 occur in the ΔH_R range from -10 to -20 kcal/mol and could cause inaccuracies in the calculated kinetic parameters. However, this relationship cannot be used, or at least should be very critically examined, in cases where unsaturated species play a critical role or observed ΔH_R values extend beyond the narrow range cited above. Subdividing the chemical space into multiple reaction families based on the structure of the radical to enhance the accuracy of the calculated kinetic parameters is appealing, particularly when reaction mechanisms and parameters are determined with automated methods such as RMG,[148] NetGen[14] and others[149] that inherently tie the molecular structure to thermodynamic and kinetic properties by molecular graph representations and group additivity.

4.4 Conclusions

This work provides a structure−reactivity relationship for hydrocarbon epoxidation reactions that is broadly applicable over a range of heats of reaction covering a spectrum of moieties connected to the O−O link that is cleaved. This effort extends previous works in the literature that examined only very narrow ranges of values for the heat of reaction, and thus chemical functionalities, making the relationship less extensible to a variety of systems. In this work, a wide range of chemical space was explored to discern key trends and establish an Evans−Polanyi relationship for this family of epoxidation reactions, particularly capturing behavior due to the presence of conjugation for the first time. The Evans−Polanyi parameters, specifically the transfer coefficient, α, close to 0.5, are consistent with a symmetric transition state that has both reactant and product character.

Although a single Evans−Polanyi relationship captured all of the reactions reasonably well, close examination revealed that there are several key structural features that affect the nature of the calculated relationship. In particular, alkylhydroperoxy species have the ability to form low-energy product complexes. When the heat of reaction was referenced to this energy well, a classic Evans−Polanyi relationship was regressed narrowly for only these reactions, an α value greater than 1.0 resulted, and a correlation distinct from the overall Evans−Polanyi relationship was evident. Based on these observations, it is possible that the use of multiple Evans−Polanyi relationships for this family broken down by structural features might be desirable to enhance the accuracy of the calculated activation energies, and it is proposed that at least one subdivision be made, separating alkylhydroperoxy radicals from larger peroxy or allyllically stabilized radicals. Implementing such a strategy today is straightforward in the

context of kinetic modeling because of the availability of numerous computational tools that enable the determination of the molecular structures of species of interest and the on-the-fly calculation of kinetic parameters during the generation of a reaction mechanism.

This work also underscores the fact that Evans−Polanyi relationships, while extremely valuable tools that facilitate detailed mechanistic models of complicated processes with diverse species, should be used cautiously. If a relationship were derived from a set of molecules with insufficient diversity, errors could be introduced when its application was expanded to larger and more complex systems. When constructing a kinetic correlation, it is critical to explore a wide range of property values to be confident in the translatability of the resulting relationship to a variety of systems. In the context of hydrocarbon oxidation, it is recommend that relationships developed primarily for saturated systems be scrutinized closely, as it was observed that the addition of an allylic group had an appreciable effect on the resulting parameters for the epoxidation reaction studied here.

Chapter 5

An expanded microkinetic model for the condensed phase, cobalt catalyzed autoxidative curing of ethyl linoleate

5.1 Introduction

For centuries, artists have used natural oils as media to create some of the world's most valued painted objects.[16] The masters of today have an even greater range of oils and faster drying, synthetic oil-based alternatives, such as alkyds, available to them.[5,150] Frequently, transition metals are added either as pigment or explicitly as catalysts to speed drying times of the paint layers. Cobalt-based catalysts in particular have been the subject of much scrutiny because they are effective catalysts but would ideally be replaced by more environmentally friendly alternatives.[28,36,122,151–153] Understanding how these materials cure and age at the molecular level is of vital importance to both ensure the long term durability of painted surfaces as they experience a variety of chemical and mechanical stresses, as well as for designing effective catalytic mimics to replace undesirable additives. The early autoxidative curing regime establishes the composition of a crosslinked network that contributes to the long term structural integrity of the paint layer. Pathways that lead to the formation of non-crosslinked, usually small molecules, are also critical to understand as these species may be prone to extraction during cleaning or migration and escape from surfaces overtime which could affect the appearance of the object.

Computational kinetic modeling, specifically microkinetic modeling, has a natural and important role to play in the process of developing a deep mechanistic understanding of the

autoxidation of these types of materials. Microkinetic models are built from elementary steps and make no assumptions about rate-limiting reactions. Consequently, the role of numerous reactive intermediates can be examined and analyzed in a way that would be extremely difficult to capture experimentally. A variety of reaction conditions can be explored without having to obtain new parameter sets. Additionally, microkinetic models can be rapidly scaled to account for increased model complexity or new proposed pathways. However, the oil-based substrates of interest are usually a mixture of C18 fatty acid esters with varying degrees of unsaturation that chemically crosslink in the presence of oxygen and lead to extensive product diversity in the model that is prohibitive depending on how explicitly unique isomers are tracked. Automated computational tools to aid in model construction and representative model compounds such as individual fatty acid ethyl or methyl esters make this problem much more tractable while still allowing for important and applicable insights on the molecular level.

Very recently, gas phase microkinetic models have been created for polyunsaturated fatty acid esters substrates, predicting behavior such as ignition time for combustion.[154] However, condensed-phase models for these species have lagged. Without transition metal catalysts or elevated temperatures to initiate radicals, the autoxidative process occurs much more slowly, over timelines where it is challenging to manage the collection of experimental data for comparison. The preliminary model for this system presented in Chapters 2 and 3 was insufficient to completely capture experimental behavior due to a lack of higher order product diversity which placed stoichiometric limits on the model.[15] However, the results were promising in that a larger, more detailed model should close gaps between experimental data and theoretical predictions, especially by automating the process of generating the reaction

mechanism which is presented here. This work presents a detailed model of the autoxidation of a fatty acid ethyl ester that also includes a transition metal catalyst. With this model it was sought to both accurately describe experimental observations and make predictions about behavior at a variety of temperatures and catalyst concentrations.

5.2 The EL model system and autoxidation mechanism

5.2.1 Ethyl linoleate as a model system

Ethyl linoleate was chosen as an appropriate model system for oil and oil-based paint coatings for several reasons. Assuming that the curing chemistry of interest occurs primarily around the regions of unsaturation in the fatty acid tail, ethyl linoleate was a reasonable balance between the much less reactive oleic acid ester with a single double bond and the complexity of the product distribution observed for linolenic acid with three double bonds. Ethyl linoleate has been identified as a useful single component oil analog and model system for autoxidation in several experiments[28,30,32–34,36] and using this molecule as the oxidizing substrate allowed this information to be leveraged for the evaluation of the performance of the model. As in previous chapters, the model system presented here mimicked experimental conditions described by Oyman et al.[30] for effective comparison (e.g. 40g of ethyl linoleate with 0.07 wt% of Cobalt(II) 2-ethyl hexanoate (CoEH) catalyst) The system was assumed to have an excess of oxygen available for autoxidation and so the oxygen concentration of the system was fixed (dC/dt =0) at the saturation limit for dissolved O_2 (0.00218 mol/L) measured at 25°C in soybean oil which has a high linoleic acid content.[72,73] The system was then treated as a homogeneous batch reactor at 25°C.

5.2.2. Mechanism and kinetic parameters

Because of the large number of species involved in kinetic models of hydrocarbons, kinetic correlations derived for similar reaction types classified together as a reaction "family" are often utilized to reduce the number of parameters needed to characterize the reaction network when values are not readily available from experiment. In this work an Evans-Polanyi type correlation was frequently employed which, to reiterate, relates the thermodynamic quantity, the heat of reaction (ΔH_R) with the activation energy, E_A, via the equation $E_A = E_0 + \alpha\Delta H_R$, where E_0 is the intrinsic reaction barrier and α is the transfer coefficient.[13] A representative pre-expontential factor for each reaction family was also used. Heats of reaction were obtained using Benson's group additivity method[52] and a database of values from the *NIST Structure and Properties Database*[54] supplemented by the Broadbelt research group's own calculations as needed. A library of chemical mechanisms and kinetic parameters are discussed in a previous work.[15] Notable additions to this library included radical addition reactions which lead to the formation of larger oligomers by the addition of peroxy radicals across the readily available double bonds in the system, in particular, conjugated double bonds. The allylic radical could then isomerize and add molecular oxygen to continue to propagate the autoxidative process or a unimolecular epoxidation first proposed by Budnik and Kochi[128] could occur. A recent work discussed the development of Evans-Polanyi parameters for this reaction explicitly including the effects of unsaturation.[114] A final summary of the optimized parameter set for the microkinetic model is included in Section 5.4.

5.3 Computational Methods

5.3.1 Automated Mechanism Generation

Automated mechanism generators have greatly impacted the field of microkinetic modeling in recent decades, allowing for the exploration of increasingly complex systems.[148,149,155] Here the automated mechanism generator NetGen[14,156,157] was employed which operates on two key principles. First, while the number of elementary reaction steps, particularly for hydrocarbon oxidation, may be large, the number of different types of chemistry occurring, i.e. the number of "reaction families", is actually quite small. For example, the abstraction of a bi-allylic hydrogen by a peroxy radical may be described as a general reaction family that applies to all peroxy radicals in the system. The generation of the molecular graphs in adjacency matrix format of the subsequent hydroperoxide and carbon centered radical is implemented via a straightforward matrix addition operation that is made facile by the second principle which is that the number of atoms actually involved in the reaction is small and those atoms not participating in the reaction can be ignored during this step. An example of this matrix transformation is shown in Figure 5.1 for a β-scission reaction where the diagonal elements represent unpaired electrons on the atom and the off diagonal elements represent the degree of any bonds between the elements.

The representative hydrogen abstraction reaction family described above could be even more generalized to the simple abstraction of any hydrogen by any radical type, but it is valuable to add further constraints to reaction rules if different radical types needed to be treated uniquely when calculating kinetic rate constants or when certain reactions are unlikely to occur. In ethyl linoleate, abstraction of allylic and bi-allylic hydrogens are much more energetically favored

than the abstraction of hydrogens from sp^3 carbons which can be excluded from the mechanism by the formulation of the rule.

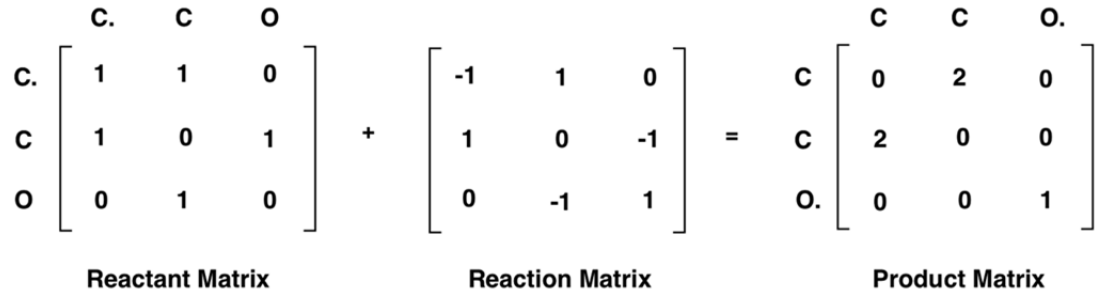

Figure 5.1. An example β-scission reaction matrix transformation where a C-O bond is broken by a carbon radical creating a C=C double bond and an oxygen radical.

Even when constraining reaction rules as described above, the mechanisms generated can be quite large. For radical systems forming oligomers through addition reactions, the mechanism can grow indefinitely without specifying a termination criteria such as the rank of stable products achieved[157] and the number of carbons allowed in a reacting molecule. Indeed, for the ethyl linoleate system and autoxidation reaction families the initial mechanism size with a termination rank criterion of 2 and a carbon limit of 40 (maximum oligomer size is a tetramer) was 68,197 species and 1,087,360 unique reactions. Since this was intractable to solve in a reliable and/or timely way, work proceeded using the rate based mechanism generation tools built into NetGen[86] which allowed for the calculation of kinetic rates on the fly and thus provided a method to pre-screen kinetically irrelevant reactions and species from the final mechanism.

The construction of a reaction network using a rate-based criterion to control the mechanism size required that the mechanism be simultaneously solved as it was formed. The particular information that must be supplied by the user to do this included reactor design

equations, reaction conditions and the necessary parameters to calculate thermodynamic and kinetic quantities as discussed above in Section 5.2.2. Additionally, the size of an initial pool of species, *s*, termed the "core" species was specified. These species are generated from the application of the reaction family rules to the set of given reactants. The new species formed from these reactions were considered "unreactive" until their rate of formation was high enough for a given time interval to exceed a calculated threshold and they were reclassified as "core" species. The reaction rules were again applied to new core species and the model was re-solved to track the rate of formation of each species in an iterative fashion until no new species were added to the core or the final reaction time was reached. This minimum rate of formation, R_{min}, threshold is calculated by determining the maximum rate of formation of the species in the current core population and multiplying it by a value, ε, that was also user-defined. Consequently, a smaller ε resulted in a smaller R_{min} and thus a larger mechanism as the threshold for promotion to a core reactive species is lowered.

Mechanisms generated with a specific ε and *s* parameter combination, were then judged to be viable based on two specific criteria. First, reaction channels to all experimentally observed products were required to be included in the model. Second, because the system included a catalytic species, it was imperative that all steps in the catalysis cycle for the decomposition of hydrogen peroxides, especially those regenerating the $Co^{(II)}$ catalyst, were included in the mechanism. Parameters for the selected mechanism that met both of these criteria and its resulting size are included in Table 5.1.

Table 5.1. Input variables *s* and ε for the automatically generated mechanism meeting the key criteria. The resulting size descriptors are presented in terms of the number of species, reactions and size of the largest oligomeric species generated.

Input Variables		**Automatically Generated Mechanism Size**		
Size of initial "core" species pool, *s*	User-defined Threshold, ε	Number of Species	Number of Unique Reactions	Maximum Oligomer Size
50	10^{-8}	1,374	2,898	6 (114 Carbons)

5.3.2 Microkinetic Modeling

With the automatically generated mechanism in hand, a stiff ordinary differential equation (ODE) solver[158] was used to generate concentration profiles. Since the cobalt catalyst is a conserved species, it was treated algebraically. While previous preliminary models of this EL system were solved using a stochastic Kinetic Monte Carlo framework based on the classic stochastic simulation algorithm (SSA) of Gillespie,[20,71] the calculations here proceed here using a deterministic model because of the ability to easily use gradient-based methods to perform parameter optimization. It should be noted that results from both the stochastic model of Chapter 2 and a deterministic version for the same mechanism are in agreement.

Parameter optimization was performed using GREG[159] which sought to minimize the objective function based on the sum of squared residuals (SSR) shown in Equation 5.1, where *y* are the lumped species concentrations of peroxides (in mmol/mol EL), the amount of oxygen absorbed by the system (in mol/mol EL) and the concentrations of volatile species hexanal and pentanal (in mmol/mol EL) for each time point *i*. A relative error in the experimental observations of 10% was used to weight the calculated residual.

$$SSR = \sum_i \left(\frac{\left(y_{obs}(i) - y_{model}(i)\right)}{0.1 \cdot y_{obs}(i)} \right)^2 \qquad (5.1)$$

5.4 Results

The microkinetic model was used to generate the concentration profiles of all 1,374 species up to 100 hours of curing time. For comparison to available experimental observations, data was lumped, such as in the case of the overall peroxide concentration, but other species were considered individually such as hexanal and pentanal. The use of computational tools to explicitly resolve and track unique isomers is valuable for the flexibility it provides for data analysis at multiple levels of resolution.

Our model results were compared to the quantitative data from Oyman et al.[30] which included the overall peroxide concentration of the system in Figure 5.2. This value comprises both hydroperoxide (ROOH) and peroxide (ROOR) groups, and both the models' total peroxide content for comparison to the experimental data and the breakdown of the contribution from hydroperoxide groups versus peroxy crosslinks are presented. From this division it became clearer that the maximum in peroxide content at about 30 hrs corresponds to the decomposition of the key intermediate hydroperoxide moieties and that the subsequent plateau was mostly indicative of the concentration peroxy bonds. The overall oxygen uptake of the system was also calculated from the model predictions and compared to experiment in Figure 5.3.

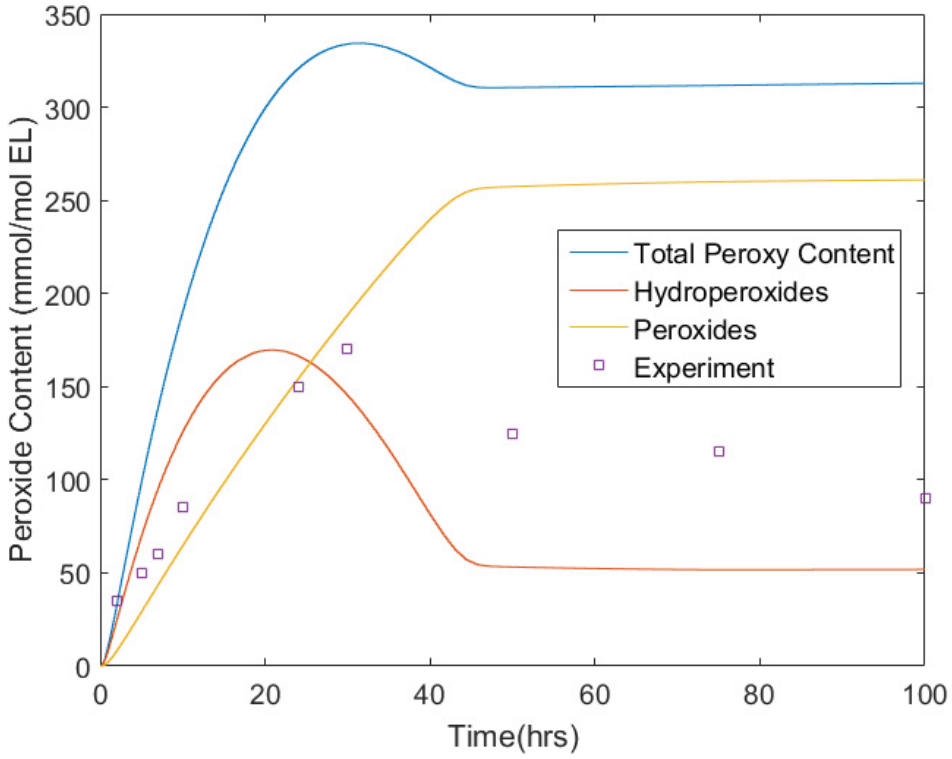

Figure 5.2. The evolution of the total peroxide content of the system (blue line) compared to results from Oyman et al.[30] The total peroxide content of the system predicted by the microkinetic model is broken down in the contributions from hydroperoxide functional groups (red line) and peroxide functional groups (yellow line).

Finally, the concentrations of the volatile species hexanal and pentanal were compared to the experimental results from Chapter 3 in Figure 5.4 which were obtained using a similar method to Oyman et al.[30] but filled in critical time points in the early 24 hours of curing in order to confirm mechanistic postulates for the formation of hexanal, in particular. Having these extra data points was extremely valuable during the process of parameter optimization. The amount of hexanal produced represents a significant improvement over the previous generations of EL models which first did not produce hexanal at all and then struggled to produce hexanal in sufficient quantities with the addition of new reaction channels due to the lack of coverage in the

model of larger oligomeric species. The final parameter set used to obtain these results is summarized in Table 5.2.

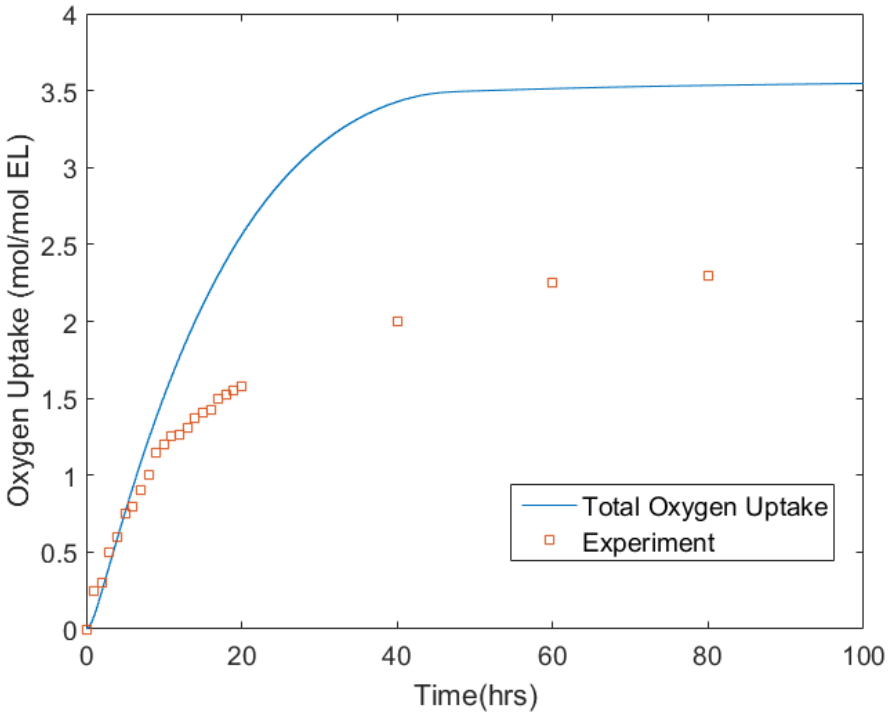

Figure 5.3. Comparison of the model prediction of the total oxygen uptake of the system (line) to experimental data from Oyman et al.[30] (points).

The parameters selected for optimization included two experimental rate constants for the abstraction of a bi-allylic hydrogen by a peroxy radical and the regeneration of the cobalt catalyst. Experience with the model has shown that the overall peroxide content and oxygen uptake is particularly sensitive to these two parameters. Similarly, adjusting kinetic parameters for radical addition and epoxidation reactions were particularly influential in controlling the concentration of hexanal in the system as radical addition reactions to conjugated double bonds create chain ends with a hydroperoxide moiety adjacent to peroxy group. When this hydroperoxide moiety is catalytically decomposed by cobalt Co(II), the resulting alkoxy radical

can undergo a facile beta scission reactions. The unimolecular decomposition of ROOR• competes with the formation of the adjacent hydroperoxy-peroxy structure so it is not surprising that the recommend parameters decreased the barrier for radical addition and also decreased the pre-exponential factor for the epoxidation reaction. Parameters were optimized within reasonable boundaries that correspond roughly to the largest expected error in rate constants generated from computational methods such as quantum chemical calculations, which is plus or minus a factor of 10.

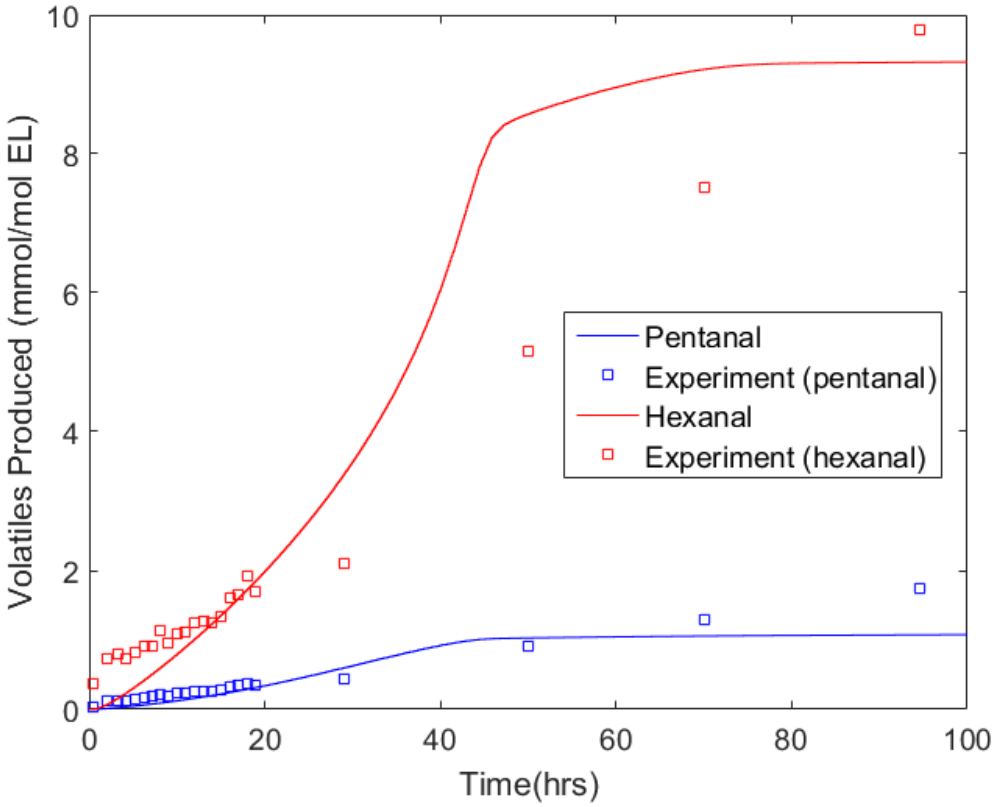

Figure 5.4. A comparison of the production of volatile species to experimental data for the small molecules pentanal (blue lines and points) and hexanal (red lines and points).

Table 5.2. Kinetic parameters for the microkinetic model with units for k and A in L/mol•s (bimolecular) or s^{-1} (unimolecular) and E_0 in kcal/mol.

Reaction Family	Representative Reactions	Reported *k*	Parameters A	E_0	α_{fwd}[a]	References
Initiation	$Co^{II} + O_2 \leftrightarrow Co^{III}OO•$	6.66×10^{-5}				36
O_2 Addition	$R• + O_2 \rightarrow ROO•$		10^8	0	0	53
Hydroperoxide formation	$ROO• + RH \rightarrow ROOH + R•$	0.9242*				62,63
Hydroperoxide decomposition	$ROOH + Co^{II} \rightarrow RO• + [Co^{III}OH^-]$	0.5				47,64,65
	$ROOH + [Co^{III}OH^-] \rightarrow [Co^{III}OOR] + H_2O$	2				
	$[Co^{III}OOR] \rightarrow Co^{II} + ROO•$	.0095*				
Radical Addition[b]	$ROO• + C{=}C \rightarrow ROOR•$		10^8, $3.61\times10^{9,c}$	11.24*	0.24	99
Epoxidation	$ROOR• \rightarrow RO(epox) + RO•$		8.59×10^{10}*	21.9	0.51	114
β-Scission	$RO• \rightarrow R'C(O)H + R''•$		10^{14}	9.5	0.85	53
Hydrogen Transfer	$R• + R'H \rightarrow RH + R'•$		10^7	9.1	0.7	53
	$RO• + R'H \rightarrow ROH + R'•$			11.9	0.91	
	$ROO• + R'C(O)H \rightarrow ROOH + R'C(O)•$			6.2	1	
	$RC(O)OO• + R'H \rightarrow RC(O)OOH + R'•$			3.05	1.1	
Disporportionation	$2ROO• \rightarrow R(O) + ROH + O_2$		10^5	0	0	53,66
	$2ROO• \rightarrow 2RO• + O_2$					
Recombination	$2R• \rightarrow RR$		10^8	RT	0	53–63
	$ROO• + R• \rightarrow ROOR$					
	$RO• + R• \rightarrow ROR$					
	$ROO• + ROO• \rightarrow ROOR + O_2$		10^6, $4.08\times10^{9,d}$			
Baeyer-Villiger	$RCOOOH + RC(O)H \rightarrow 2RCOOH$		1.2×10^4	8.5	0	53

[a]See Pfaendenter and Broadbelt [53] for definitions of $\alpha_{fwd.,}$ [b]Radical addition reactions forming allylic radicals are allowed to rapidly isomerize, however this reaction family is used only for bookkeeping purposes. [c,d] Separate pre-exponential factors were utilized for small molecules HO• and HOO• respectively, *optimized

The overall agreement between model and experiment was qualitatively good, matching key structural features in the experimental data. However, the good quantitative agreement in the early 10 hours of curing falls off at longer times scales for peroxide concentration and oxygen uptake where the concentrations are overestimated, oxygen uptake by a seemingly very precise 1 mol of O_2. However, optimizing parameters to reduce this disagreement resulted in the suppression of the production of hexanal relative to the results presented above. A deeper exploration of the mechanistic steps included in the model based on the rate-based criterion reveals why this overestimate of oxygen uptake and peroxide content are tied to the production of hexanal in a stoichiometric way.

By examining the structure of the alkoxy radicals that decompose to form hexanal, it became clear that they were primarily "over-oxidized" reactants, a term which reflects that the net moles of oxygen added to the molecule exceeds that of the predicted experimental value (slightly greater than 2). By revisiting Figure 3.10 and following the chain of reactions reproduced in Figure 5.6 to observe where oxygen is absorbed by the system on the pathway to form hexanal reveals how 3 mols of O_2 are readily incorporated into the reacting species.

Because oxygen adds so rapidly to carbon-centered radicals, the model favors the production of species like C) in Figure 5.6. Pathways competitive with mechanistic step 3 exist (examples shown as routes to species D & E in Figure 5.6), but did either not pass the rate-based threshold in the mechanism generation phase or are not very competitive with oxygen addition. Additionally, if species D & E can be formed in higher quantities, channels to the formation of hexanal must also be included in the model. Currently the model includes pathways from species D to hexanal, but again contribute in a minor way, but pathways from species E are not included.

This analysis offers insight into two ways to enhance model agreement. First, there is the inclusion of more reactions in the mechanism during the network generation step to incorporate more routes to hexanal from less oxidized species. Secondly, is curbing the rate of oxygen addition by using a different pre-exponential factor, particularly for higher rank, larger products to avoid over oxidation. Support for this comes from the fact that at early time scales where oxygen is primarly being absorbed to form species A, model agreement with experiment is good, but drifts at longer times. It is possible that for larger molecules, oxygen addition is not as rapid due to increased steric constraints and the possibility of more facile intra-molecular reactions which is not captured in the current generation of the model. By subdividing the oxygen addition reaction family to be described by multiple kinetic parameters, model agreement for the oxygen addition and peroxide content can be tuned and improved without overly suppressing hexanal production. These postulates can be easily tested within the framework of the microkinetic model.

Additionally, the experimental set-up for obtaining peroxide data used the largest quantity of EL material in the smallest container. Compared to the oxygen uptake and headspace analysis experimental geometries, the percentage of surface area of the sample exposed to air is much lower. Although EL does not form a skin while curing, the layer thickness may imply some mass transport limitations and an oxygen concentration gradient through the sample that may make optimizing agreement with all three data sets simultaneously a challenge.

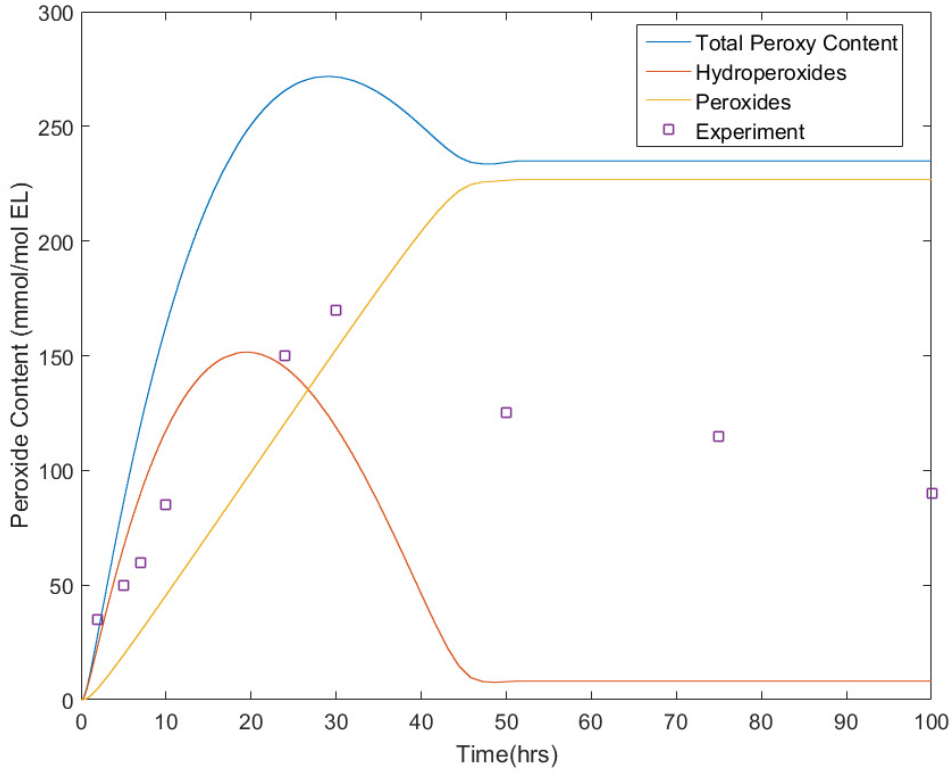

Figure 5.5 Model predictions for the peroxide content of the system generated with 67 model parameters. The two additional parameters suppressed the addition of oxygen to larger radicals and therefore reduced the amount of peroxides in the system to better agree with experiment.[30]

A comparison of Figure 5.2 and Figure 5.5 demonstrates the most significant improvement when two additional pre-exponential factors, a factor of 20 lower than the reported 10^8 M s^{-1} in Table 5.2, were implemented to describe subdivisions in the oxygen addition family to account for molecular size and steric hindrance. Implementing more parameters is a logical way to improve model agreement, however best practice for making changes such as this that alter the ratios of rates between competing mechanistic steps would be to regenerate the reaction network with these newly optimized parameters to ensure consistency and a complete mechanism.

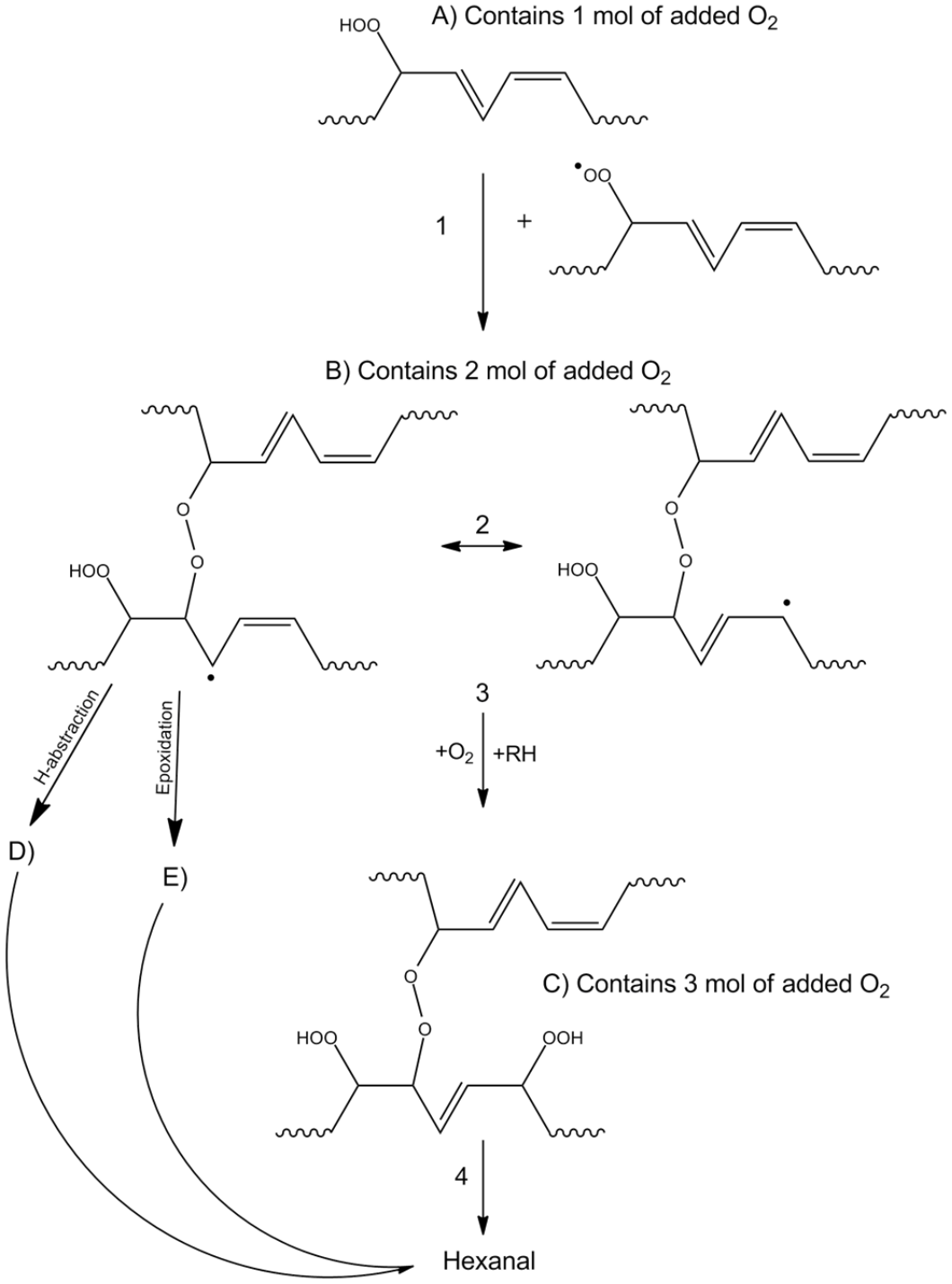

Figure 5.6. Schematic of representative mechanistic steps that lead to hexanal from over-oxidized reactant C). Ideally if mechanistic step 3 could be avoided by increasing the competition to form reactants D) & E) and ensuring routes exist in the model to form hexanal from these species, model agreement could be improved.

The evolution of oligomers is presented in Figure 5.7. Species were categorized based on the number of carbon atoms in the molecule (EL initially contains 20) with each oligomer type representing a range of molecule sizes. Dimers were classified as compounds with a carbon number C, $20 < C \leq 40$, trimers were described as $40 < C \leq 60$, etc. Muizebelt et al.[32] observed mass fragments from mass spectrometry corresponding to pentamers and Oyman et al.[30] resolved peaks via size exclusion chromatography (SEC) for up to tetramers as well as higher order species.

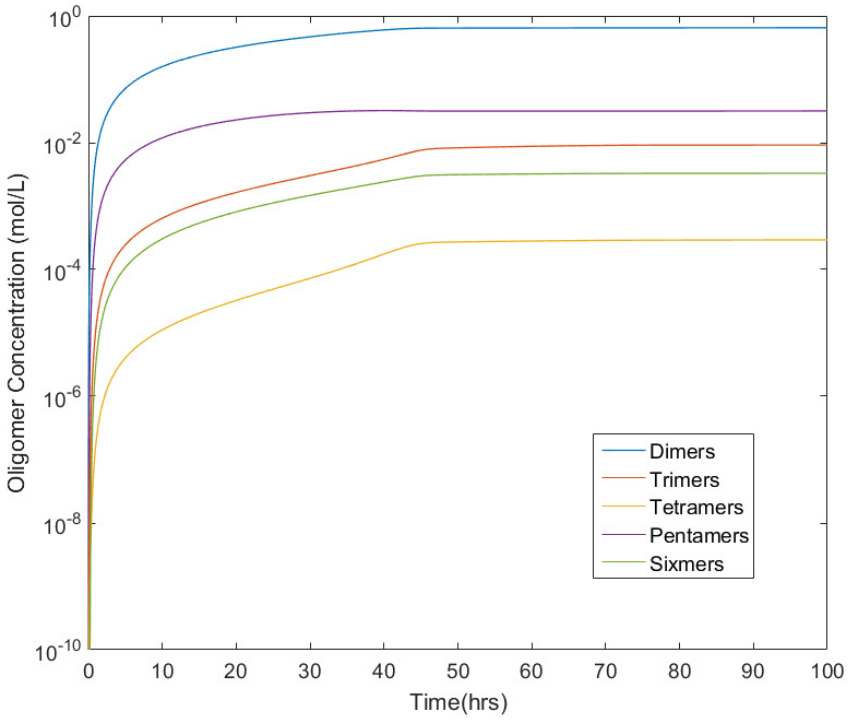

Figure 5.7. The evolution of the concentration of oligomeric species. Species were classified as dimers, trimers, etc. based on the number of carbons in the molecule.

Our model also predicts the concentration of other oxygen containing functional groups, particularly ketones, alcohols and carboxylic acids as shown in Figure 5.8 which were observed in another work by Oyman et al.[34] but not quantified. Muizebelt et al.[32] also observed a

significant concentration of epoxide functional groups (~10 mol% at 24 hours) during the oxidation of ethyl linoleate with a cobalt catalyst which the model seems to capture well as the predicted concentration on the order of 100 mM is approximately 10% of the concentration of the initial starting material.

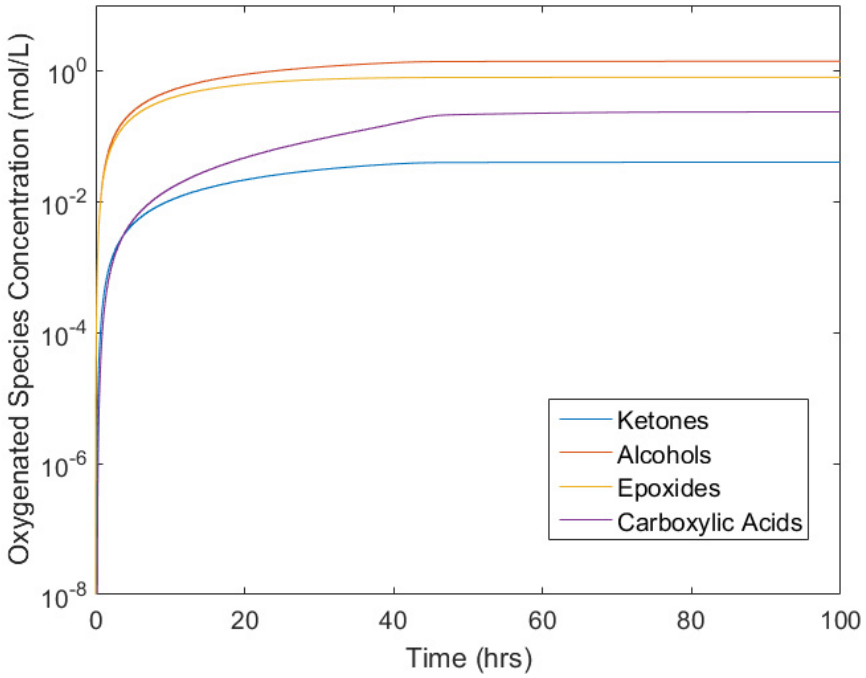

Figure 5.8. The microkinetic model predictions for key functional groups containing oxygen during the first 100 hrs of cure time. These species were observed experimentally but not necessarily well quantified for model comparison.

Muizebelt also observed the slow decay in the number of double bonded carbons in the system which persisted in the system for up to a year. The predictions for the evolving concentration of double bonds in the system during the early cure regime include an initial drop followed by a regime of extremely slow consumption as shown in Figure 5.9. Further analysis of these double bonds reproduced the progression observed by Oyman et al.[34] that non-conjugated double bonds are transformed to conjugated double bonds which then are further consumed via

radical addition to form single isolated allylic groups as oxidation proceeds. The model prediction of the percentage of conjugated double bonds in the system (~25 %) at 24 hours matches with the experimental value presented by Oyman et al.[34] from ^{13}C NMR that approximately 1 out 4 double bonded carbons per EL molecule are due to conjugated C=C double bonds.

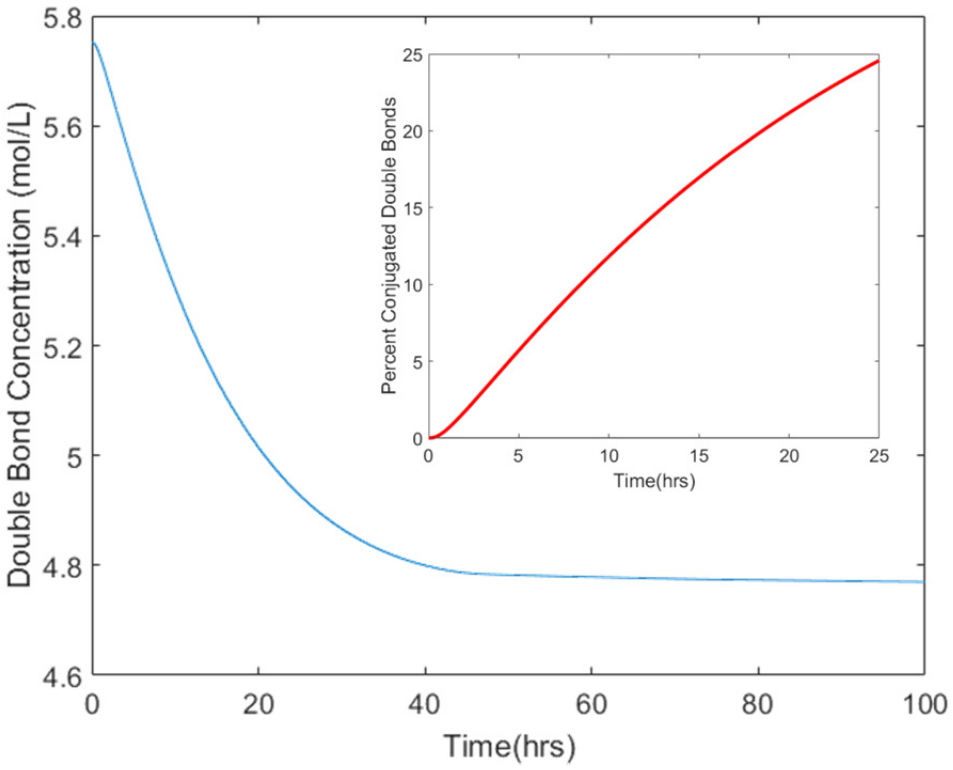

Figure 5.9. Microkinetic model predictions for the consumption of double bonds over 100 hours of curing time. The inset tracks the percentage of double bonds that exist in conjugated form.

After examining the descriptive capabilities of the model its predictive capabilities were explored. The model was used to observe the effect of the concentration of the catalyst. The influence of the catalyst concentration on the rate of autoxidation was shown most dramatically in the rate of consumption of hydroperoxides in Figure 5.10 as the peak shifted dramatically to

the left as the amount of cobalt in the system increased. Starting from the initial amount of 0.07 wt %, the amount of catalyst was steadily increased until a peak in the hydroperoxide curve was no longer observed at 1.4 wt %. Note that this amount is still less than when catalyst can start to become inactive by complexing with a second cobalt species.[47,152]

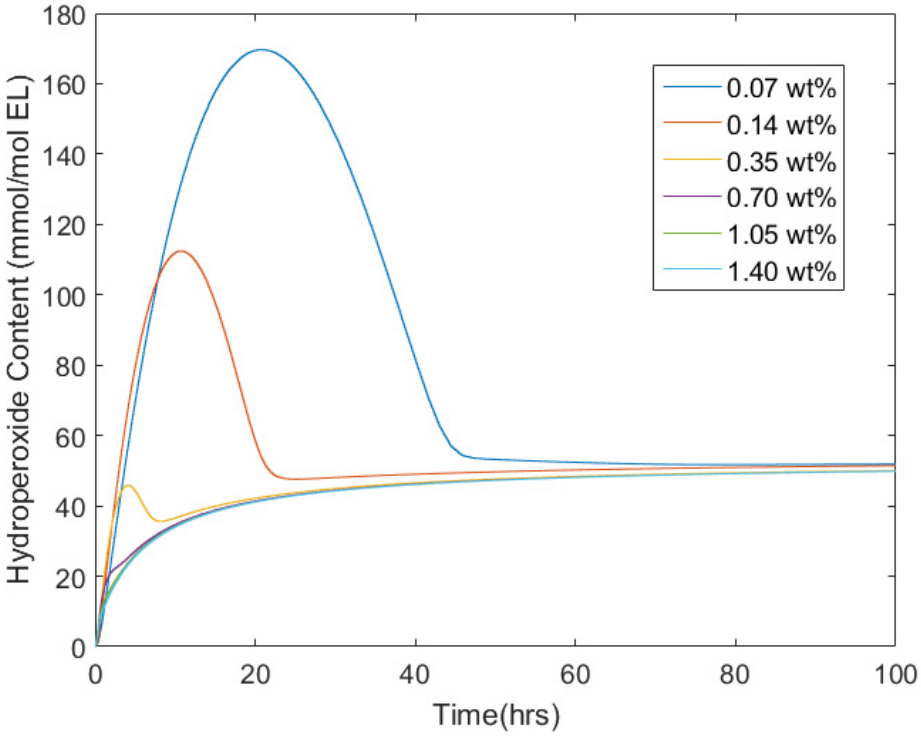

Figure 5.10. Microkinetic model predictions of the concentration profiles for lumped hydroperoxide species at catalyst concentrations ranging from 0.07 to 1.4 wt%. Increasing the amount of cobalt in the system dramatically increased the rate of consumption of these functional groups to form radicals.

Finally, the microkinetic model was used to examine the effects of temperature on the rate of autoxidative curing. Although the range of temperatures selected from 25°C to 60°C is relatively narrow and mild, it includes temperatures relevant for art conservation under typical storage and display conditions as well as temperatures used to artificially age paint mock-ups for study. The effect is best visualized by the rapid increase in the rate of double bond consumption as shown in Figure 5.11 as a proxy for the consumption of the EL substrate.

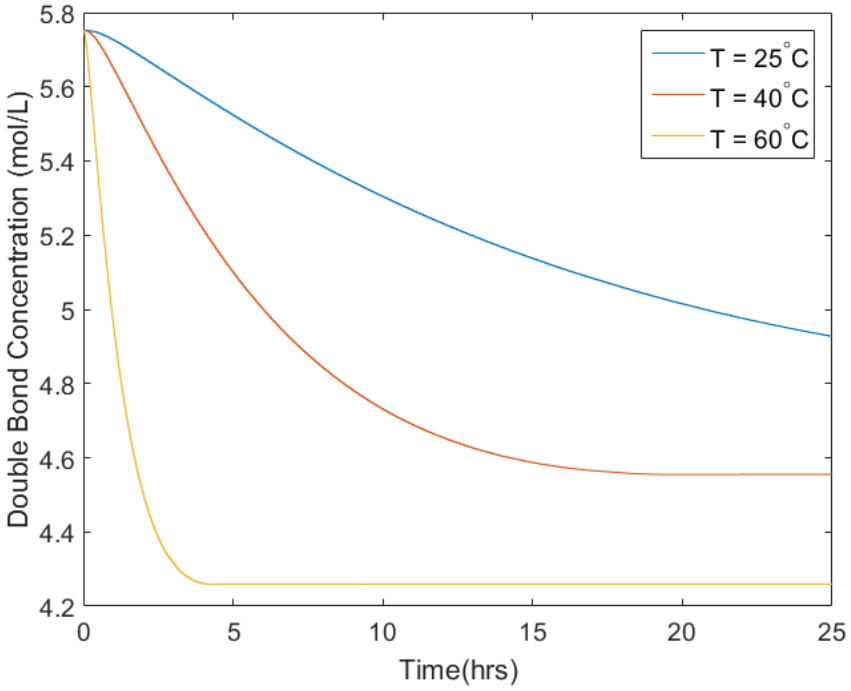

Figure 5.11. Microkinetic model predictions for the consumption of double bonds at increasing temperatures from 25 to 60°C for 25 hours.

5.5 Conclusions

The microkinetic model constructed using rate based automated mechanism generation techniques represents a significant improvement over previous generations of the EL model due to enhanced mechanistic detail and subsequent descriptive power for metrics of model performance that were previously problematic such as oxygen uptake and the production of hexanal. The predictive capabilities of the model were tested by varying two main system parameters, the reaction temperature and catalyst concentration. Increasing both of these parameters displayed similar effects, namely that the rate of production and consumption of hydroperoxides was rapidly increased and the length of time required to convert the EL substrate changed from on the order of days to hours.

The evolution of several key chemical moieties such as ketones, alcohols and carboxylic acids were also predicted. While the concentrations of these species have not been explicitly quantified experimentally for this model system, this data would be useful to continue to push the model towards increasing complexity and therefore an increasingly applicable representation of a paint layer. In particular, the quantification of carboxylic acid functionality would be relevant to the field of cultural heritage science as free fatty acid groups are expected to complex with transition metals to form soaps in later stages of aging.[160] When these soaps aggregate and migrate, significant damage can occur to paint layers.[161]

Models of low temperature, condensed phase oxidation in the presence of transition metals offer significant value as a method to obtain deeper mechanistic insights for a variety of fields interested in autoxidative processes, including and beyond art conservation. For instance, in biological systems these pathways are studied for their possible contribution to disease[43,162] or in the food industry where oxidation of oils can lead to undesirable odors or tastes.[120,163] Constructing detailed kinetic models for these large polyunsaturated fatty acid ester substrates is a complex undertaking where the boundaries can be continually pushed with ever-improving computational methods and resources.

Chapter 6

Summary and Future Perspectives

Several important overall conclusions can be drawn from this work describing the construction of a microkinetic model for the autoxidative curing of ethyl linoleate. The model results presented in Chapter 2 highlight the necessity of computational automation for the construction of detailed mechanistic models for polyunsaturated hydrocarbon systems, as manual construction can lead to the imposition of stoichiometric limits on the reaction progress and an inability to achieve qualitative and quantitative agreement for some metrics. However, even in this relatively small model, error in the prevailing mechanistic assumption in the literature for the production of the small volatile molecule hexanal was evident.

This error was discovered because of the resolution of the model at the molecular level which might have been otherwise missed if the model only predicted lumped concentrations of the chemical moieties of interest. Accurate mechanisms for these small molecule non-crosslinked species are key for extracting valuable information for the cultural heritage science community about extractable components of cured paint layers that may be at risk during cleaning.

The review of mechanistic postulates for the production hexanal in Chapter 3 again highlights the usefulness of microkinetic models for interrogating mechanistic assumptions, as the kinetic relevance of multiple competing reaction channels can be assessed simultaneously. From the evaluation of the set of assembled mechanistic pathways and their associated kinetic parameters within the context of the microkinetic model, scission of higher rank oligomers was

determined to be the major source of volatile hexanal. Enhanced confidence in this proposed mechanism was derived from the creation of a more complete experimental data set to compare against modeling results in the early cure regime (< 24 hrs) where the emergence of kinetic signatures would be observed.

Chapter 4 adds a cautionary note to the development of the kinetic model. Because experimental rate constants for most of the elementary steps considered in this model are rare, the accuracy of the model is highly dependent on achieving good estimates for rate constants from computational methods. Due to the relatively mild reaction conditions of interest, small variations Arrhenius parameters can have a large impact on derived rate constants and thus the model results. While the use of kinetic correlations is a very useful strategy to develop large and detailed models for hydrocarbon oxidation, if they are created from a very limited number of substrates or only regressed over a narrow thermodynamic range the extensibility of these correlations may be suspect. In the case of epoxidation reactions, we observed completely different regression behavior between unsaturated and saturated radical reactants and thus recommend that at least two correlations be used to accurately parameterize this reaction family.

The second generation model presented in Chapter 5 of this thesis represents the most detailed model of the condensed phase curing reactions of a large, polyunsaturated fatty acid ester to date that also includes the active role of a transition metal catalyst. Tempering the size of the automatically generated reaction mechanism using a rate-based screening criterion resulted in a mechanism that contained routes to all experimentally observed moieties, contained routes to form a diversity of large crosslinked species, and was still reasonably sized enough to be solved quickly for 100 hours of curing time. The model displayed improved qualitative and quantitative

agreement for several metrics. The model was also able to predict accelerated rates of curing for increased concentrations of cobalt catalyst as well as increased temperature and it is anticipated that the predictive power of the model could be expanded even further with more quantitative experimental training data sets.

Opportunities to build on this work and generate kinetic models for increasingly relevant oil-paint model systems include simulating mixtures of fatty acid esters with varying degrees of unsaturation in the fatty acid tail. Because of the nature of automated mechanism generation which applies a set of chemistry rules to a particular molecular substructure, the scale up between ethyl linoleate with two bi-allylic hydrogens and linolenic acid with four is natural although the product distribution is extremely more complex and requires large computational resources to manage at such a high level of detail.

Additionally, the model could be extended to examine longer time scales by calculating kinetic rate constants for hydrolysis reactions which break down ester bonds as the paint binder ages and lead to the formation of diacid and free fatty acid species. Conservators often use these diacids as a metric to estimate of the age of a painting as a function of the degree of hydrolysis or as evidence to determine if an oil binder was pre-treated before use to shorten drying times.[164,165] The complexation of free fatty acid components with metallic species in oil paint layers is also an extremely active area of research in the field where computational kinetic models could provide useful insight given that the time scales of such phenomena are difficult to capture experimentally.[166,167]

The detailed and dynamic description of the curing system generated by fully mechanistic models could also be used to provide guidelines for models of oil paint conducted at different time and length scales. For example, atomistic molecular dynamics simulations can be used to explore the interactions of solvent molecules used for cleaning and treatment with the cured network to assess the expected diffusion and penetration from the surface into a paint layer as well as how other properties such as the modulus and glass transition temperature might be affected. Formulating the initial starting state for these simulations could be directed by data from the microkinetic model in terms of the extracted percentages of crosslink type (RR, ROR, or ROOR) and other functional groups in the system.

The construction of a microkinetic model for the curing of an oil-based paint model system has introduced an important platform for interpreting experimental results and deepening the current understanding of the underlying chemical mechanisms. Adding computation and simulation to the cultural heritage science toolkit for studying curing and aging pathways offers an ability to interrogate mechanistic assumptions, correlate the chemical evolution of the system with changes in mechanical properties,[168] and extract information relevant for designing improved artificial aging protocols to create increasingly accurate mock ups for testing conservation treatments and appropriate storage and display conditions of priceless artworks. Indeed, oil-based paint media are not the only materials that can benefit from the mechanistic understanding generated by modeling tools. Objects containing relatively modern plastics and rubbers can be particularly sensitive to thermal and photodegradative processes.[98] Adapting models for the curing and aging of materials such as polystyrene[24,169] to the cultural heritage context opens many new avenues for investigation, achieving a primary aim of the field.

References

(1) Leona, M.; Van Duyne, R. P.; Trentelman, K.; Casadio, F.; Berrie, B.; Faber, K. T.; Ernst, R.; Sgamellotti, A.; Whitmore, P. *Chemistry and Materials Research at the Interface between Science and Art*; 2009.

(2) Feller, R. L. *Accelerated Aging: Photochemical and Thermal Aspects*; Research in conservation; Getty Conservation Institute: Marina del Rey, CA, 1994.

(3) Erhardt, D.; Tumosa, C. S.; Mecklenburg, M. F. Long Term Chemical and Physical Processes in Oil Paint Films. *Stud. Conserv.* **2005**, *50* (2), 143–150.

(4) Erhardt, D.; Tumosa, C. S.; Mecklenburg, M. F. Natural and Accelerated Thermal Aging of Oil Paint Films. In *Tradition and Innovation, Advances in Conservation, IIC*; Melbourne, 2000; pp 65–69.

(5) Ploeger, R.; Scalarone, D.; Chiantore, O. The Characterization of Commercial Artists Alkyd Paints. *J. Cult. Herit.* **2008**, *9* (4), 412–419 DOI: 10.1016/j.culher.2008.01.007.

(6) Lazzari, M.; Chiantore, O. Drying and Oxidative Degradation of Linseed Oil. *Polym. Degrad. Stab.* **1999**, *65* (2), 303–313.

(7) Sutherland, K. Measurements of Solvent Cleaning Effects on Oil Paintings. *J. Am. Inst. Conserv.* **2006**, *45* (3), 211–226.

(8) Sutherland, K. Solvent-Extractable Components of Linseed Oil Paint Films. *Stud. Conserv.* **2003**, *48* (2), 111–135.

(9) Mills, J.; White, R. *Organic Chemistry of Museum Objects, Second Edition*, 2nd ed.; Butterworth-Heinemann, 2000.

(10) Jensen, F. *Introduction to Computational Chemistry*, 2nd ed.; Wiley: West Sussex, 2007.

(11) Lewars, E. *Computational Chemistry: Introduction to the Theory and Applications of Molecular and Quantum Mechanics*; Springer: Dordrecht [Netherlands]; London; New York, 2011.

(12) Gorelsky, S. I. Software for Computational Chemistry. In *Comprehensive Coordination Chemistry II*; Elsevier, 2003; Vol. 2, pp 687–689.

(13) Evans, M. G.; Polanyi, M. Inertia and Driving Force of Chemical Reactions. *Trans Faraday Soc* **1938**, *34*, 11–24.

(14) Broadbelt, L. J.; Stark, S. M.; Klein, M. T. Computer Generated Pyrolysis Modeling: On-the-Fly Generation of Species, Reactions, and Rates. *Ind. Eng. Chem. Res.* **1994**, *33* (4), 790–799.

(15) Oakley, L. H.; Casadio, F.; Shull, K. R.; Broadbelt, L. J. Microkinetic Modeling of the Autoxidative Curing of an Alkyd and Oil-Based Paint Model System. *Appl. Phys. A* **2015**, *121* (3), 869–878 DOI: 10.1007/s00339-015-9363-1.

(16) Eastlake, C. L. *Materials for a History of Oil Painting*, 1st ed.; Longman, Brown, Green, and Longmans: London, 1847; Vol. 1.

(17) Mecklenburg, M. F.; Tumosa, C. S. Traditional Oil Paints: The Effects of Long-Term Chemical and Mechanical Properties on Restoration Efforts. *MRS Bull.* **2001**, *26* (1), 51–54 DOI: 10.1557/mrs2001.19.

(18) Ploeger, R.; Scalarone, D.; Chiantore, O. Thermal Analytical Study of the Oxidative Stability of Artists' Alkyd Paints. *Polym. Degrad. Stab.* **2009**, *94* (11), 2036–2041 DOI: 10.1016/j.polymdegradstab.2009.07.018.

(19) Vinu, R.; Broadbelt, L. J. Unraveling Reaction Pathways and Specifying Reaction Kinetics for Complex Systems. *Annu. Rev. Chem. Biomol. Eng.* **2012**, *3* (1), 29–54 DOI: 10.1146/annurev-chembioeng-062011-081108.

(20) Gillespie, D. T. A General Method for Numerically Simulating the Stochastic Time Evolution of Coupled Chemical Reactions. *J. Comput. Phys.* **1976**, *22* (4), 403–434.

(21) Wang, L.; Broadbelt, L. J. Explicit Sequence of Styrene/Methyl Methacrylate Gradient Copolymers Synthesized by Forced Gradient Copolymerization with Nitroxide-Mediated Controlled Radical Polymerization. *Macromolecules* **2009**, *42* (20), 7961–7968.

(22) Wang, L.; Broadbelt, L. J. Tracking Explicit Chain Sequence in Kinetic Monte Carlo Simulations. *Macromol. Theory Simul.* **2011**, *20* (1), 54–64.

(23) Wang, L.; Broadbelt, L. J. Model-Based Design for Preparing Styrene/Methyl Methacrylate Structural Gradient Copolymers. *Macromol. Theory Simul.* **2011**, *20* (3), 191–204.

(24) Vinu, R.; Levine, S. E.; Wang, L.; Broadbelt, L. J. Detailed Mechanistic Modeling of Poly (Styrene Peroxide) Pyrolysis Using Kinetic Monte Carlo Simulation. *Chem. Eng. Sci.* **2012**, *69* (1), 456–471.

(25) Hartshorn, J. H. Applications of FTIR to Paint Analysis. In *Analysis of Paints and Related Materials: Current Techniques for Solving Coatings Problems*; American Society for Testing and Materials: Philadelphia, 1992; pp 127–147.

(26) Warzeska, S. T.; Zonneveld, M.; van Gorkum, R.; Muizebelt, W. J.; Bouwman, E.; Reedijk, J. The Influence of Bipyridine on the Drying of Alkyd Paints: A Model Study. *Prog. Org. Coat.* **2002**, *44* (3), 243–248.

(27) Mallégol, J.; Lemaire, J.; Gardette, J.-L. Drier Influence on the Curing of Linseed Oil. *Prog. Org. Coat.* **2000**, *39* (2), 107–113.

(28) Liu, Z.; Kooijman, H.; Spek, A. L.; Bouwman, E. New Manganese-Based Catalyst Systems for Alkyd Paint Drying. *Prog. Org. Coat.* **2007**, *60* (4), 343–349 DOI: 10.1016/j.porgcoat.2007.08.003.

(29) Oyman, Z. O.; Ming, W.; Linde, R. van der. Oxidation of Drying Oils Containing Non-Conjugated and Conjugated Double Bonds Catalyzed by a Cobalt Catalyst. *Prog. Org. Coat.* **2005**, *54* (3), 198–204 DOI: 10.1016/j.porgcoat.2005.06.004.

(30) Oyman, Z. O.; Ming, W.; van der Linde, R.; van Gorkum, R.; Bouwman, E. Effect of [Mn(acac)3] and Its Combination with 2,2-Bipyridine on the Autoxidation and Oligomerisation of Ethyl Linoleate. *Polymer* **2005**, *46* (6), 1731–1738 DOI: 10.1016/j.polymer.2004.12.045.

(31) Ellis, G.; Claybourn, M.; Richards, S. E. The Application of Fourier Transform Raman Spectroscopy to the Study of Paint Systems. *Spectrochim. Acta Part Mol. Spectrosc.* **1990**, *46* (2), 227–241 DOI: 10.1016/0584-8539(90)80092-D.

(32) Muizebelt, W. J.; Hubert, J. C.; Venderbosch, R. A. M. Mechanistic Study of Drying of Alkyd Resins Using Ethyl Linoleate as a Model Substance. *Prog. Org. Coat.* **1994**, *24*, 263–279.

(33) Muizebelt, W. J.; Donkerbroek, J. J.; Nielen, M. W. F.; Hussem, J. B.; Biemond, M. E. F.; Klaasen, R. P.; Zabel, K. H. Oxidative Crosslinking of Alkyd Resins Studied with Mass Spectrometry and NMR Using Model Compounds. *J. Coat. Technol.* **1998**, *70* (876), 83–93.

(34) Oyman, Z. O.; Ming, W.; van der Linde, R. Oxidation of 13C-Labeled Ethyl Linoleate Monitored and Quantitatively Analyzed by 13C NMR. *Eur. Polym. J.* **2006**, *42* (6), 1342–1348 DOI: 10.1016/j.eurpolymj.2005.12.003.

(35) Muizebelt, W. J.; Nielen, M. W. F. Oxidative Crosslinking of Unsaturated Fatty Acids Studied with Mass Spectrometry.pdf. *J. Mass Spectrom.* **1996**, *31*, 545–554.

(36) Bouwman, E.; Gorkum, R. A Study of New Manganese Complexes as Potential Driers for Alkyd Paints. *J. Coat. Technol. Res.* **2007**, *4* (4), 491–503 DOI: 10.1007/s11998-007-9041-0.

(37) Mallégol, J.; Gonon, L.; Commereuc, S.; Verney, V. Thermal (DSC) and Chemical (Iodometric Titration) Methods for Peroxides Measurements in Order to Monitor Drying Extent of Alkyd Resins. *Prog. Org. Coat.* **2001**, *41* (1), 171–176.

(38) Van den Berg, J. D. J.; Van den Berg, K. J.; Boon, J. J. Determination of the Degree of Hydrolysis of Oil Paint Samples Using a Two-Step Derivatisation Method and on-Column GC/MS. *Prog. Org. Coat.* **2001**, *41* (1), 143–155.

(39) Iedema, P. D.; Hermans, J. J.; Keune, K.; van Loon, A.; Stols-Witlox, M. J. N. Mathematical Modeling of Mature Oil Paints. In *Preprints*; International Council of Museums: Melbourne, 2014.

(40) Garcia-Ochoa, F.; Querol, J.; Romero, A. Modeling of the Liquid-Phase N-Octane Oxidation Catalyzed by Cobalt. *Ind. Eng. Chem. Res.* **1990**, *29* (10), 1989–1994.

(41) Broadbelt, L. J.; Pfaendtner, J. Lexicography of Kinetic Modeling of Complex Reaction Networks. *AIChE J.* **2005**, *51* (8), 2112–2121 DOI: 10.1002/aic.10599.

(42) Denisov, E. T.; Afanas'ev, I. B. *Oxidation and Antioxidants in Organic Chemistry and Biology*; Crc Press-Taylor & Francis Group: Boca Raton, 2005.

(43) Gardner, H. W. Oxygen Radical Chemistry of Polyunsaturated Fatty Acids. *Free Radic. Biol. Med.* **1989**, *7* (1), 65–86.

(44) Frankel, E. N. *Lipid Oxidation*; Woodhead Publishing: Cambridge, 2012.

(45) Van Gorkum, R.; Bouwman, E. The Oxidative Drying of Alkyd Paint Catalysed by Metal Complexes. *Coord. Chem. Rev.* **2005**, *249* (17), 1709–1728.

(46) Soucek, M. D.; Khattab, T.; Wu, J. Review of Autoxidation and Driers. *Prog. Org. Coat.* **2012**, *73* (4), 435–454 DOI: 10.1016/j.porgcoat.2011.08.021.

(47) Spier, E.; Neuenschwander, U.; Hermans, I. Insights into the Cobalt(II)-Catalyzed Decomposition of Peroxide. *Angew. Chem. Int. Ed.* **2013**, *52* (5), 1581–1585 DOI: 10.1002/anie.201207920.

(48) Spier, E.; Hermans, I. Enhancing the Deperoxidation Activity of Cobalt(II)Acetylacetonate by the Addition of Octanoic Acid. *ChemPhysChem* **2013**, *14* (14), 3384–3388 DOI: 10.1002/cphc.201300460.

(49) Frankel, E. N. Volatile Lipid Oxidation Products. *Prog. Lipid Res.* **1983**, *22* (1), 1–33.

(50) Hancock, R. A.; Leeves, N. J.; Nicks, P. F. Studies in Autoxidation: Part I. The Volatile by-Products Resulting from the Autoxidation of Unsaturated Fatty Acid Methyl Esters. *Prog. Org. Coat.* **1989**, *17* (3), 321–336.

(51) Pfaendtner, J.; Broadbelt, L. J. Mechanistic Modeling of Lubricant Degradation. 2. The Autoxidation of Decane and Octane. *Ind. Eng. Chem. Res.* **2008**, *47* (9), 2897–2904 DOI: 10.1021/ie071481z.

(52) Benson, S. W. *Thermochemical Kinetics: Methods for the Estimation of Thermochemical Data and Rate Parameters*, 2nd ed.; John Wiley & Sons: New York, 1976.

(53) Pfaendtner, J.; Broadbelt, L. J. Mechanistic Modeling of Lubricant Degradation. 1. Structure-Reactivity Relationships for Free-Radical Oxidation. *Ind. Eng. Chem. Res.* **2008**, *47* (9), 2886–2896.

(54) Stein, S. E.; Rukkers, J. M.; Brown, R. L. *NIST Standard Reference Database 25: NIST Structures and Properties Database and Estimation Program*; Gaithersberg, MD, 1991.

(55) Sumathi, R.; Green Jr., W. H. A Priori Rate Constants for Kinetic Modeling. *Theor. Chem. Acc. Theory Comput. Model. Theor. Chim. Acta* **2002**, *108* (4), 187–213 DOI: 10.1007/s00214-002-0368-4.

(56) Henry, D. J.; Radom, L. Theoretical Thermochemistry of Radicals. In *Quantum-Mechanical Prediction of Thermochemical Data*; Cioslowski, J., Ed.; Springer, 2001; pp 161–197.

(57) Menon, A. S.; Wood, G. P. F.; Moran, D.; Radom, L. Bond Dissociation Energies and Radical Stabilization Energies: An Assessment of Contemporary Theoretical Procedures. *J. Phys. Chem. A* **2007**, *111* (51), 13638–13644 DOI: 10.1021/jp076521r.

(58) Coote, M. L. Reliable Theoretical Procedures for the Calculation of Electronic-Structure Information in Hydrogen Abstraction Reactions. *J. Phys. Chem. A* **2004**, *108* (17), 3865–3872 DOI: 10.1021/jp049863v.

(59) Lin, C. Y.; Hodgson, J. L.; Namazian, M.; Coote, M. L. Comparison of G3 and G4 Theories for Radical Addition and Abstraction Reactions. *J. Phys. Chem. A* **2009**, *113* (15), 3690–3697 DOI: 10.1021/jp900649j.

(60) Zheng, X.; Blowers, P. The Application of Composite Energy Methods to N-Butyl Radical β-Scission Reaction Kinetic Estimations. *Theor. Chem. Acc.* **2007**, *117* (2), 207–212 DOI: 10.1007/s00214-006-0129-x.

(61) Wang, F.; Cao, D. B.; Liu, G.; Ren, J.; Li, Y. W. Theoretical Study of the Competitive Decomposition and Isomerization of 1-Hexyl Radical. *Theor. Chem. Acc.* **2010**, *126* (1–2), 87–98 DOI: 10.1007/s00214-009-0685-y.

(62) Denisov, E. T. *Liquid-Phase Reaction Rate Constants*; Plenum Press: New York, 1974.

(63) Emanuel, N. M.; Denisov, E. T.; Maizus, Z. K. *Liquid-Phase Oxidation of Hyrdocarbons*; Plenum Press: New York, 1967.

(64) Neuenschwander, U.; Hermans, I. Thermal and Catalytic Formation of Radicals during Autoxidation. *J. Catal.* **2012**, *287*, 1–4 DOI: 10.1016/j.jcat.2011.12.009.

(65) Naqvi, S. M. D.; Khan, F. Selective Homogeneous Oxidation System for Producing Hydroperoxides Concentrate: Kinetics of Catalytic Oxidation of Gas Oils. *Ind. Eng. Chem. Res.* **2009**, *48* (12), 5642–5655.

(66) Denisov, E. T.; Denisova, T. G.; Pokidova, T. S. *Handbook of Free Radical Initiators*; John Wiley & Sons: New Jersey, 2003.

(67) Min, D. B.; Boff, J. M. Chemistry and Reaction of Singlet Oxygen in Foods. *Compr. Rev. Food Sci. Food Saf.* **2002**, *1* (2), 58–72.

(68) Frankel, E. N. Chemistry of Free Radical and Singlet Oxidation of Lipids. *Prog. Lipid Res.* **1984**, *23* (4), 197–221.

(69) Frankel, E. N.; Neff, W. E.; Rohwedder, W. K.; Khambay, B. P. S.; Garwood, R. F.; Weedon, B. C. L. Analysis of Autoxidized Fats by Gas Chromatography-Mass Spectrometry: II. Methyl Linoleate. *Lipids* **1977**, *12* (11), 908–913.

(70) Gillespie, D. T. Concerning the Validity of the Stochastic Approach to Chemical Kinetics. *J Stat Phys* **1977**, *16*, 311–318.

(71) Gillespie, D. T. Stochastic Simulation of Chemical Kinetics. *Annu. Rev. Phys. Chem.* **2007**, *58* (1), 35–55 DOI: 10.1146/annurev.physchem.58.032806.104637.

(72) *Lipid Technologies and Applications*; Gunstone, F. D., Padley, F. B., Eds.; Marcel Dekker: New York, 1997.

(73) Choe, E.; Min, D. B. Mechanisms and Factors for Edible Oil Oxidation. *Compr. Rev. Food Sci. Food Saf.* **2006**, *5* (4), 169–186.

(74) Gao, H.; Oakley, L. H.; Konstantinov, I. A.; Arturo, S. G.; Broadbelt, L. J. Acceleration of Kinetic Monte Carlo Method for the Simulation of Free Radical Copolymerization through Scaling. *Ind. Eng. Chem. Res.* **2015**, *54* (48), 11975–11985 DOI: 10.1021/acs.iecr.5b03198.

(75) Evans, C. D.; List, G. R.; Dolev, A.; McConnell, D. G.; Hoffmann, R. L. Pentane from Thermal Decomposition of Lipoxidase-Derived Products. *Lipids* **1967**, *2* (5), 432–434.

(76) Jeleń, H. H.; Obuchowska, M.; Zawirska-Wojtasiak, R.; Wąsowicz, E. Headspace Solid-Phase Microextraction Use for the Characterization of Volatile Compounds in Vegetable Oils of Different Sensory Quality. *J. Agric. Food Chem.* **2000**, *48* (6), 2360–2367 DOI: 10.1021/jf991095v.

(77) Jalan, A.; Alecu, I. M.; Meana-Pañeda, R.; Aguilera-Iparraguirre, J.; Yang, K. R.; Merchant, S. S.; Truhlar, D. G.; Green, W. H. New Pathways for Formation of Acids and Carbonyl Products in Low-Temperature Oxidation: The Korcek Decomposition of γ-Ketohydroperoxides. *J. Am. Chem. Soc.* **2013**, *135* (30), 11100–11114 DOI: 10.1021/ja4034439.

(78) Wang, S. Hock Rearrangement (Hock Cleavage). In *Comprehensive Organic Name Reactions and Reagents*; John Wiley & Sons: Hoboken, N.J.; Vol. 2, pp 1438–1441.

(79) Juita; Dlugogorski, B. Z.; Kennedy, E. M.; Mackie, J. C. Mechanism of Formation of Volatile Organic Compounds from Oxidation of Linseed Oil. *Ind. Eng. Chem. Res.* **2012**, *51* (16), 5653–5661 DOI: 10.1021/ie202536n.

(80) Morita, M.; Tokita, M. Hydroxy Radical, Hexanal, and Decadienal Generation by Autocatalysts in Autoxidation of Linoleate Alone and with Eleostearate. *Lipids* **2008**, *43* (7), 589–597 DOI: 10.1007/s11745-008-3170-9.

(81) Gardner, H. W.; Plattner, R. D. Linoleate Hydroperoxides Are Cleaved Heterolytically into Aldehydes by a Lewis Acid in Aprotic Solvent. *Lipids* **1984**, *19* (4), 294–299.

(82) Schneider, C.; Boeglin, W. E.; Yin, H.; Stec, D. F.; Hachey, D. L.; Porter, N. A.; Brash, A. R. Synthesis of Dihydroperoxides of Linoleic and Linolenic Acids and Studies on Their Transformation to 4-Hydroperoxynonenal. *Lipids* **2005**, *40* (11), 1155–1162.

(83) Frimer, A. A. The Reaction of Singlet Oxygen with Olefins: The Question of Mechanism. *Chem. Rev.* **1979**, *79* (5), 359–387.

(84) Spickett, C. M. The Lipid Peroxidation Product 4-Hydroxy-2-Nonenal: Advances in Chemistry and Analysis. *Redox Biol.* **2013**, *1* (1), 145–152 DOI: 10.1016/j.redox.2013.01.007.

(85) Morita, M.; Tokita, M. The Real Radical Generator Other than Main-Product Hydroperoxide in Lipid Autoxidation. *Lipids* **2006**, *41* (1), 91–95.

(86) Susnow, R. G.; Dean, A. M.; Green, W. H.; Peczak, P.; Broadbelt, L. J. Rate-Based Construction of Kinetic Models for Complex Systems. *J. Phys. Chem. A* **1997**, *101* (20), 3731–3740.

(87) Fjällström, P.; Andersson, B.; Nilsson, C.; Andersson, K. Drying of Linseed Oil Paints: A Laboratory Study of Aldehyde Emissions. *Ind. Crops Prod.* **2002**, *16* (3), 173–184.

(88) Knudsen, H. N.; Clausen, P. A.; Wilkins, C. K.; Wolkoff, P. Sensory and Chemical Evaluation of Odorous Emissions from Building Products with and without Linseed Oil. *Build. Environ.* **2007**, *42* (12), 4059–4067 DOI: 10.1016/j.buildenv.2006.05.009.

(89) Clausen, P. A.; Knudsen, H. N.; Larsen, K.; Kofoed-Sørensen, V.; Wolkoff, P.; Wilkins, C. K. Use of Thermal Desorption Gas Chromatography–olfactometry/Mass Spectrometry for the Comparison of Identified and Unidentified Odor Active Compounds Emitted from Building Products Containing Linseed Oil. *J. Chromatogr. A* **2008**, *1210* (2), 203–211 DOI: 10.1016/j.chroma.2008.09.073.

(90) Haghighat, F.; De Bellis, L. Material Emission Rates: Literature Review, and the Impact of Indoor Air Temperature and Relative Humidity. *Build. Environ.* **1998**, *33* (5), 261–277 DOI: 10.1016/S0360-1323(97)00060-7.

(91) Uhde, E.; Salthammer, T. Impact of Reaction Products from Building Materials and Furnishings on Indoor Air quality—A Review of Recent Advances in Indoor Chemistry. *Atmos. Environ.* **2007**, *41* (15), 3111–3128 DOI: 10.1016/j.atmosenv.2006.05.082.

(92) Jiménez, A.; Beltrán, G.; Aguilera, M. . Application of Solid-Phase Microextraction to the Analysis of Volatile Compounds in Virgin Olive Oils. *J. Chromatogr. A* **2004**, *1028* (2), 321–324 DOI: 10.1016/j.chroma.2003.11.096.

(93) Muik, B.; Lendl, B.; Molina-Díaz, A.; Ayora-Cañada, M. J. Direct Monitoring of Lipid Oxidation in Edible Oils by Fourier Transform Raman Spectroscopy. *Chem. Phys. Lipids* **2005**, *134* (2), 173–182 DOI: 10.1016/j.chemphyslip.2005.01.003.

(94) Krist, S.; Stuebiger, G.; Unterweger, H.; Bandion, F.; Buchbauer, G. Analysis of Volatile Compounds and Triglycerides of Seed Oils Extracted from Different Poppy Varieties (Papaver Somniferum L.). *J. Agric. Food Chem.* **2005**, *53* (21), 8310–8316 DOI: 10.1021/jf0580869.

(95) Krist, S.; Stuebiger, G.; Bail, S.; Unterweger, H. Analysis of Volatile Compounds and Triacylglycerol Composition of Fatty Seed Oil Gained from Flax and False Flax. *Eur. J. Lipid Sci. Technol.* **2006**, *108* (1), 48–60 DOI: 10.1002/ejlt.200500267.

(96) Lattuati-Derieux, A.; Thao, S.; Langlois, J.; Regert, M. First Results on Headspace-Solid Phase Microextraction-Gas Chromatography/Mass Spectrometry of Volatile Organic Compounds Emitted by Wax Objects in Museums. *J. Chromatogr. A* **2008**, *1187* (1–2), 239–249 DOI: 10.1016/j.chroma.2008.02.015.

(97) Curran, K.; Underhill, M.; Gibson, L. T.; Strlic, M. The Development of a SPME-GC/MS Method for the Analysis of VOC Emissions from Historic Plastic and Rubber Materials. *Microchem. J.* **2016**, *124*, 909–918 DOI: 10.1016/j.microc.2015.08.027.

(98) Curran, K.; Strlič, M. Polymers and Volatiles: Using VOC Analysis for the Conservation of Plastic and Rubber Objects. *Stud. Conserv.* **2015**, *60* (1), 1–14 DOI: 10.1179/2047058413Y.0000000125.

(99) Vinu, R.; Broadbelt, L. J. Unraveling Reaction Pathways and Specifying Reaction Kinetics for Complex Systems. *Annu. Rev. Chem. Biomol. Eng.* **2012**, *3*, 29–54.

(100) Gardner, H. W.; Selke, E. Volatiles from Thermal Decomposition of Isomeric Methyl (12S, 13S)-(E)-12, 13-Epoxy-9-Hydroperoxy-10-Octadecenoates. *Lipids* **1984**, *19* (6), 375–380.

(101) Frisch, M. J.; Trucks, G. W.; Schlegel, H. B.; Scuseria, G. E.; Robb, M. A.; Cheeseman, J. R.; Scalmani, G.; Barone, V.; Mennucci, B.; Petersson, G. A.; Nakasuji, H.; Caricato, M.; Li, X.; Hratchian, H. P.; Izmaylov, A. F.; Bloino, J.; Zheng, G.; Sonnenberg, J. L.; Hada, M.; Ehara, M.; Toyota, K.; Fukuda, R.; Hasegawa, J.; Ishida, M.; Nakajima, T.; Honda, Y.; Kitao, O.; Nakai, H.; Vreven, T.; Montgomery, J. A.; Peralta, J. E.; Ogliaro, F.; Bearpark, M.; Heyd, J. . J.; Brothers, E.; Kudin, K. N.; Staroverov, V. N.; Kobayashi, R.; Normand, J.; Raghavachari, K.; Rendell, A.; Burant, J. C.; Iyengar, S. S.; Tomasi, J.; Cossi, M.; Rega, N.; Millam, J. M.; Klene, M.; Knox, J. E.; Cross, J. B.; Bakken, V.; Adamo, C.; Jaramillo, J.; Gomperts, R.; Stratmann, R. E.; Yazyev, O.; Austin, A. . J.; Cammi, R.; Pomelli, C.; Ochterski, J. W.; Martin, R. L.; Morokuma, K.; Zakrzewski, V. G.; Voth, G. A.; Salvador, P.; Dannenberg, J. J.; Dapprich, S.; Daniels, A. D.; Farkas, O.; Foresman, J. B.; Ortiz, J. V.; Cioslowski, J.; Fox, D. J. *Gaussian 09*; Gaussian, Inc.: Wallingford CT, 2009.

(102) Curtiss, L. A.; Redfern, P. C.; Raghavachari, K. Gaussian-4 Theory. *J. Chem. Phys.* **2007**, *126* (8), 084108 DOI: 10.1063/1.2436888.

(103) Pfaendtner, J.; Yu, X.; Broadbelt, L. J. The 1-D Hindered Rotor Approximation. *Theor. Chem. Acc.* **2007**, *118* (5–6), 881–898 DOI: 10.1007/s00214-007-0376-5.

(104) Moore, J. W.; Pearson, R. G. *Kinetics and Mechanism*, 3rd ed.; John Wiley & Sons: New York, 1981.

(105) Hirschfelder, J. O.; Wigner, E. Some Quantum Mechanical Considerations in the Theory of Reactions Involving an Activation Energy. *J. Chem. Phys.* **1939**, *7*, 616–628 DOI: 10.1063/1.1750500.

(106) Gillespie, D. T. A General Method for Numerically Simulating the Stochastic Time Evolution of Coupled Chemical Reactions. *J Comp Phys* **1976**, *22*, 403–434.

(107) Jensen, R. K.; Korcek, S.; Mahoney, L. R.; Zinbo, M. Liquid-Phase Autoxidation of Organic Compounds at Elevated Temperatures. 1. The Stirred Flow Reactor Technique and Analysis of Primary Products from N-Hexadecane Autoxidation at 120-180. Degree. C. *J. Am. Chem. Soc.* **1979**, *101* (25), 7574–7584.

(108) Jensen, R. K.; Korcek, S.; Mahoney, L. R.; Zinbo, M. Liquid-Phase Autoxidation of Organic Compounds at Elevated Temperatures. 2. Kinetics and Mechanisms of the Formation of Cleavage Products in N-Hexadecane Autoxidation. *J. Am. Chem. Soc.* **1981**, *103* (7), 1742–1749.

(109) Jensen, R. K.; Korcek, S.; Zinbo, M.; Johnson, M. D. Initiation in Hydrocarbon Autoxidation at Elevated Temperatures. *Int. J. Chem. Kinet.* **1990**, *22* (10), 1095–1107.

(110) Hamilton, E. J.; Korcek, S.; Mahoney, L. R.; Zinbo, M. Kinetics and Mechanism of the Autoxidation of Pentaerythrityl Tetraheptanoate at 180–220° C. *Int. J. Chem. Kinet.* **1980**, *12* (9), 577–603.

(111) Scalarone, D.; Lazzari, M.; Chiantore, O. Thermally Assisted Hydrolysis and Methylation-Pyrolysis-Gas Chromatography/Mass Spectrometry of Light-Aged Linseed Oil. *J. Anal. Appl. Pyrolysis* **2001**, *58*, 503–512.

(112) NIST. *Standard Reference Database 17*; 2015.

(113) Pfaendtner, J.; Yu, X.; Broadbelt, L. J. Quantum Chemical Investigation of Low-Temperature Intramolecular Hydrogen Transfer Reactions of Hydrocarbons. *J. Phys. Chem. A* **2006**, *110* (37), 10863–10871 DOI: 10.1021/jp061649e.

(114) Oakley, L. H.; Casadio, F.; Shull, K. R.; Broadbelt, L. J. Theoretical Study of Epoxidation Reactions Relevant to Hydrocarbon Oxidation. *Ind. Eng. Chem. Res.* **2017**, *56* (26), 7454–7461 DOI: 10.1021/acs.iecr.7b01443.

(115) Farmer, E. H.; Bloomfield, G. F.; Sundralingam, A.; Sutton, D. A. The Course and Mechanism of Autoxidation Reactions in Olefinic and Polyolefinic Substances, Including Rubber. *Trans. Faraday Soc.* **1942**, *38*, 348–356.

(116) Juita; Dlugogorski, B. Z.; Kennedy, E. M.; Mackie, J. C. Mechanism of Formation of Volatile Organic Compounds from Oxidation of Linseed Oil. *Ind. Eng. Chem. Res.* **2012**, *51* (16), 5653–5661 DOI: 10.1021/ie202536n.

(117) Somers, K. P.; Simmie, J. M. Benchmarking Compound Methods (CBS-QB3, CBS-APNO, G3, G4, W1BD) against the Active Thermochemical Tables: Formation Enthalpies of Radicals. *J. Phys. Chem. A* **2015**, *119* (33), 8922–8933 DOI: 10.1021/acs.jpca.5b05448.

(118) Dobarganes, M. C.; Marquez-Ruiz, G. Formation and Analysis of Oxidized Monomeric, Dimeric and Higher Oligomeric Triglycerides. In *Deep Frying: Chemistry, Nutrition and Practical Applications*; 2007; pp 87–110.

(119) Blaine, S.; Savage, P. E. Reaction Pathways in Lubricant Degradation 2. N-Hexadecane Autoxidation. *Ind. Eng. Chem. Res.* **1991**, *30* (9), 2185–2191.

(120) Lee, J.; Kim, D.; Chang, P.; Lee, J. Headspace-Solid Phase Microextraction (HS-SPME) Analysis of Oxidized Volatiles from Free Fatty Acids (FFA) and Application for Measuring Hydrogen Donating Antioxidant Activity. *Food Chem.* **2007**, *105* (1), 414–420 DOI: 10.1016/j.foodchem.2006.12.059.

(121) Buttrey, D. N. Cellulose Nitrate. In *Cellulose Plastics*; Cleaver-Hume Press Ltd.: London, 1947; pp 53–86.

(122) Vangorkum, R.; Bouwman, E. The Oxidative Drying of Alkyd Paint Catalysed by Metal Complexes. *Coord. Chem. Rev.* **2005**, *249* (17–18), 1709–1728 DOI: 10.1016/j.ccr.2005.02.002.

(123) Yaluris, G.; Rekoske, J. E.; Aparicio, L. M.; Madon, R. J.; Dumesic, J. A. Isobutane Cracking over Y-Zeolites I. Development of a Kinetic Model. *J. Catal.* **1995**, *153*, 56–64.

(124) Saeys, M.; Reyniers, M.-F.; Marin, G. B.; Van Speybroeck, V.; Waroquier, M. Ab Initio Calculations for Hydrocarbons: Enthalpy of Formation, Transition State Geometry, and Activation Energy for Radical Reactions. *J. Phys. Chem. A* **2003**, *107* (43), 9147–9159 DOI: 10.1021/jp021706d.

(125) Lee, Y.; von Gunten, U. Quantitative Structure–activity Relationships (QSARs) for the Transformation of Organic Micropollutants during Oxidative Water Treatment. *Water Res.* **2012**, *46* (19), 6177–6195 DOI: 10.1016/j.watres.2012.06.006.

(126) Blowers, P.; Masel, R. I. An Extension of the Marcus Equation for Atom Transfer Reactions. *J. Phys. Chem. A* **1999**, *103* (35), 7047–7054 DOI: 10.1021/jp990039u.

(127) Sharma, S.; Raman, S.; Green, W. H. Intramolecular Hydrogen Migration in Alkylperoxy and Hydroperoxyalkylperoxy Radicals: Accurate Treatment of Hindered Rotors. *J. Phys. Chem. A* **2010**, *114* (18), 5689–5701 DOI: 10.1021/jp9098792.

(128) Budnik, R. A.; Kochi, J. K. Epoxidation of Olefins with Molecular Oxygen in the Presence of Cobalt Complexes. *J. Org. Chem.* **1976**, *41* (8), 1384–1389.

(129) Benson, S. W. Effects of Resonance and Structure on the Thermochemistry of Organic Peroxy Radicals and the Kinetics of Combustion Reactions1. *J. Am. Chem. Soc.* **1965**, *87* (5), 972–979.

(130) Baldwin, R. R.; Stout, D. R.; Walker, R. W. Arrhenius Parameters for the Addition of HO 2 Radicals to Ethene between 400 and 500° C. *J. Chem. Soc. Faraday Trans.* **1991**, *87* (14), 2147–2150.

(131) Bloodworth, A. J.; Davies, A. G.; Griffin, I. M.; Muggleton, B.; Roberts, B. P. Rate Constants for the Formation of Oxiranes From. Beta.-Peroxyalkyl Radicals. Gem-Dialkyl Effect in Homolytic Ring Closure. *J. Am. Chem. Soc.* **1974**, *96* (24), 7599–7601.

(132) Sheng, C. Y.; Bozzelli, J. W.; Dean, A. M.; Chang, A. Y. Detailed Kinetics and Thermochemistry of C2H5+ O2: Reaction Kinetics of the Chemically-Activated and Stabilized CH3CH2OO Adduct. *J. Phys. Chem. A* **2002**, *106* (32), 7276–7293.

(133) Wijaya, C. D.; Sumathi, R.; Green, W. H. Thermodynamic Properties and Kinetic Parameters for Cyclic Ether Formation from Hydroperoxyalkyl Radicals. *J. Phys. Chem. A* **2003**, *107* (24), 4908–4920 DOI: 10.1021/jp027471n.

(134) Chan, W.-T.; Pritchard, H. O.; Hamilton, I. P. Dissociative Ring-Closure in Aliphatic Hydroperoxyl Radicals. *Phys. Chem. Chem. Phys.* **1999**, *1* (16), 3715–3719.

(135) Miyoshi, A. Systematic Computational Study on the Unimolecular Reactions of Alkylperoxy (RO2), Hydroperoxyalkyl (QOOH), and Hydroperoxyalkylperoxy (O2QOOH) Radicals. *J. Phys. Chem. A* **2011**, *115* (15), 3301–3325 DOI: 10.1021/jp112152n.

(136) Cord, M.; Sirjean, B.; Fournet, R.; Tomlin, A.; Ruiz-Lopez, M.; Battin-Leclerc, F. Improvement of the Modeling of the Low-Temperature Oxidation of N-Butane: Study of the Primary Reactions. *J. Phys. Chem. A* **2012**, *116* (24), 6142–6158 DOI: 10.1021/jp211434f.

(137) Villano, S. M.; Huynh, L. K.; Carstensen, H.-H.; Dean, A. M. High-Pressure Rate Rules for Alkyl + O2 Reactions. 2. The Isomerization, Cyclic Ether Formation, and β-Scission Reactions of Hydroperoxy Alkyl Radicals. *J. Phys. Chem. A* **2012**, *116* (21), 5068–5089 DOI: 10.1021/jp3023887.

(138) Bugler, J.; Power, J.; Curran, H. J. A Theoretical Study of Cyclic Ether Formation Reactions. *Proc. Combust. Inst.* **2017**, *36* (1), 161–167 DOI: 10.1016/j.proci.2016.05.006.

(139) Peng, C.; Ayala, P. Y.; Schlegel, H. B.; Frisch, M. J. Using Redundant Internal Coordinates to Optimize Equilibrium Geometries and Transition States. *J. Comput. Chem.* **1996**, *17* (1), 49–56.

(140) Liu, S.; Srinivasan, S.; Grady, M. C.; Soroush, M.; Rappe, A. M. Backbiting and β-Scission Reactions in Free-Radical Polymerization of Methyl Acrylate. *Int. J. Quantum Chem.* **2014**, *114* (5), 345–360 DOI: 10.1002/qua.24572.

(141) Wang, H.; Bozzelli, J. W. Thermochemistry and Kinetic Analysis of the Unimolecular Oxiranyl Radical Dissociation Reaction: A Theoretical Study. *ChemPhysChem* **2016**, *17* (13), 1983–1992 DOI: 10.1002/cphc.201600152.

(142) Curtiss, L. A.; Redfern, P. C.; Raghavachari, K.; Pople, J. A. Gaussian-3X (G3X) Theory: Use of Improved Geometries, Zero-Point Energies, and Hartree–Fock Basis Sets. *J. Chem. Phys.* **2001**, *114* (1), 108 DOI: 10.1063/1.1321305.

(143) Pfaendtner, J.; Yu, X.; Broadbelt, L. J. *Calctherm*; 2006.

(144) Montgomery, J. A.; Frisch, M. J.; Ochterski, J. W.; Petersson, G. A. A Complete Basis Set Model Chemistry. VI. Use of Density Functional Geometries and Frequencies. *J. Chem. Phys.* **1999**, *110* (6), 2822.

(145) Zhang, K.; Banyon, C.; Togbé, C.; Dagaut, P.; Bugler, J.; Curran, H. J. An Experimental and Kinetic Modeling Study of N-Hexane Oxidation. *Combust. Flame* **2015**, *162* (11), 4194–4207 DOI: 10.1016/j.combustflame.2015.08.001.

(146) Lay, T. H.; Bozzelli, J. W. Enthalpies of Formation and Group Additivity of Alkyl Peroxides and Trioxides. *J. Phys. Chem. A* **1997**, *101* (49), 9505–9510.

(147) Pfaendtner, J.; Broadbelt, L. J. Contra-Thermodynamic Behavior in Intermolecular Hydrogen Transfer of Alkylperoxy Radicals. *ChemPhysChem* **2007**, *8* (13), 1969–1978 DOI: 10.1002/cphc.200700161.

(148) Gao, C. W.; Allen, J. W.; Green, W. H.; West, R. H. Reaction Mechanism Generator: Automatic Construction of Chemical Kinetic Mechanisms. *Comput. Phys. Commun.* **2016**, *203*, 212–225 DOI: 10.1016/j.cpc.2016.02.013.

(149) Vandewiele, N. M.; Van Geem, K. M.; Reyniers, M.-F.; Marin, G. B. Genesys: Kinetic Model Construction Using Chemo-Informatics. *Chem. Eng. J.* **2012**, *207–208*, 526–538 DOI: 10.1016/j.cej.2012.07.014.

(150) Learner, T.; Institute, G. C. *Analysis Of Modern Paints*; Getty Publications, 2005.

(151) de Boer, J. W.; Wesenhagen, P. V.; Wenker, E. C. M.; Maaijen, K.; Gol, F.; Gibbs, H.; Hage, R. The Quest for Cobalt-Free Alkyd Paint Driers. *Eur. J. Inorg. Chem.* **2013**, *2013* (21), 3581–3591 DOI: 10.1002/ejic.201300205.

(152) Dubrulle, L.; Lebeuf, R.; Thomas, L.; Fressancourt-Collinet, M.; Nardello-Rataj, V. Catalytic Activity of Primary and Secondary Driers towards the Oxidation and Hydroperoxide Decomposition Steps for the Chemical Drying of Alkyd Resin. *Prog. Org. Coat.* **2017**, *104*, 141–151 DOI: 10.1016/j.porgcoat.2016.12.018.

(153) Gezici-Koç, Ö.; Thomas, C. A. A. M.; Michel, M.-E. B.; Erich, S. J. F.; Huinink, H. P.; Flapper, J.; Duivenvoorde, F. L.; van der Ven, L. G. J.; Adan, O. C. G. In-Depth Study of Drying Solvent-Borne Alkyd Coatings in Presence of Mn- and Fe- Based Catalysts as Cobalt Alternatives. *Mater. Today Commun.* **2016**, *7*, 22–31 DOI: 10.1016/j.mtcomm.2016.03.001.

(154) Rodriguez, A.; Herbinet, O.; Battin-Leclerc, F.; Frassoldati, A.; Faravelli, T.; Ranzi, E. Experimental and Modeling Investigation of the Effect of the Unsaturation Degree on the Gas-Phase Oxidation of Fatty Acid Methyl Esters Found in Biodiesel Fuels. *Combust. Flame* **2016**, *164*, 346–362 DOI: 10.1016/j.combustflame.2015.11.032.

(155) Van Geem, K. M.; Reyniers, M.-F.; Marin, G. B.; Song, J.; Green, W. H.; Matheu, D. M. Automatic Reaction Network Generation Using RMG for Steam Cracking of N-Hexane. *AIChE J.* **2006**, *52* (2), 718–730 DOI: 10.1002/aic.10655.

(156) Broadbelt, L. J.; Stark, S. M.; Klein, M. T. Computer Generated Reaction Modelling: Decomposition and Encoding Algorithms for Determining Species Uniqueness. *Comput. Chem. Eng.* **1995**, *20* (2), 113–129.

(157) Broadbelt, L. J.; Stark, S. M.; Klein, M. T. Termination of Computer-Generated Reaction Mechanisms: Species Rank-Based Convergence Criterion. *Ind. Eng. Chem. Res.* **1995**, *34* (8), 2566–2573.

(158) Stewart, W. E.; Caracotsios, M.; Sorensen, J. P. *Double Precision Differential-Algebraic Sensitive Analysis Code (DDASAC)*; Madison, WI, 1997.

(159) Stewart, W. E.; Caracotsios, M.; Sorensen, J. P. *Generalized Regression Software (GREG)*; Madison, WI, 1997.

(160) Catalano, J.; Yao, Y.; Murphy, A.; Zumbulyadis, N.; Centeno, S. A.; Dybowski, C. Nuclear Magnetic Resonance Spectra and 207Pb Chemical-Shift Tensors of Lead Carboxylates Relevant to Soap Formation in Oil Paintings. *Appl. Spectrosc.* **2014**, *68* (3), 280–286 DOI: 10.1366/13-07209.

(161) Hermans, J. J.; Keune, K.; Loon, A. van; Iedema, P. D. The Crystallization of Metal Soaps and Fatty Acids in Oil Paint Model Systems. *Phys Chem Chem Phys* **2016** DOI: 10.1039/C6CP00487C.

(162) Pryor, W. A.; Porter, N. A. Suggested Mechansims for the Production of 4-Hydroxy-2-Nonenal from the Autoxidation of Polyunsaturated Fatty Acids. *Free Radic. Biol. Med.* **1990**, *8*, 541–543.

(163) Kochhar, S. P. Oxidative Pathways to the Formation of off-Flavours. In *Food Taints and Off-Flavours*; Saxby, M. J., Ed.; Chapman & Hall: New York, 1996.

(164) Bonaduce, I.; Carlyle, L.; Colombini, M. P.; Duce, C.; Ferrari, C.; Ribechini, E.; Selleri, P.; Tiné, M. R. A Multi-Analytical Approach to Studying Binding Media in Oil Paintings: Characterisation of Differently Pre-Treated Linseed Oil by DE-MS, TG and GC/MS. *J. Therm. Anal. Calorim.* **2012**, *107* (3), 1055–1066 DOI: 10.1007/s10973-011-1586-6.

(165) Bonaduce, I.; Carlyle, L.; Colombini, M. P.; Duce, C.; Ferrari, C.; Ribechini, E.; Selleri, P.; Tiné, M. R. New Insights into the Ageing of Linseed Oil Paint Binder: A Qualitative and Quantitative Analytical Study. *PLoS ONE* **2012**, *7* (11), e49333 DOI: 10.1371/journal.pone.0049333.

(166) Plater, M. J.; De Silva, B.; Gelbrich, T.; Hursthouse, M. B.; Higgitt, C. L.; Saunders, D. R. The Characterisation of Lead Fatty Acid Soaps in “protrusions” in Aged Traditional Oil Paint. *Polyhedron* **2003**, *22* (24), 3171–3179 DOI: 10.1016/S0277-5387(03)00461-3.

(167) Cotte, M.; Checroun, E.; Nolf, W. D.; Taniguchi, Y.; Viguerie, L. D.; Burghammer, M.; Walter, P.; Rivard, C.; Salomé, M.; Janssens, K.; Susini, J. Lead Soaps in Paintings: Friends or Foes? *Stud. Conserv.* **2017**, *62* (1), 2–23 DOI: 10.1080/00393630.2016.1232529.

(168) Sturdy, L.; Casadio, F.; Kokkori, M.; Muir, K.; Shull, K. R. Quartz Crystal Rheometry: A Quantitative Technique for Studying Curing and Aging in Artists' Paints. *Polym. Degrad. Stab.* **2014**, *107*, 348–355 DOI: 10.1016/j.polymdegradstab.2014.02.009.

(169) M Kruse, T.; Sang Woo, O.; J Broadbelt, L. Detailed Mechanistic Modeling of Polymer Degradation: Application to Polystyrene. *Chem. Eng. Sci.* **2001**, *56* (3), 971–979.